70-22,984

FIORINO, Jr., Thomas Daniel, 1941-
AN INTEGRAL APPROXIMATION FOR SHOCK SHAPES OVER SLENDER BODIES IN INVISCID HYPERSONIC FLOW.

The University of Oklahoma, Ph.D., 1970
Engineering, aeronautical

University Microfilms, A XEROX Company, Ann Arbor, Michigan

THIS DISSERTATION HAS BEEN MICROFILMED EXACTLY AS RECEIVED

Downloaded from SHAREOK. Persistent Handle URL: https://hdl.handle.net/11244/2799

THE UNIVERSITY OF OKLAHOMA

GRADUATE COLLEGE

AN INTEGRAL APPROXIMATION FOR SHOCK SHAPES OVER SLENDER BODIES IN INVISCID HYPERSONIC FLOW

A DISSERTATION

SUBMITTED TO THE GRADUATE FACULTY

in partial fulfillment of the requirements for the

degree of

DOCTOR OF PHILOSOPHY

BY

THOMAS DANIEL FIORINO, JR.

Norman, Oklahoma

1970

AN INTEGRAL APPROXIMATION FOR SHOCK SHAPES OVER SLENDER BODIES IN INVISCID HYPERSONIC FLOW

APPROVED BY:

Maurice Rasmussen

E J Blasi

Martin C. Twitty

Robert F. Petty

DISSERTATION COMMITTEE

ACKNOWLEDGMENTS

Most of this work was accomplished during a tour of duty with the Air Force Institute of Technology Civilian Institutions program at the University of Oklahoma. Thanks are due to those who have made this program possible and also to Col. Joseph Meyers, Commander of the Air Force Flight Dynamics Laboratory, for allowing me to be absent from duty while completing this project at the University.

I am most grateful to my advisor Dr. Maurice Rasmussen for the help, encouragement, and inspiration he has given me throughout the graduate program. Without his initial efforts and suggestions as well as contributions throughout the course of study, this work could not have been completed. The contributions of Dr. Martin Jischke are greatly appreciated and deserve a special note of thanks. Also, the time and effort of Dr. Tom Love, Dr. Edward Blick, Dr. Darrell Harden, and Dr. Robert Petry are sincerely appreciated. Many thanks are extended to Mary Lou Stokes not only for the typing and assistance with the format, but also for accomplishing these tasks in a friendly and efficient manner.

I would like to thank my wife Dorothy and my children Steve, Ellen, and Tim for their own special contributions.

This work is dedicated to the memory of my beloved grandfathers, Soccorso Ciardi and Francesco Fiorino.

ABSTRACT

The governing equations for the flow over a slender body are developed in terms of the equivalence principle of Hayes, and are written in integral form. A quadrature solution for the body shape in terms of a specified shock is obtained (inverse problem). Also, for blunted shocks the entropy-displacement effect is evaluated in terms of the shock parameters. By means of the same governing equations a solution for the shock shape over a non-growing body is presented (a special case of the direct problem). Physically, this represents the flow over circular cylinders and flat-plates. In addition, expressions for the pressure distribution and drag are developed and applied to the inverse and direct problems.

The general solution for the inverse problem is applied to conical, ogival, power-law, and hyperbolic shocks. The corresponding body shapes are analytic and expressed in terms of the shock parameters and ratio of specific heats. The body generating a parabolic shock is found to grow asymptotically, whereas the body from blast-wave theory is non-growing. The general solution for the direct problem is applied to circular cylinders and flat-plates with varying nose bluntness. The corresponding shocks, given by simple algebraic expressions in terms of the body parameters and ratio of specific heats, are found to grow more slowly than those predicted by the blast-wave solutions.

TABLE OF CONTENTS

Page

ACKNOWLEDGMENTS iii

ABSTRACT. iv

LIST OF TABLES. viii

LIST OF ILLUSTRATIONS ix

NOMENCLATURE. xii

Chapter

I. INTRODUCTION. 1

II. THEORETICAL DEVELOPMENT 6

Fundamental Concepts. 6

Basic Equations 9

Conservation of Mass 9

Momentum Equation. 11

Conservation of Energy 15

The Inverse Problem 17

The Direct Problem for the Non-Growing Body 19

Pressure and Drag Equations 22

III. POINTED SHOCKS. 27

Generalities. 27

The Conical Shock 27

Axisymmetric Case-Cone 27

Planar Case-Wedge. 29

Table of Contents (Continued)

The Ogival Shock 31

Axisymmetric Case-Ogive of Revolution 31

Planar Case-Plane Ogive 37

IV. SLIGHTLY BLUNTED SHOCKS. 44

General Considerations 44

Power-Law Shock. 45

Body Shape. 45

Entropy-Displacement Effect 51

Body Shape as a Function of n 52

Pressure Distribution 60

Hyperbolic Shock 61

Axisymmetric Case 63

Planar Case 68

V. CONSTANT RADIUS AND CONSTANT THICKNESS BODIES. 75

Shock Shape and Pressure Distribution. 75

Comparisons with other Theories and Experiments. 79

Additional Considerations. 103

VI. INTERPRETATION OF BODY SHAPES. 107

VII. CONCLUSIONS. 116

Concluding Remarks 116

Recommendations for Future Research. 118

LIST OF REFERENCES 119

Table of Contents (Continued)

APPENDICES

A. H_0, H_1, H_2, G_1 AND G_2 FOR THE OGIVE OF REVOLUTION. . 125

B. A_1, B_1, AND C_1 FOR THE OGIVE OF REVOLUTION 127

LIST OF TABLES

Table Page

4-1 Body Shape Associated with a Power-Law Shock (Zero Order Problem). 55

LIST OF ILLUSTRATIONS

Figure		Page
2.1	Illustration of the Equivalence Principle.	8
2.2	Equivalent Plane Terminology	10
2.3	Terminology for Slender Body Drag.	24
3.1	Curvature Ratio for the Ogive of Revolution.	33
3.2	Variation of m with K_δ for the Ogive of Revolution	34
3.3	Variation of n with K_δ for the Ogive of Revolution	35
3.4	Initial Pressure Gradient on the Ogive of Revolution . . .	38
3.5	Curvature Ratio for the Plane Ogive.	41
3.6	Initial Pressure Gradient on the Plane Ogive	42
4.1	Illustration of the Entropy-Displacement Effect.	49
4.2	Body Shape for an Axisymmetric Power-Law Shock	56
4.3	Body Shape for a Plane Power-Law Shock	56
4.4	Body Shapes for an Axisymmetric Parabolic Shock	59
4.5	Body Shapes for a Plane Parabolic Shock.	59
4.6	Body Pressures for an Axisymmetric Parabolic Shock	62
4.7	Body Pressures for a Plane Parabolic Shock	62
4.8	Body Supporting an Axisymmetric Hyperbolic Shock	66
4.9	Drag Coefficient for an Axisymmetric Hyperbolic Shock. . .	69
4.10	Body Supporting a Plane Hyperbolic Shock	72
4.11	Body Pressure for a Plane Hyperbolic Shock	72
5.1	Illustration of the Shock Attachment	76
5.2	Location of the Nose for the Theoretical Body.	80

List of Illustrations (Continued)

5.3 Variation of f_1 and f_1^* with γ. 82

5.4 Variation of f_o and f_o^* with γ. 83

5.5 Shock Shape for a Circular Cylinder with a Pointed Hemispherical Nose (γ=7/5) 86

5.6 Shock Shape for a Circular Cylinder with a Pointed Hemispherical Nose (γ=5/3) 87

5.7 Shock Shape for a Circular Cylinder with a Conical Nose. . 88

5.8 Surface Pressure on a Circular Cylinder with a Pointed Hemispherical Nose (γ=5/3) 89

5.9 Surface Pressure on a Circular Cylinder with a Conical Nose 90

5.10 Shock Coordinates for a Circular Cylinder with a Modified Hemispherical Nose 91

5.11 Shock Coordinates for a Circular Cylinder with a Hemispherical Nose 92

5.12 Shock Coordinates for a Circular Cylinder with a 90° Conical Nose 93

5.13 Shock Coordinates for a Circular Cylinder with a Flat Nose 94

5.14 Surface Pressure on a Circular Cylinder with a Modified Hemispherical Nose 95

5.15 Surface Pressure on a Circular Cylinder with a Hemispherical Nose. 96

LIST OF ILLUSTRATIONS (Continued)

Figure		Page
5.16	Surface Pressure on a Circular Cylinder with a 90° Conical Nose	97
5.17	Surface Pressure on a Circular Cylinder with a Flat Nose	98
5.18	Shock Coordinates for a Flat Leading-Edge Plate in Helium	100
5.19	Shock Coordinates for a Flat-Plate with a Hemicylindrical Leading-Edge	101
5.20	Shock Coordinates for a Flat Leading-Edge Plate in Air	102
5.21	The Slender Cone-Cylinder	103
5.22	Comparison of Shock Shapes for a Slender Cone-Cylinder	105
6.1	Variation of the Shock Power-Law Exponent for Axisymmetric Bodies	109
6.2	Variation of the Shock Power-Law Exponent for Planar Bodies	110
6.3	Comparison of the Variation of n_s with n_b Between the Present Theory and Experiments (j=1)	112
6.4	Comparison of the Variation of n_s with n_b Between the Present Theory and Experiments (j=0)	113

NOMENCLATURE

The following nomenclature is used throughout this work unless noted otherwise.

a	$(\gamma p/\rho)^{\frac{1}{2}}$, isentropic speed of sound
A	parameter used in shock shapes, see Eqs. (4.1), (4.30), (4.40)
b	δ/β
B	parameter used in shock shapes, see Eqs. (4.30), (4.40)
C	$V_b(0)H(0)^{1/\gamma}$, constant of integration, see Eq. (2.18)
C_D	$D/(\frac{1}{2}\rho_\infty v_\infty^2 s)$, drag coefficient
Cp	$p/(\frac{\gamma}{2} p_\infty M_\infty^2)$, pressure coefficient
d	body diameter or thickness
$D(t)$ $D(x)$	drag force to time t, or up to a station x
$\hat{e}$	unit vector, see Fig. (2.2c)
$\bar{E}$	energy per unit length (j=1), or per unit area (j=0) added instantaneously by a blunt nose
e	$p/[(\gamma-1)\rho]$, specific internal energy
G	function, see Eq. (2.16)
H	function, see Eq. (2.16)
$\bar{I}$	momentum per unit length (j=1), or per unit area (j=0) added instantaneously by a blunt nose
j	0,1 for the planar or axisymmetric case, respectively
K_δ	$M_\infty\delta$, hypersonic similarity parameter

K_j, K_{j+2}	constants of integration, see Eqs. (2.24), (2.26), (5.2)
ℓ	parameter, see Eq. (3.14); body length
M	v/a, Mach number
n	power-law exponent; parameter, see Eq. (3.16)
$\hat{n}$	unit outward normal vector from the surface under consideration
p	pressure
p''	pressure between layer Δr and body; assumed equal to p_b
r(x)	radius or half thickness in the physical plane
r_o	initial contribution to the body radius or thickness as a result of the blunt nose, see Eq. (4.7)
R(t)	radius or half thickness in the equivalent plane
$\bar{r}$	r/d; also r/B, see Eq. (4.40)
r'	d/dx(r)
r''	$d^2/dx^2(r)$
s	$2(\pi R_s)^j$, shock surface area in the equivalent plane
t	x/v_∞, time
$\bar{v}$	velocity
v_2	speed of gas particles in the shock layer, see Eq. (2.9)
V(t),V(x)	volume per unit length (j=1), or per unit area (j=0)
W	$(8B^2/A^4)r^2$
W_x	$(8B^2/A^2)x$
x	axial coordinate
x_o	position on x-axis when $r=r_o$, see Eq. (4.3)
β	characteristic value of the shock slope; semivertex angle of a conical shock

γ	Cp/Cv, specific heat ratio for a perfect gas
δ	characteristic value of the body slope; semivertex angle of a conical body
Δr	thin gas layer adjacent to shock, see Fig. (2.2)
ε	$(\gamma-1)/(\gamma+1)$, limiting density ratio across a normal shock
ζ_{j+1}	parameter for power-law body shapes, see Eq. (4.6)
ρ	gas density
$\sum$	surface surrounding an arbitrary region of gas, see Fig. (2.2)
τ	thickness ratio
ω	parameter used in shock shapes, see Eq. (3.8)

Subscripts

∞	free stream condition
b	body surface
s	shock surface
N	nose of body

Mathematical Symbols

$\frac{D}{Dt}( )$	substantial or Eulerian derivative
$\simeq$	approximately equal to
$\sim$	asymptotically equal to
$d\tau$	differential volume
$\dot{( )}$	derivative of quantity with respect to time

AN INTEGRAL APPROXIMATION FOR SHOCK SHAPES OVER SLENDER BODIES IN INVISCID HYPERSONIC FLOW

CHAPTER I

INTRODUCTION

The treatment of hypersonic flows over slender bodies has been the subject of many papers over the past twenty-five years. Some of the earliest works in this area are attributed to Guderly [1], Hayes [2], Sedov [3], and Tsien [4]. From these contributions the ideas of "hypersonic similitude" and the "equivalence principle" have been formulated.

Similarity solutions for the unsteady constant-energy flow behind the spherical blast-wave were first treated by Sedov [5] and Taylor [6]. Subsequently, solutions of the hypersonic flow equations over slender bodies were obtained by Bam-Zelikovich *et al.* [7] and Goldsworthy [8]. However, a more general treatment was accomplished in 1954 by Van Dyke [9] and the concept of "hypersonic small disturbance theory" was formalized. Van Dyke's approach facilitated the solution of the steady-state equations for hypersonic flow. In his development expansions for large Mach number, $M_\infty >> 1$, and small characteristic body slope, $\delta << 1$, were made such that the combination $M_\infty \delta$ was a constant.

Thus, the two-dimensional steady hypersonic flow problem was reduced to the simpler, yet still complex, problem of one-dimensional unsteady flow. About this time Sakurai [10,11] studied the constant-energy or "blast-wave" problem by removing the condition of strong shocks and, independently, Lin [12] obtained a solution for the cylindrical blast-wave.

In a study published in 1956, Cheng and Pallone [13] accounted for nose bluntness effects on the downstream flow within the framework of hypersonic small disturbance theory. Following this work Lees and Kubota [14] studied the self-similar flows over blunt-nosed slender bodies. These theories demonstrated that the flow over a flat-plate or circular cylinder was analogous to the constant-energy planar and cylindrical problem, and also, that the nose drag of these bodies is related to the instantaneous energy released in the constant-energy problem. Along these same lines Chernyi [15] and Cheng *et al.* [16] developed integral methods for the solution of hypersonic flow past slender blunted bodies. Their analyses were accomplished within the restrictions of small disturbance theory and the approximation of a thin shock-layer.

Unfortunately, the blast-wave analogy and similarity solutions do not provide an uniformly valid solution throughout the flow field. They fail near the nose since the body slope is not small and in a layer near the body surface referred to as the "entropy layer". The entropy layer arises because the changes in entropy and temperature, caused by the nose bluntness and propagated along the streamlines

wetting the body, are lower than the entropy and temperature predicted by the small-disturbance solutions. To overcome this limitation Sychev [17] studied the inverse problem by determining the body that produces the outer small-disturbance flow associated with a blast-wave. He chose a parabolic shock shape and, accounting for the finite entropy change across the shock, numerically calculated a body shape which he found to grow asymptotically.

Guiraud [18] had pointed out that the entropy-layer is a region of non-uniformity characteristic of singular perturbation problems and could be treated with the method of "inner and outer expansions". In 1962 Yakura [19] successfully solved the same problem investigated by Sychev with an expansion procedure, that is, matched asymptotic expansions. Yakura was able to obtain an "outer" expansion valid in the shock layer, but outside of the entropy layer, and an "inner" solution valid in the entropy layer. By means of a proper matching of the two expansions, an uniformily valid solution was found

Prior and subsequent to Yakura's work, there have been a number of expansion techniques applied to the direct problem, notably, Freeman [20,21], Vaglio-Laurin [22], Guiraud [23], and Guiraud *et al.* [24]. Common to all of these approaches is a difficulty in the matching procedure requiring a certain integral to vanish. Since the integral could not be proven to vanish theoretically, disagreement arose over whether it could be assumed to vanish. Stewartson and Thompson [25] were able to show numerically that the integral in question is indistinguishable from zero, but the non-vanishing of other terms still leaves some doubt as to the validity of the matching procedure

Recently an uniformly valid solution for the inviscid hypersonic flow past blunted bodies has been accomplished by Schneider [26] for the inverse problem. He obtained an analytical solution for the flow quantities in quadrature form. Contrary to Yakura's approach, Schneider's success is a result of judicious choices for the order of magnitude of pertinent flow quantities, rather than on a systematic expansion procedure. Although the works mentioned in this brief historical sketch enable simplification of the solutions for the hypersonic flow over slender bodies they are by no means "simple" solutions. Only in a few cases can the shock shapes, pressure distributions, etc., be obtained explicitly in terms of known parameters, e.g., Chernyi [27]. The purpose of this study is to develop an approximate method that yields simple analytical solutions for the shock shapes over slender bodies in hypersonic flow. To accomplish this we shall initially follow the integral approach of Chernyi [15,28] and treat, in general, the inverse problem.

In Chapter II the governing equations for the flow over a slender body are developed in terms of the equivalence principle of Hayes [2]. These equations written in integral form have been presented by Chernyi [15,28]. A general solution for the body shape in terms of the specified shock shape is then obtained in quadrature form. By means of the same fundamental equations, a solution for a particular direct problem is obtained, that is, the shock shape for the non-growing body. Physically this represents the shock supported by a circular cylinder or flat-plate. In addition, general equations for the pressure distribution

and drag are developed which are applicable to both the direct and inverse problems.

Chapters III and IV deal with applications of the inverse problem. In Chapter III conical and ogival shocks are specified. The resulting body shapes are found to be cones, wedges, and ogives. In addition, the pressure distributions are presented in terms of the shock shapes. Chapter IV is a treatment of the body shapes supporting power-law and hyperbolic shocks, as well as the associated pressure distributions. We find that these bodies are blunted and, generally, not similar to the shock shape.

Chapters V and VI are devoted to applications of the general solution for the non-growing body and an interpretation of the variation in body shape with power-law exponent. In Chapter V constant radius and constant thickness bodies with varying nose bluntness are specified, and the shock shapes and related pressure distributions are determined. Chapter VI deals with an interpretation of the variation of n_b with n_s, where n is the power-law exponent, for slender blunted bodies supporting power-law shocks. The range $0 \leq n_b \leq 1$ is considered, and comparisons with other theories and experiments are made.

Although there are a large number of theories dealing with the hypersonic flow over slender bodies, the number of related experiments are limited. Comparisons among the present theory, other theories, and experiments are made where possible in Chapters III-VI. Further discussions of these topics can be found in references [28-34].

CHAPTER II

THEORETICAL DEVELOPMENT

Fundamental Concepts

A supersonic flow in which the free stream Mach number M_∞ is sufficiently high that linearized theory is inadequate for describing its essential features, is called hypersonic flow. Throughout this paper we shall be concerned with the inviscid hypersonic flow of a perfect gas past slender bodies. Consequently, the basic equations will be developed within the framework of hypersonic small disturbance theory and the equivalence principle.

Small disturbance theory is that portion of hypersonic flow theory which is applicable to slender bodies. The slenderness of the bodies is described in terms of the parameter δ which we designate as a characteristic body slope. All bodies are considered to be at zero angle of inclination. The inviscid hypersonic small disturbance assumptions pertinent to the present development are:

(1) $M_\infty >> 1$

(2) $\delta << 1$

(3) $M_\infty \delta >> 1$

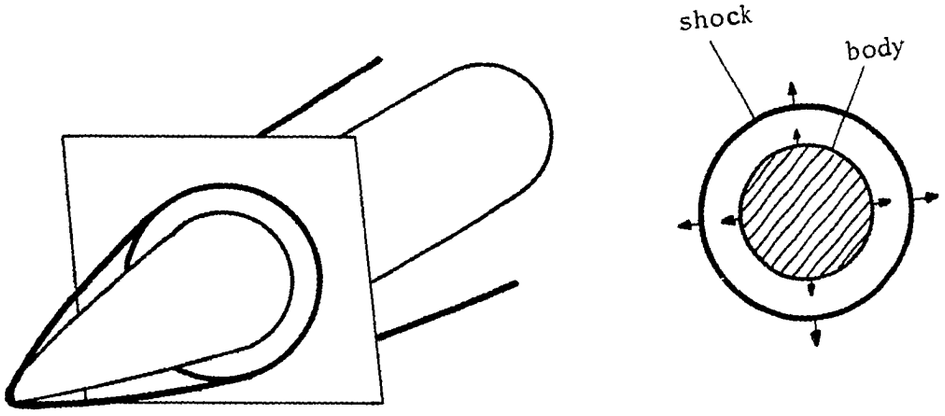
(4) $\varepsilon << 1$

where $\varepsilon = (\gamma-1)/(\gamma+1)$ is the limiting density ratio across a normal shock.

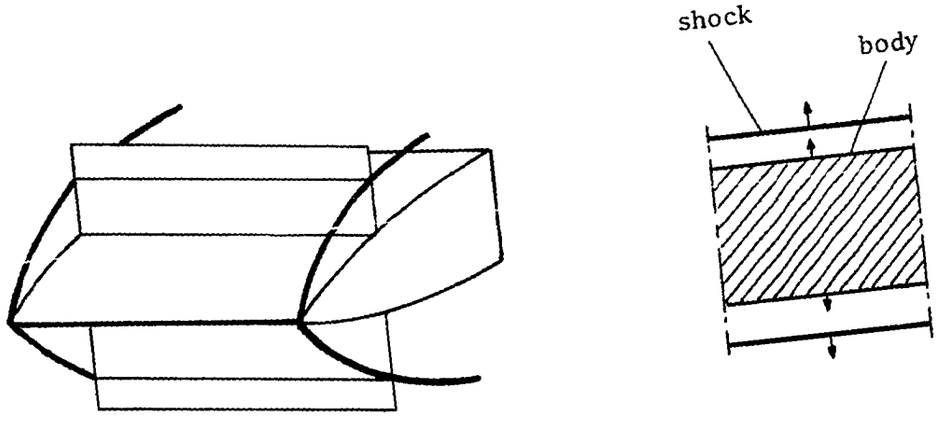
Assumption (1) is necessary for all hypersonic flow theories. Assumption (2) insures a slender body. Assumption (3) is the strong shock requirement. From this we define the hypersonic similarity parameter $K_\delta \equiv M_\infty \delta$. Assumption (4) involves the gas properties and insures a small density ratio. This assumption is also necessary for the thin shock layer approximation.

The equivalence principle of Hayes [2] can be stated quite simply with the aid of Fig. (2.1). Consider a plane section of initially undisturbed gas which is penetrated by a slender body. It is known that the gradients of the flow quantities normal to the plane are small compared with those parallel to the plane. Physically this means that the motion of the gas is essentially confined to the plane section and that motion out of the plane is negligible, that is, all gas motion is perpendicular to the longitudinal body axis. Thus, for our purposes, a statement of the equivalence principle is: the steady two-dimensional flow over an axisymmetric or planar body is equivalent to the one-dimensional unsteady motion in a plane section.

In the following sections we shall develop the equations of continuity, momentum, and energy for the unsteady problem. As illustrated in Fig. (2.1) we can view this motion as a body (or piston) and shock expanding in a plane. The axisymmetric case is used for the development of the basic equations; however, the final form of these equations enable applications to either axisymmetric (j=1) or planar (j=0) flows. In the equivalent plane the dependent variables are the shock radius or thickness R_s, body radius or thickness R_b, and the



(a) axisymmetric case



(b) planar case

Figure 2.1. Illustration of the equivalence principle.

pressure p; and the time t is the independent variable. In the physical plane the dependent variables are the shock radius or thickness r_s, the body radius or thickness r_b, and the pressure p; and the axial coordinate x is the independent variable. The transformation into physical coordinates is simply $t = x/v_\infty$. The symbols R and r will be used to designate both radius and thickness since it will be clear in each case whether the axisymmetric or planar problem is being considered.

Basic Equations

Conservation of Mass

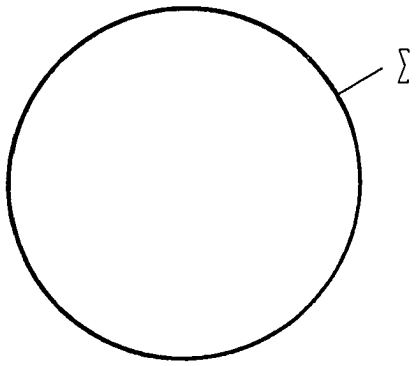
Consider an undisturbed, axisymmetric, plane section of gas confined by a fixed surface Σ, Fig. (2.2a), at some time $t<0$. At some later time $t>0$, a disturbance caused by the shock and body propagates outward, Fig. (2.2b). According to the law of conservation of mass, the total mass of gas within Σ must remain constant. As a result the substantial derivative of the mass at any time t must be

$$\frac{D}{Dt}\iiint_{\Sigma-b}\rho d\tau = 0 \ , \qquad (2.1)$$

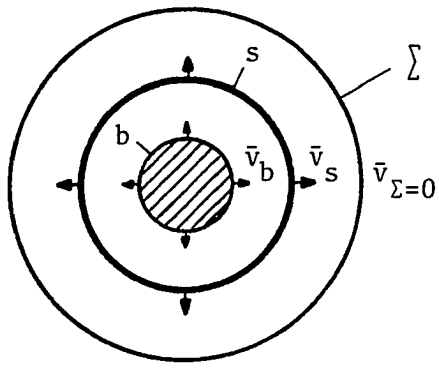
where ρ is the gas density and b(t) represents the boundary of the body. Equation (2.1) can be written in the form

$$\frac{D}{Dt}\iiint_{\Sigma-b}\rho d\tau = \frac{d}{dt}\iiint_{\Sigma-s}\rho d\tau + \frac{d}{dt}\iiint_{s-b}\rho d\tau \ ,$$

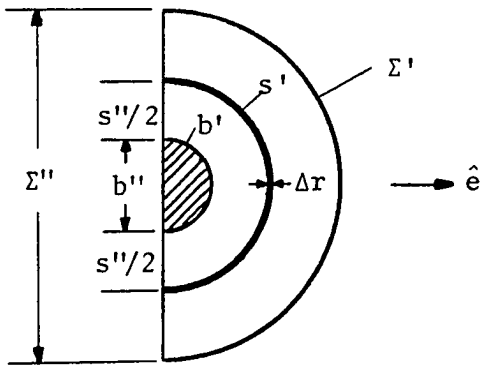
where s(t) is the surface area of the shock. It follows that



(a) $t < 0$



(b) $t > 0$



(c) $t > 0$

Figure 2.2. Equivalent plane terminology.

$$\frac{d}{dt}\iiint_{s-b} \rho d\tau = -\frac{d}{dt}\iiint_{\Sigma-s} \rho d\tau \ .$$

Since the density between Σ and the shock surface s(t) is constant ($\rho=\rho_\infty$), the application of Liebnitz's rule to the above equation yields

$$\frac{d}{dt}\iiint_{s-b} \rho d\tau = -\oiint_{\Sigma} \rho_\infty \bar{v}_\Sigma \cdot \hat{n} ds - \oiint_{s} \rho_\infty \bar{v}_s \cdot \hat{n} ds \ . \qquad (2.2)$$

In Eq. (2.2) $\hat{n}$ is a unit normal pointing outward from the region enclosed by the surface under consideration, $\bar{v}_s$ is the velocity of the shock surface, and $\bar{v}_\Sigma$ equals zero since Σ is stationary. Integration of Eq. (2.2) yields the total mass of the disturbed gas at time t as

$$\iiint_{s-b} \rho d\tau = \rho_\infty V_s \ , \qquad (2.3)$$

where $V_s = (2-j)\pi^j R_s^{j+1}$ is the "volume" of the shock in a plane section at time t.

Momentum Equation

Since the geometry of the gas and body motion is symmetric, the analysis can be simplified if we consider the momentum equation in a meridian plane to one side of the axis of symmetry as in Fig. (2.2c). The gas is inviscid, hence, the time rate of change of momentum of the gas must equal the sum of the hydrodynamic pressure forces. Expressed in integral form Newton's Second Law is

$$\frac{D}{Dt}\iiint_{\Sigma'-b'} \rho\bar{v}\cdot\hat{e}\,d\tau = -\oiint_{\Sigma'+\Sigma''} p\hat{n}ds\cdot\hat{e}\ , \qquad (2.4)$$

where $\hat{e}$ is a unit vector in the direction indicated in Fig. (2.2c). Equation (2.4) can be recast as

$$\frac{d}{dt}\iiint_{s'-b'} \rho\bar{v}\cdot\hat{e}\,d\tau = -\iint_{s'} p_\infty\hat{n}\cdot\hat{e}\ ds - \iint_{s''} p''\hat{n}\cdot\hat{e}ds - \iint_{b'} p_b\hat{n}\cdot\hat{e}\ ds$$

$$= -\iint_{s''+b''} p_\infty ds + \iint_{s''} p''ds + \iint_{b''} p_b ds\ ,$$

or, with a rearrangement of terms

$$\frac{d}{dt}\iiint_{s'-b'} \rho\bar{v}\cdot\hat{e}\,d\tau = \iint_{s''+b''} (p_b-p_\infty)ds + \iint_{s''} (p''-p_b)ds\ . \qquad (2.5)$$

Equation (2.5) can be further simplified with the following considerations. We have assumed that the gas is strongly compressed across the shock and as a result most of the gas in the disturbed region is concentrated in a thin layer close to the shock. Most of the pressure change occurs near the shock, whereas in the rest of the shock layer the pressure change is small. Thus, we shall assume that the thin layer next to the shock (Δr) contains all of the gas, that Δr is negligibly small, and that pressure changes between this layer and the body can be neglected.

The above assumptions allow us to write the integral on the left-hand side of Eq. (2.5) in the form

$$\iiint_{s'-b'} \rho\bar{v}\cdot\hat{e}d\tau = \iint_{s'} \rho_2 v_2 \Delta r\hat{n}ds\cdot\hat{e} \quad , \tag{2.6}$$

where ρ_2 and v_2 are the density and speed of the gas in the layer Δr. Furthermore, we note that

$$\iint_{s'} \rho_2 v_2 \Delta r\hat{n}ds\cdot\hat{e} = \rho_2 v_2 \Delta r \iint_{s'} \hat{n}ds\cdot\hat{e} \quad ,$$

but

$$\iint_{s'} \hat{n}ds\cdot\hat{e} = s/\pi \quad .$$

Therefore,

$$\iint_{s'} \rho_2 v_2 \Delta r\hat{n}ds\cdot\hat{e} = (\rho_2 v_2 \Delta r s)/\pi \quad ,$$

where $s = 2\pi R_s$ is the "surface-area" of the shock in the equivalent plane at time t. In the final result the "surface-area" of the shock for planar flow can be obtained from the formula $s = 2(\pi R_s)^j$.

The total mass of the gas in the layer Δr is given by $\rho_2(\Delta r)s$ and from the continuity equation is equal to $\rho_\infty V_s$. We can now recast Eq. (2.5) in the form

$$\frac{\rho_\infty}{\pi}\frac{d}{dt}(v_2 V_s) = \iint_{s''+b''} (p_b - p_\infty)ds + \iint_{s''} (p'' - p_b)ds \quad . \tag{2.7}$$

The right-hand side of Eq. (2.7) can be evaluated as follows:

$$\iint_{s''+b''} (p_b-p_\infty)ds = (p_b-p_\infty) \iint_{s''+b''} ds = \frac{s}{\pi} (p_b-p_\infty)$$

and

$$\iint_{s''} (p''-p_b)ds = (p''-p_b)\iint_{s''} ds = 2\Delta r(p''-p_b) \quad .$$

However, if we impose the assumption that Δr is negligibly small, the momentum equation takes the form

$$\rho_\infty \frac{d}{dt} (v_2 V_s) = (p_b-p_\infty)s \quad . \tag{2.8}$$

The term v_2 now represents the speed of all gas particles in the shock layer caused by the propagation of a normal shock into an ambient medium. In terms of the shock speed and the acoustic speed in the undisturbed medium v_2 can be expressed as

$$v_2 = \frac{2}{\gamma+1} (\dot{R}_s - a_\infty^2/\dot{R}_s) \quad . \tag{2.9}$$

Integration of Eq. (2.8) yields an equation for the total impulse added to the gas at time t as

$$\rho_\infty v_2 V_s = \int_{o^+}^{t} (p_b-p_\infty)sdt + \bar{I} \quad , \tag{2.10}$$

where $\bar{I}$ is the momentum per unit length or area added instantaneously by the blunt nose of an axisymmetric or planar body, respectively.

Conservation of Energy

We shall treat the inviscid, adiabatic flow of a perfect gas and neglect all body forces. With these assumptions the energy equation can be written in the form

$$\frac{D}{Dt}\iiint_{\Sigma-b}\rho(e+\bar{v}^2/2)d\tau = -\oiint_{\Sigma}p_\infty\bar{v}_\Sigma\cdot\hat{n}ds - \oiint_{b}p_b\bar{v}_b\cdot\hat{n}ds \quad . \tag{2.11}$$

Since $\bar{v}_\Sigma$ is equal to zero, and for a body of revolution or uniform plane surface p_b is a function of time only, Eq. (2.11) is recast as

$$\frac{D}{Dt}\iiint_{\Sigma-b}\rho(e+\bar{v}^2/2)d\tau = p_b\oiint_{b}v_b ds \quad .$$

The substantial derivative of the internal and kinetic energy can be expressed as

$$\frac{D}{Dt}\iiint_{\Sigma-b}\rho(e+\bar{v}^2/2)d\tau = \frac{d}{dt}\iiint_{\Sigma-s}\rho(e+\bar{v}^2/2)d\tau + \frac{d}{dt}\iiint_{s-b}\rho(e+\bar{v}^2/2)d\tau \quad .$$

In the region between Σ and the shock surface ρ is equal to ρ_∞, e is equal to e_∞, and $\bar{v}$ is equal to zero. Thus, the last two equations can be combined to read

$$p_b\oiint_{b}v_b ds = \rho_\infty e_\infty\frac{d}{dt}\iiint_{\Sigma-s}d\tau + \frac{d}{dt}\iiint_{s-b}\rho(e+\bar{v}^2/2)d\tau \quad .$$

We now note that

$$\rho_\infty e_\infty \frac{d}{dt} \iiint_{\Sigma-s} d\tau = - \rho_\infty e_\infty \frac{dV_s}{dt} \quad ,$$

$$p_b \oiint_b v_b ds = p_b \frac{dV_b}{dt}$$

and

$$e = \frac{1}{\gamma-1} \frac{p}{\rho} \quad .$$

Therefore, we have

$$\frac{d}{dt} \iiint_{s-b} \left(\frac{p}{\gamma-1} + \rho\frac{\bar{v}^2}{2}\right) d\tau = \frac{p_\infty}{\gamma-1} \frac{dV_s}{dt} + p_b \frac{dV_b}{dt} \quad . \tag{2.12}$$

Application of the thin shock layer assumption to Eq. (2.12) and subsequent integration yields

$$\frac{p_b}{\gamma-1} (V_s - V_b) + \frac{1}{2} \rho_\infty V_s v_2^2 = \frac{p_\infty}{\gamma-1} V_s + \int_{o^+}^{t} p_b \frac{dV_b}{dt} dt + \bar{E} \quad . \tag{2.13}$$

Equation (2.13) is the desired form of the energy equation. The constant of integration $\bar{E}$ is the energy per unit length or area, added instantaneously by the blunt nose of an axisymmetric or planar body, respectively. It is equivalent to the concentrated nose drag force D_N for axisymmetric bodies and the nose drag force per unit width for planar bodies.

Equations (2.10) and (2.13) are equivalent to those utilized by Cherni [27,28,35] in the application of unsteady motion to hypersonic

flow problems. In the following two sections we shall depart somewhat from Chernyi's approach. Equations (2.10) and (2.13) will be applied to obtain analytic solutions in quadrature form for the inverse problem and the direct problem for a non-growing body.

The Inverse Problem

In the inverse problem the shock shape is specified and the body shape is to be determined as part of the solution. The desired result is a quadrature solution for the body shape in terms of the shock parameters and γ. To accomplish this we differentiate Eq. (2.13), and replace the body pressure in the resulting expression with the use of Eq. (2.8). Subsequently, we obtain

$$\frac{1}{2}\rho_\infty \frac{d}{dt}(V_s v_2^2) + \frac{\rho_\infty}{\gamma-1}\frac{d}{dt}\left[\frac{V_s}{s}\frac{d}{dt}(V_s v_2)\right] - \frac{1}{\gamma-1}\frac{d}{dt}\left\{V_b\left[p_\infty + \frac{\rho_\infty}{s}\frac{d}{dt}(V_s v_2)\right]\right\} = \frac{dV_b}{dt}\left[p_\infty + \frac{\rho_\infty}{s}\frac{d}{dt}(V_s v_2)\right]. \tag{2.14}$$

A rearrangement of terms and use of the relation $\frac{\gamma p}{\rho} = a^2$ for the isentropic sound speed yields

$$\left[a_\infty^2 + \frac{\gamma}{s}\frac{d}{dt}(V_s v_2)\right]\frac{dV_b}{dt} + \frac{V_b}{\gamma}\frac{d}{dt}\left[a_\infty^2 + \frac{\gamma}{s}\frac{d}{dt}(V_s v_2)\right] = \frac{\gamma-1}{2}\frac{d}{dt}(V_s v_2^2) + \frac{d}{dt}\left[\frac{V_s}{s}\frac{d}{dt}(V_s v_2)\right]. \tag{2.15}$$

When we define the quantities

$$a_\infty^2 + \frac{\gamma}{s}\frac{d}{dt}(V_s v_2) \equiv H$$

and

$$\frac{\gamma-1}{2}\frac{d}{dt}(V_s v_2^2) + \frac{d}{dt}\left[\frac{V_s}{s}\frac{d}{dt}(V_s v_2)\right] \equiv G \,, \tag{2.16}$$

Eq. (2.15) can be recast in the form

$$H\frac{dV_b}{dt} + \frac{V_b}{\gamma}\frac{dH}{dt} = G$$

or

$$\frac{d}{dt}\left[H^{1/\gamma} V_b\right] = H^{\frac{1-\gamma}{\gamma}} G \,. \tag{2.17}$$

Integration of Eq. (2.17) yields

$$(2-j)\pi^j R_b^{\,j+1} = \frac{1}{H(t)^{1/\gamma}}\int_o^t \frac{G(t)}{H(t)^{(\gamma-1)/\gamma}}\,dt + \frac{C}{H(t)^{1/\gamma}} \tag{2.18a}$$

or, in physical coordinates with the application of the transformation $t = \frac{x}{V_\infty}$,

$$(2-j)\pi^j r_b^{\,j+1} = \frac{V_\infty^{-1}}{H(x)^{1/\gamma}}\int_o^x \frac{G(x)}{H(x)^{(\gamma-1)/\gamma}}\,dx + \frac{C}{H(x)^{1/\gamma}} \tag{2.18b}$$

where $C = H(0)^{1/\gamma} V_b(0)$.

Equation (2.18) is the general solution for the inverse problem. It will become apparent in Chapters III and IV that the first term on the right-hand side of Eq. (2.18) is an approximate form of the body shape obtained with the self-similar solutions. The second

term on the right-hand side is a result of the nose bluntness. We recall that in the momentum and energy equations the bluntness was accounted for by the instantaneous addition of momentum ($\bar{I}$) and energy ($\bar{E}$) at time equal to zero. To obtain Eq. (2.18) we differentiated and integrated a combined form of the momentum and energy equation. The constant of integration C is essentially a manifestation of the original initial conditions (i.e., nose bluntness). If the nose is pointed H(0) is a constant, but $V_b(0)$ is equal to zero. It follows that for pointed bodies C is equal to zero. For blunted bodies H(0) is infinite because r_s' is infinite at the origin and $V_b(0)$ is zero. Thus, strictly interpreted C is indeterminate for blunted bodies. However, in Chapter IV we shall develop an expression for $C/H^{1/\gamma}$ and demonstrate that this term can be treated as the entropy-displacement thickness.

The Direct Problem for the Non-Growing Body

In general a solution of the direct problem, that is, specification of the body shape and determination of the shock shape as part of the solution, does not lend itself to the technique used in the previous section. However, if we consider the case of the constant-radius or constant-thickness body, a solution similar to Eq. (2.18) can be obtained for the shock shape.

A constant-radius body in the unsteady problem is equivalent to the steady flow over a circular cylinder in the physical plane. We restrict our consideration to M_∞ equal to infinity or a_∞ equal to zero. For the axisymmetric case $V_s = \pi R_s^2$, $V_b = \pi R_b^2$, and $s = 2\pi R_s$, consequently

we write

$$H = \frac{\gamma}{\gamma+1} \frac{1}{R_s} \frac{d}{dt} (R_s^2 \dot{R}_s) \tag{2.19}$$

and

$$\frac{G}{\pi} = \frac{\gamma-1}{2} \left(\frac{2}{\gamma+1}\right)^2 \frac{d}{dt} (R_s^2 \dot{R}_s^2) + \frac{1}{\gamma+1} \frac{d}{dt} \left[R_s \frac{d}{dt} (R_s^2 \dot{R}_s)\right]. \tag{2.20}$$

The substitution of Eqs. (2.19) and (2.20) into (2.16) yields (with R_b = constant)

$$\frac{d}{dt} \left[\frac{R_b^2}{R_s} \frac{d}{dt} (R_s^2 \dot{R}_s) \right] =$$

$$2\varepsilon \frac{d}{dt} (R_s^2 \dot{R}_s^2) + \frac{d}{dt} \left[R_s \frac{d}{dt} (R_s^2 \dot{R}_s)\right],$$

where $\varepsilon = (\gamma-1)/(\gamma+1)$. Integration and rearrangement gives

$$\frac{R_s^2 - R_b^2}{R_s} \frac{d}{dt} (R_s^2 \dot{R}_s) + 2\varepsilon R_s^2 \dot{R}_s^2 = C_1 \quad ,$$

where C_1 is a constant of integration. Furthermore we write

$$\frac{d}{dt} = \dot{R}_s \frac{d}{dR_s}$$

and thus we have

$$\frac{R_s^2 - R_b^2}{R_s^2} \frac{1}{2R_s} \frac{d}{dR_s} (R_s^2 \dot{R}_s)^2 + 2\varepsilon \left(\frac{R_s^2 \dot{R}_s}{R_s}\right)^2 = C_1 \quad . \tag{2.21}$$

The following change of variables

$$\phi = (R_s^2 \dot{R}_s)^2$$

$$\eta = R_s^2$$

enables us to write Eq. (2.21) in the form

$$(\eta - R_b^2) \frac{d\phi}{d\eta} + 2\varepsilon\phi = C_1 \eta \ ,$$

which has the general solution

$$\phi = \frac{C_1}{2\varepsilon} \left[\eta - \frac{(\eta - R_b^2)}{2\varepsilon+1}\right] + C_2(\eta - R_b^2)^{-2\varepsilon} \ , \tag{2.22}$$

where C_2 is the second constant of integration. By replacing ϕ with our original variables and rearranging terms in Eq. (2.22) we obtain

$$\left(\frac{d\eta}{dt}\right)^2 = \frac{K_1'}{\eta} \left[\eta + \frac{R_b^2}{2\varepsilon}\right] + \frac{K_3'}{\eta} (\eta - R_b^2)^{-2\varepsilon} \ , \tag{2.23}$$

where K_1' and K_3' are constants. Integration of Eq. (2.23) yields

$$t = \frac{1}{K_1} \int_{R_{s1}}^{R_s} \frac{R^2 dR}{[R^2 + R_{b/2\varepsilon}^2 + K_3(R^2 - R_b^2)^{-2\varepsilon}]^{\frac{1}{2}}} \ . \tag{2.24}$$

Here K_1 and K_3 are constants of integration and R_{s1} is the shock radius at t_1, where t_1 is taken equal to zero.

A similar analysis can be performed for the constant thickness body which is equivalent to the steady flow over a flat plate in the physical plane. We again restrict our consideration to M_∞ equal to infinity.

In this case $V_s = 2R_s$, $V_b = 2R_b$ and $s = 2$. The analysis proceeds in the same manner as the axisymmetric problem with the final result

$$t = \frac{1}{K_o} \int_{R_{s1}}^{R_s} \frac{RdR}{[R+R_b/2\varepsilon+K_2(R-R_b)^{-2\varepsilon}]^{\frac{1}{2}}} , \qquad (2.25)$$

where K_o and K_2 are constants of integration.

Equations (2.24) and (2.25) describe the shock shapes for constant radius and constant thickness bodies, respectively. Evaluations of the constants K_j and K_{2+j} will be considered in Chapter V. Written in unified form Eqs. (2.24) and (2.25) become

$$t = \frac{1}{K_j} \int_{R_{s1}}^{R_s} \frac{R^{1+j}dR}{[R^{1+j}+R_{b/2\varepsilon}^{1+j}+K_{2+j}(R^{1+j}-R_b^{1+j})^{-2\varepsilon}]^{\frac{1}{2}}} . \qquad (2.26)$$

Pressure and Drag Equations

A general expression for the pressure on the body surface can be obtained by combining Eqs. (2.8) and (2.9). The result is

$$\frac{p_b-p_\infty}{\rho_\infty} = \frac{2}{\gamma+1} \frac{1}{s} \frac{d}{dt} [V_s(\dot{R}_s - \frac{a_\infty^2}{\dot{R}_s})] ,$$

and if the standard definition of the pressure coefficient is applied we obtain

$$C_{p_b} = \frac{4}{\gamma+1} \frac{1}{sv_\infty^2} \frac{d}{dt} [V_s(\dot{R}_s - \frac{a_\infty^2}{\dot{R}_s})] . \qquad (2.27)$$

Substitution of the appropriate values for V_s and s into Eq. (2.27) and differentiation enable us to present the pressure coefficient in the form

$$C_{p_b} = \frac{2(2-j)}{\gamma+1}\left\{\frac{1}{v_\infty^2}\left[(1+j)\dot{R}_s^2 + R_s\ddot{R}_s\right] + \frac{1}{M_\infty^2}\left(\frac{R_s\ddot{R}_s}{\dot{R}_s^2} - j-1\right)\right\} .$$

If we apply the transformation $t = x/v_\infty$, the pressure coefficient can be expressed as

$$C_{p_b} = \frac{2(2-j)}{\gamma+1}\left[(1+j)r_s'^2 + r_s r_s'' + \frac{1}{M_\infty^2}\left(\frac{r_s r_s''}{r_s'^2} - j-1\right)\right] . \qquad (2.28)$$

This expression is also presented by Hayes and Probstein [30, p. 360]. In the limit M_∞ equal to infinity, γ equal to unity, Eq. (2.28) reduces to

$$C_{p_b} = (2-j)\left[(1+j)r_s'^2 + r_s r_s''\right] , \qquad (2.29)$$

which is the slender-body Newton-Busemann result. Cole [36] obtained this equation by proceeding to the same limits in the small disturbance equations.

It was mentioned previously that the energy per unit length and per unit area in the unsteady problem can be thought of as the drag force and the drag force per unit width of axisymmetric and planar slender bodies in the physical plane. If we consider the steady integral conservation equations for mass, momentum and energy for the body depicted in Fig. (2.3), the drag up to a station x can be written as

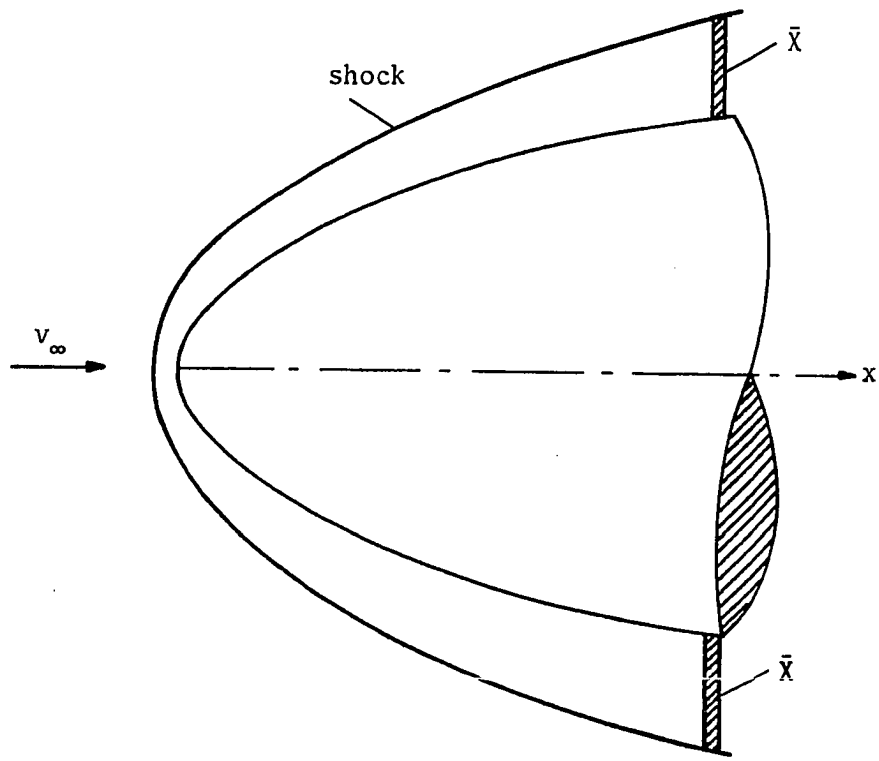


Figure 2.3. Terminology for slender body drag.

$$D(x) = \iint_{\bar{X}} \rho(e-e_\infty+v^2/2)ds \quad , \tag{2.30}$$

where $\bar{X}$ is a plane section between the shock and body. Equation (2.30), recast in terms of the equivalent plane variables (see Fig. 2.2), has the form

$$\begin{aligned} D(t) &= \iiint_{s-b} \rho(e-e_\infty+v^2/2)d\tau \ , \\ &= \frac{p_b}{\gamma-1}(V_s-V_b) + \frac{1}{2}\rho_\infty V_s v_2^2 - \frac{p_\infty V_s}{\gamma-1} \ . \end{aligned} \tag{2.31}$$

The above expression is equivalent to the last two terms in Eq. (2.13). Thus, we write for the total drag

$$D(t) = \bar{E} + \int_{0^+}^{t} p_b \frac{dV_b}{dt}\, dt \quad .$$

However, for applications, the most useful form for the drag is given by Eq. (2.31). The dependence on p_b can be removed with the substitution of the body pressure from Eq. (2.8) into Eq. (2.31). With this accomplished we have

$$D(t) = \frac{\rho_\infty}{\gamma-1}\left(\frac{V_s-V_b}{s}\right)\frac{d}{dt}(V_s v_2) + \frac{1}{2}\rho_\infty V_s v_2^2 - \frac{p_\infty V_b}{\gamma-1} \quad .$$

Furthermore, if the counterpressure is neglected and the transformation into physical coordinates is made, the drag expressed in unified form is

$$D(x) = \frac{\rho_\infty v_\infty^2 2^{2-j} \pi^j}{\gamma+1} \left\{ \frac{1}{\gamma-1} \frac{(r_s^{1+j} - r_b^{1+j})}{(2r_s)^j} \frac{d}{dx} \left[r_s' r_s^{1+j} \left(1 - \frac{1}{M_\infty^2 r_s'^2}\right)\right] \right.$$

$$\left. + \frac{r_s'^2 r_s^{1+j}}{\gamma+1} \left(1 - \frac{1}{M_\infty^2 r_s'^2}\right)^2 \right\}. \qquad (2.32)$$

Equation (2.32) is a general relation for the drag of slender bodies in hypersonic flow as a result of the hydrodynamic pressure forces.

CHAPTER III

POINTED SHOCKS

Generalities

In this chapter we shall consider pointed shocks that are conical or ogival. It is known that shocks of this type are supported by cones, wedges, and ogives. We shall not consider pointed shocks generated by more complicated body shapes.

Since the body is pointed the nose drag is zero and it follows that C is equal to zero in Eq. (2.18). Hence, for pointed shocks the body shape is given by the quadrature only.

The Conical Shock

Axisymmetric Case-Cone

In the physical plane the shock shape is specified as

$$r_s = \beta x \quad , \tag{3.1}$$

where β is the shock inclination. Substitution of Eq. (3.1) into the general expressions (2.16) for H and G yields

$$H = \frac{2\gamma}{\gamma+1} \beta^2 v_\infty^2 - \frac{\gamma-1}{\gamma+1} a_\infty^2 \ ,$$

and

$$G = \frac{1}{v_\infty} \frac{4\pi}{\gamma+1} (\beta^2 v_\infty^2 - a_\infty^2)(\frac{2\gamma}{\gamma+1} \beta^2 v_\infty^2 - \frac{\gamma-1}{\gamma+1} a_\infty^2) x \ .$$

If these functions are substituted into Eq. (2.18b) straight forward evaluation of the quadrature yields

$$r_b^2 = \frac{2}{\gamma+1} (\beta^2 - \frac{1}{M_\infty^2}) \ x^2 \ . \qquad (3.2)$$

Thus the body shape for a conical shock is a cone, and if we define the body inclination δ as

$$\delta^2 \equiv \frac{2}{\gamma+1} (\beta^2 - \frac{1}{M_\infty^2}) \ ,$$

then the ratio of the shock radius to body radius is

$$\frac{\beta}{\delta} = (\frac{\gamma+1}{2} + \frac{1}{K_\delta^2})^{\frac{1}{2}} \ . \qquad (3.3)$$

In the limit K_δ equal to infinity Eq. (3.3) has the form

$$\frac{\beta}{\delta} = (\frac{\gamma+1}{2})^{\frac{1}{2}} \ , \qquad K_\delta = \infty \ .$$

Rasmussen [37] obtained Eq. (3.3) as part of an approximate solution of the hypersonic small disturbance form of the stream-function equation for the flow past a cone at zero angle of incidence. This expression also agrees with the asymptotic relation given by Chernyi [28, p. 227] for a cone with slight nose bluntness. Also, Eq. (3.3) agrees well with the exact computations of Sims [38] for small cone angles and large Mach numbers.

To obtain the pressure distribution on the surface of the cone we substitute Eq. (3.1) and its derivatives into Eq. (2.28) and get

$$C_{p_b}/\delta^2 = 2 \quad . \tag{3.4}$$

The pressure on the surface of a cone given by Eq. (3.4) is a good approximation only for values of γ near unity and for very large Mach numbers. This result is not unexpected because in the development of Eq. (2.28) the pressure was assumed constant between the shock and body. However, for a cone this is only approximately true since the pressure actually increases somewhat from the shock to the body. Thus, Eq. (3.4) is the first approximation to the pressure given by the small disturbance equations and is correct in the Newtonian limit γ equal to unity, M_∞ equal to infinity.

Planar Case-Wedge

The shock shape is again given by Eq. (3.1), but for the plane shock we have

$$H = \frac{2\gamma}{\gamma+1}\beta^2 v_\infty^2 - \frac{\gamma-1}{\gamma+1}a_\infty^2 \quad ,$$

and

$$G = \frac{4}{\gamma+1}\frac{v_\infty}{\beta}\left(\beta^2 - \frac{1}{M_\infty^2}\right)\left(\frac{2\gamma}{\gamma+1}\beta^2 v_\infty^2 - \frac{\gamma-1}{\gamma+1}a_\infty^2\right) \quad .$$

Substitution of these expressions into Eq. (2.18b) and subsequent integration yields

$$r_b = \frac{2}{\gamma+1}\frac{1}{\beta}\left(\beta^2 - \frac{1}{M_\infty^2}\right)x \quad . \tag{3.5a}$$

We define δ as

$$\delta = \frac{2}{\gamma+1}\frac{1}{\beta}\left(\beta^2 - \frac{1}{M_\infty^2}\right) \quad , \tag{3.5b}$$

and, keeping only the physically relevant solution, we obtain for the ratio of shock and body angle

$$\frac{\beta}{\delta} = \frac{\gamma+1}{4} + \left[\left(\frac{\gamma+1}{4}\right)^2 + \frac{1}{K_\delta^2}\right]^{\frac{1}{2}} \quad . \tag{3.6}$$

In the limit K_δ equal to infinity Eq. (3.6) has the form

$$\frac{\beta}{\delta} = \frac{\gamma+1}{2} \quad , \qquad K_\delta = \infty \quad .$$

Equation (3.6) is recognized as the result obtained by Van Dyke [9, p. 8] from a solution of the hypersonic small disturbance equations, and is originally due to Linnell [39]. Chernyi [28, p. 80] shows that this result follows from an application of the equivalence principle to the flow over a wedge. Also Eq. (3.6) follows directly by applying the hypersonic small disturbance assumption to the oblique shock relations.

The pressure on the surface of a wedge is found by inserting Eq. (3.1) into Eq. (2.28) with j equal to zero. The result is

$$\frac{C_{pb}}{\delta^2} = \frac{\gamma+1}{2} + \left[\left(\frac{\gamma+1}{2}\right)^2 + \frac{4}{K_\delta^2}\right]^{\frac{1}{2}} \quad . \tag{3.7}$$

We find that Eq. (3.7) agrees exactly with the small disturbance result obtained by Van Dyke (9, p.8]. This is not surprising since for a wedge

the pressure is constant between the shock and body, which is what we assumed in developing Eq. (2.28).

The Ogival Shock

Axisymmetric Case-Ogive of Revolution

In a manner similar to that used by Van Dyke [9], we shall specify the shock shape as a power series expansion about the cone as follows:

$$r_s = \beta x(1 + \lambda x + \omega x^2 + \ldots) \quad . \tag{3.8}$$

Here β is the initial shock slope and λ and ω are parameters determined by a particular shape.

Substitution of (3.8) into (2.16) and expansion for small x yields the following expressions for H and G:

$$H = H_0(1 + H_1 x + H_2 x^2 + \ldots) \quad , \tag{3.9}$$

$$G = \frac{4\pi}{v_\infty(\gamma+1)} (\beta^2 v_\infty^2 - a_\infty^2) H_0 x(1 + G_1 x + G_2 x^2 + \ldots) \quad . \tag{3.10}$$

Expressions for H_0, H_1, H_2, G_1, and G_2 can be found in Appendix A.

Equations (3.9) and (3.10) are now substituted into Eq. (2.18b). Although the algebraic process is tedious, expansion for small x, integration, and manipulation yield the result

$$r_b = \delta x[1 + A_1 \lambda x + (B_1 \omega + C_1 \lambda^2) x^2 + \ldots] \quad , \tag{3.11}$$

where δ is the initial body slope, given in terms of β by (3.5b). Relations for the parameters A_1, B_1, and C_1 are listed in appendix B.

Van Dyke [9, pp. 14-16] obtained an approximate shock shape for the ogive of revolution by a numerical solution of the small disturbance equations. He specified the body shape as

$$r_b = \tau b[x + \frac{1}{2}\frac{c}{b}x^2 + \frac{1}{6}\frac{d}{b}x^3 + \ldots]$$

and the corresponding shock wave as

$$r_s = \tau[x + \frac{1}{2}\ell c\, x^2 + \frac{1}{6}(md+nc^2)x^3 + \ldots] \ .$$

A comparison between our equations and those of Van Dyke can be made if we let

$$\tau = \beta \ , \tag{3.12}$$

$$b = \frac{\delta}{\beta} \ , \tag{3.13}$$

$$\ell = \frac{1}{A_1 b} \tag{3.14}$$

$$m = \frac{1}{B_1 b} \ , \tag{3.15}$$

$$n = \frac{-3C_i}{2B_1(A_1 b)^2} \ , \tag{3.16}$$

where ℓ is the curvature ratio between the shock and body, and m and n are parameters that relate the shock shape to the body shape. Several values of ℓ, m, and n vs. K_δ computed by Van Dyke are shown in Figs. (3.1-3.3) along with the plots of Eqs. (3.14-3.16). The present theory appears to be in reasonably good agreement with small disturbance theory for all values of m and n. In Fig. (3.3) there is a notable discrepancy

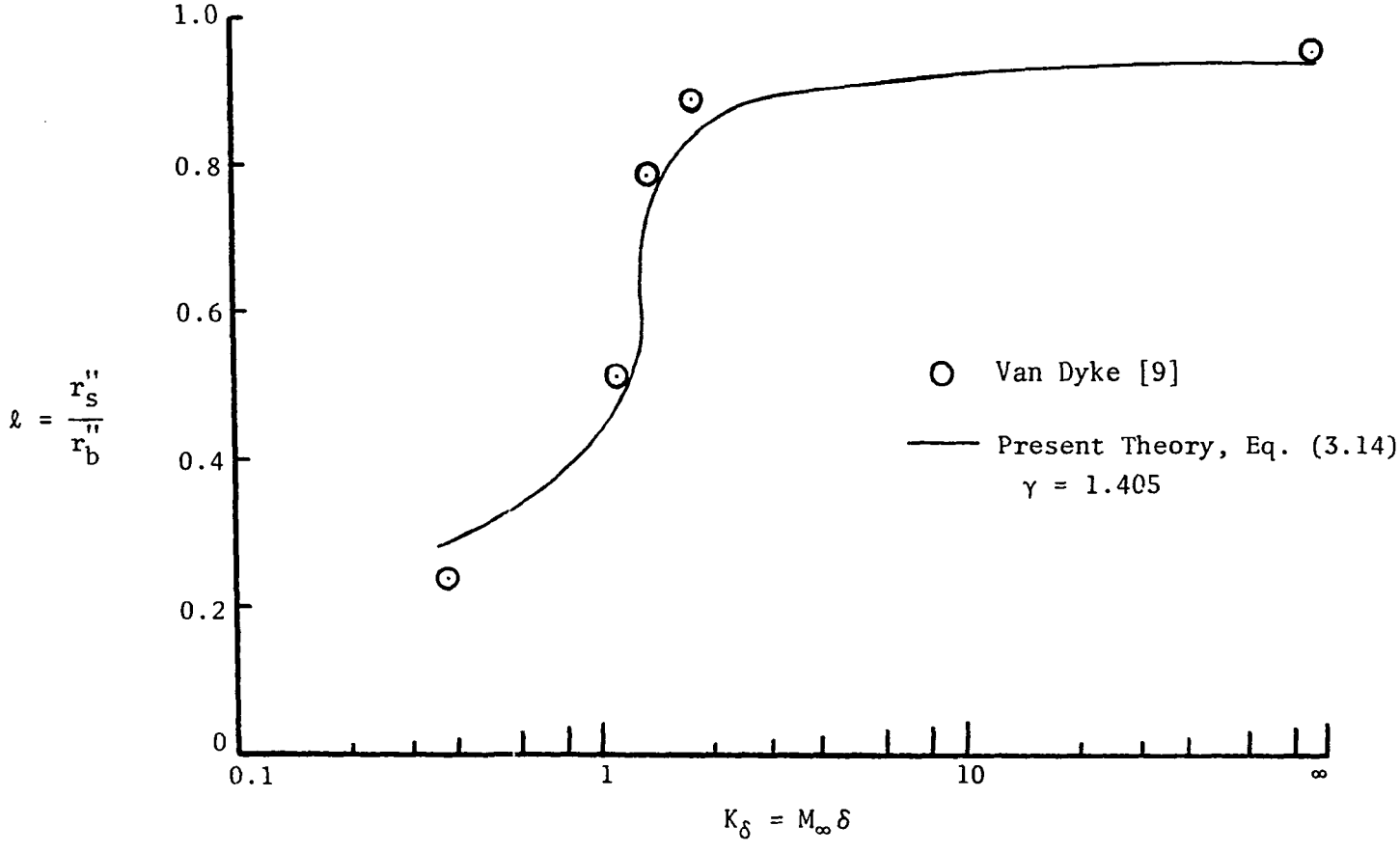


Figure 3.1. Curvature ratio for the ogive of revolution.

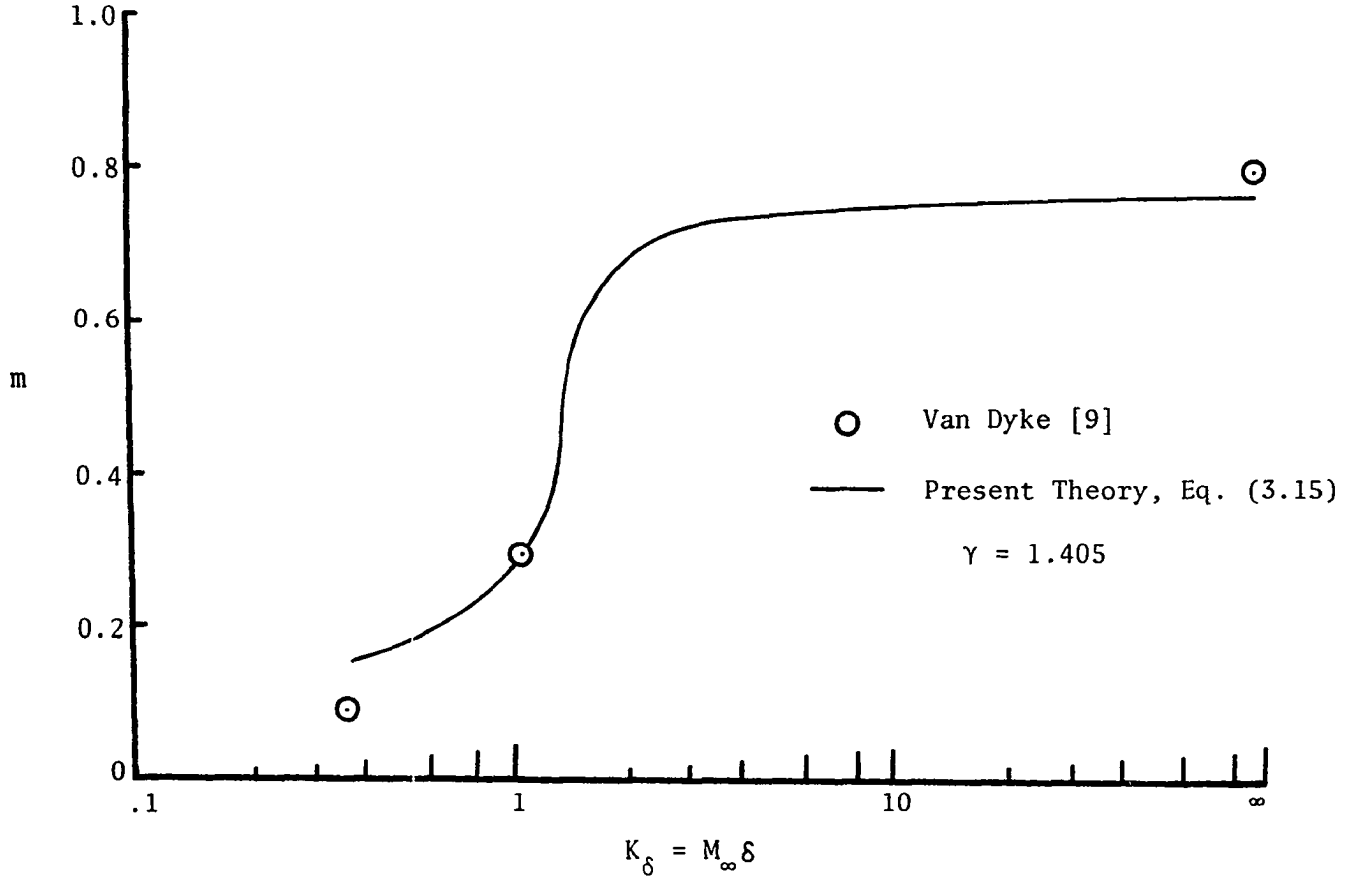


Figure 3.2. Variation of m with K_δ for the ogive of revolution.

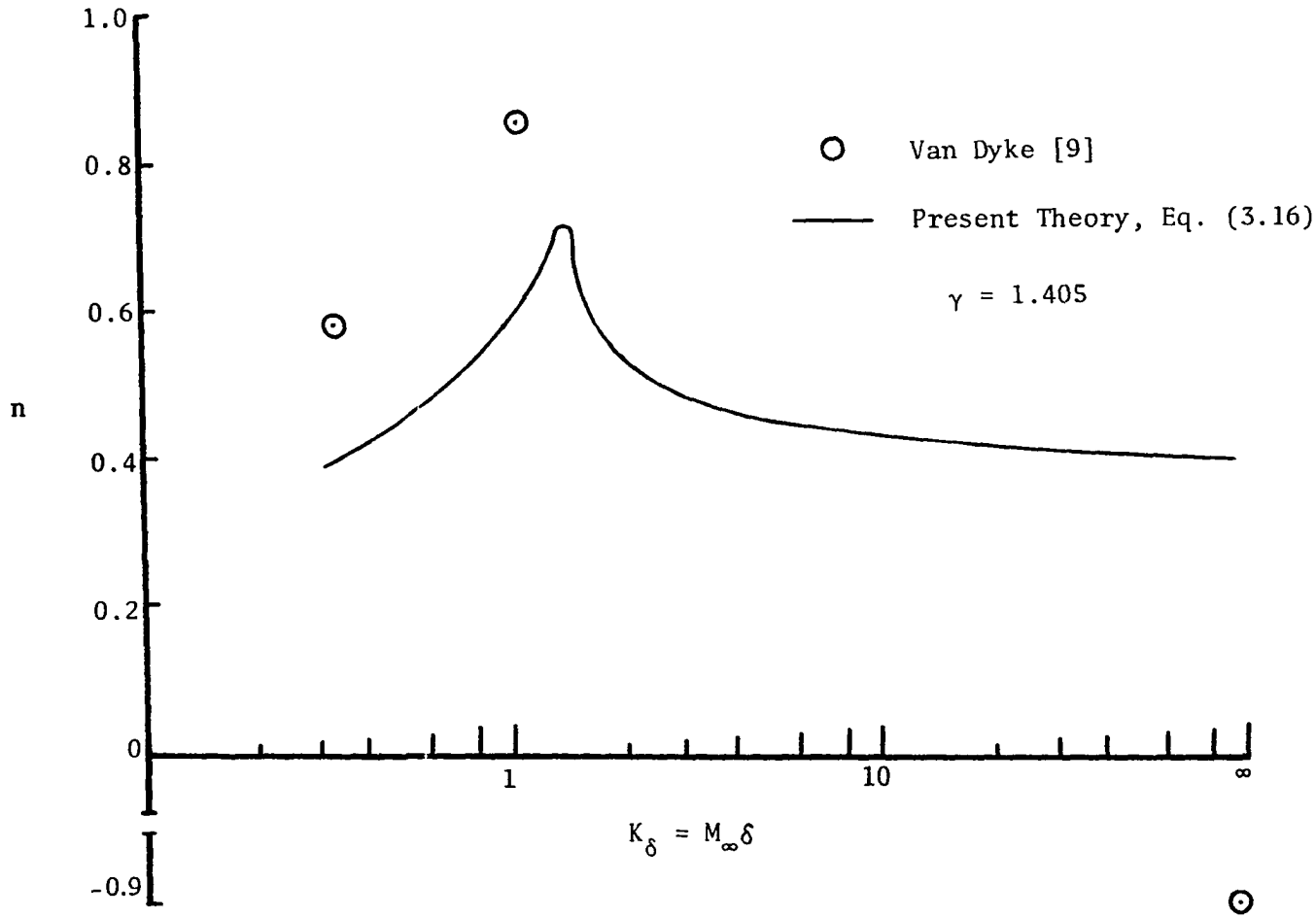


Figure 3.3. Variation of n with K_δ for the ogive or revolution.

in the values for n in the limit K_δ equal to infinity. This could indicate a limitation on the present theory for large K_δ. However, Van Dyke noted that the greatest numerical error in his computations was expected for this case.

When we describe the shock and body given by Eqs. (3.8) and (3.11) as

$$r_s = \bar{r}_o' x + \frac{\bar{r}_o''}{2} x^2 + \frac{\bar{r}_o'''}{6} x^3 + \ldots$$

and

$$r_b = r_o' x + \frac{r_o''}{2} x^2 + \frac{r_o'''}{6} x^3 + \ldots$$

the first two terms of the pressure coefficient, also expressed as a power series expansion, are given by

$$C_{pb} = r_o'^2 \left(\frac{C_p}{r_o'^2}\right) + r_o' r_o'' \left[\frac{\partial C_p}{\partial (r_o' r_o'' x)}\right] x + \ldots .$$

With the aid of Eq. (2.28) and the shock and body equations, the initial surface pressure coefficient and initial pressure gradient can be found.

The initial pressure coefficient is

$$C_{pb}/r_o'^2 = 2 \quad ,$$

which is the value expected since the body shape as x approaches the origin is conical. Thus the surface pressure should be identical to the value we obtained for a cone with a slope r_o'. The initial pressure gradient is found to be

$$\frac{\partial C_p}{\partial (r_o' r_o'' x)} = \frac{2}{\gamma+1} \frac{1}{A_1} \left[\frac{5}{2} (\gamma+1) + \frac{6}{K_\delta^2} \right] \quad . \tag{3.17}$$

A plot of Eq. (3.17) is compared with the small disturbance results of Van Dyke in Fig. (3.4). For values of K_δ near unity the agreement is not good. As K_δ increases the agreement improves and for K_δ equal to infinity and γ equal to 1.405, the pressure gradient from Eq. (3.17) is 4.3 compared to 4.93 given by Van Dyke. Also shown are the limiting values given by the cone-expansion and tangent-cone methods.

In the limit γ equal to unity, M_∞ equal to infinity, Eq. (3.17) yields

$$\frac{\partial C_p}{\partial (r_o' r_o'' x)} = 5.0 \quad ,$$

which is the Newton-Busemann, or Newtonian plus centrifugal result.

Planar Case-Plane Ogive

Following the approach for the ogive of revolution, we specify a two term expansion about the wedge as follows:

$$r_s = \beta x(1 + \lambda x + \ldots) \quad , \tag{3.18}$$

where β is the initial shock slope and λ is a parameter determined by a particular shape.

The functions H and G can be expressed as

$$H = H_0(1 + H_1 x + \ldots) \quad , \tag{3.19}$$

$$G = \frac{2}{\gamma+1} \frac{(\beta^2 v_\infty^2 - a_\infty^2)}{\beta v_\infty} H_0(1 + G_1 x + \ldots) \quad , \tag{3.20}$$

where

$$H_0 = a_\infty^2 + \frac{2\gamma}{\gamma+1} (\beta^2 v_\infty^2 - a_\infty^2) \quad ,$$

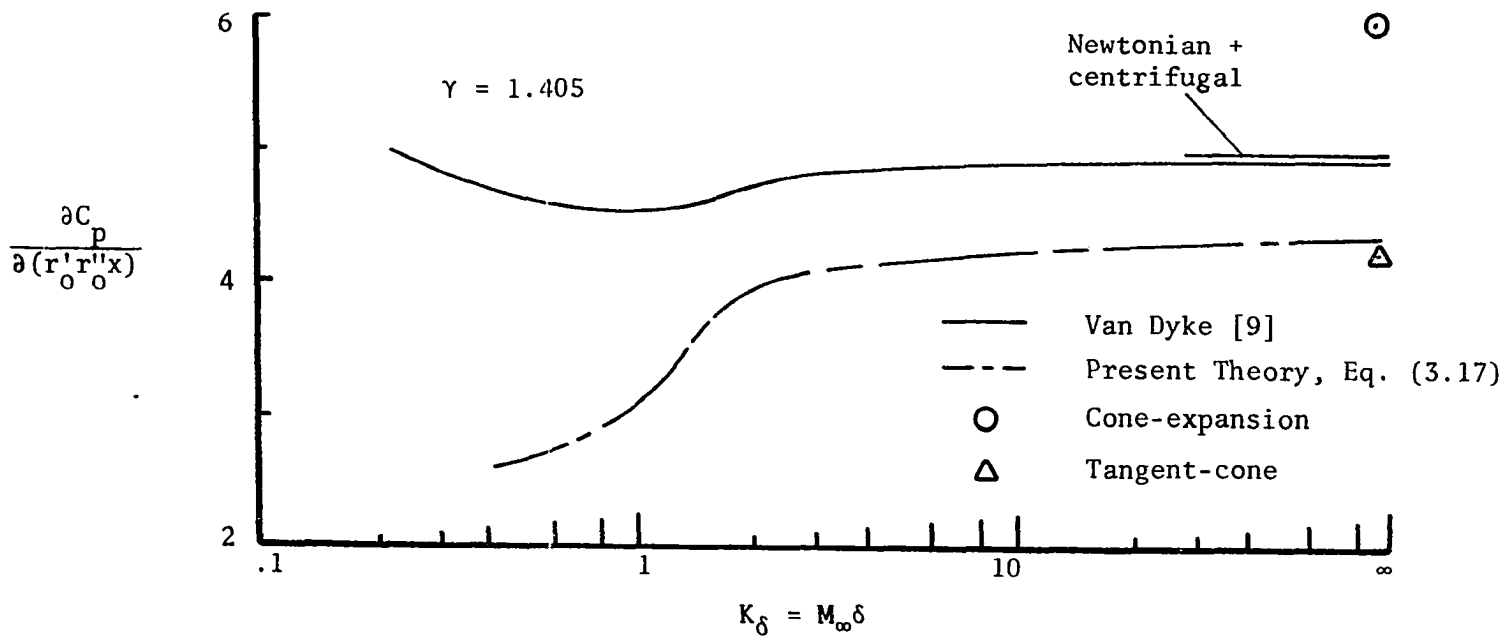


Figure 3.4. Initial pressure gradient on the ogive of revolution.

$$H_1 = \frac{4\gamma}{\gamma+1}\frac{\lambda}{H_0}(3\beta^2 v_\infty^2 + a_\infty^2) \quad ,$$

$$G_1 = \frac{2\lambda}{H_0}\left[\varepsilon(5\beta^2 v_\infty^2 + 3a_\infty^2) + \frac{\beta^2 v_\infty^2(7\beta^2 v_\infty^2 + a_\infty^2)}{\beta^2 - a_\infty^2}\right] \quad .$$

After Eqs. (3.19) and (3.20) are substituted into Eq. (2.18b) and expansion for small x and integration is performed, the body can be expressed as

$$r_b = \delta x(1 + A_1 \lambda x + \ldots) \quad , \tag{3.21}$$

where δ is the initial body slope given by (3.5b). The parameter A_1 for the plane ogive is

$$A_1 = \frac{2[2(3\gamma-2)K_\beta^4 + (3\gamma+7)K_\beta^2 + 5-\gamma]}{(1+\gamma K_\beta K_\delta)(\gamma+1)^2 K_\beta K_\delta}$$

where

$$K_\beta = \frac{\gamma+1}{4}K_\delta + \left[\left(\frac{\gamma+1}{4}\right)^2 K_\delta^2 + 1\right]^{\frac{1}{2}} ; \qquad K_\beta \equiv M_\infty \beta \quad .$$

In a manner analogous to that for the ogive of revolution, Van Dyke specified the body for the plane ogive as

$$r_b = \tau b\left(x + \frac{1}{2}\frac{c}{b}x^2 + \ldots\right)$$

and the corresponding shock wave as

$$r_s = \tau\left(x + \frac{1}{2}\ell c\, x^2 + \ldots\right) \quad .$$

A comparison between our equations and those of Van Dyke can be made by referring to Eqs. (3.12-14). The curvature ratio ℓ is plotted in Fig. (3.5). This present theory agrees well with the small disturbance results for most values of K_δ, although agreement is noticeably better for $K_\delta >> 1$.

The pressure coefficient can be expressed as a two term series expansion

$$C_{p_b} = r_o'^2 \left(\frac{C_p}{r_o'^2} \right) + r_o' r_o'' \left[\frac{\partial C_p}{\partial (r_o' r_o'' x)} \right] x + \ldots \quad .$$

Following the procedure used for the ogive of revolution, we obtain the initial surface pressure as

$$C_{p_b}/r_o'^2 = \frac{\gamma+1}{2} + \left[\left(\frac{\gamma+1}{2} \right)^2 + \frac{4}{K_\delta^2} \right]^{\frac{1}{2}} \quad ,$$

which is as expected since this is the value for the wedge. The initial pressure gradient is found to be

$$\frac{\partial C_p}{\partial (r_o' r_o'' x)} = \frac{4}{\gamma+1} \frac{1}{A_1} \left[\frac{3}{2} (\gamma+1) \frac{\beta}{\delta} + \frac{4}{K_\delta^2} \right] , \qquad (3.22)$$

where β/δ is given by Eq. (3.6).

Equation (3.22) is displayed in Fig. (3.6) and compared with the plot of an expression obtained by Van Dyke. The agreement is relatively good for K_δ greater than unity. In the limit γ equal to unity, M_∞ equal to infinity Eq. (3.22) yields the Newton-Busemann value, that is,

$$\frac{\partial C_p}{\partial (r_o' r_o'' x)} = 6.0 \quad .$$

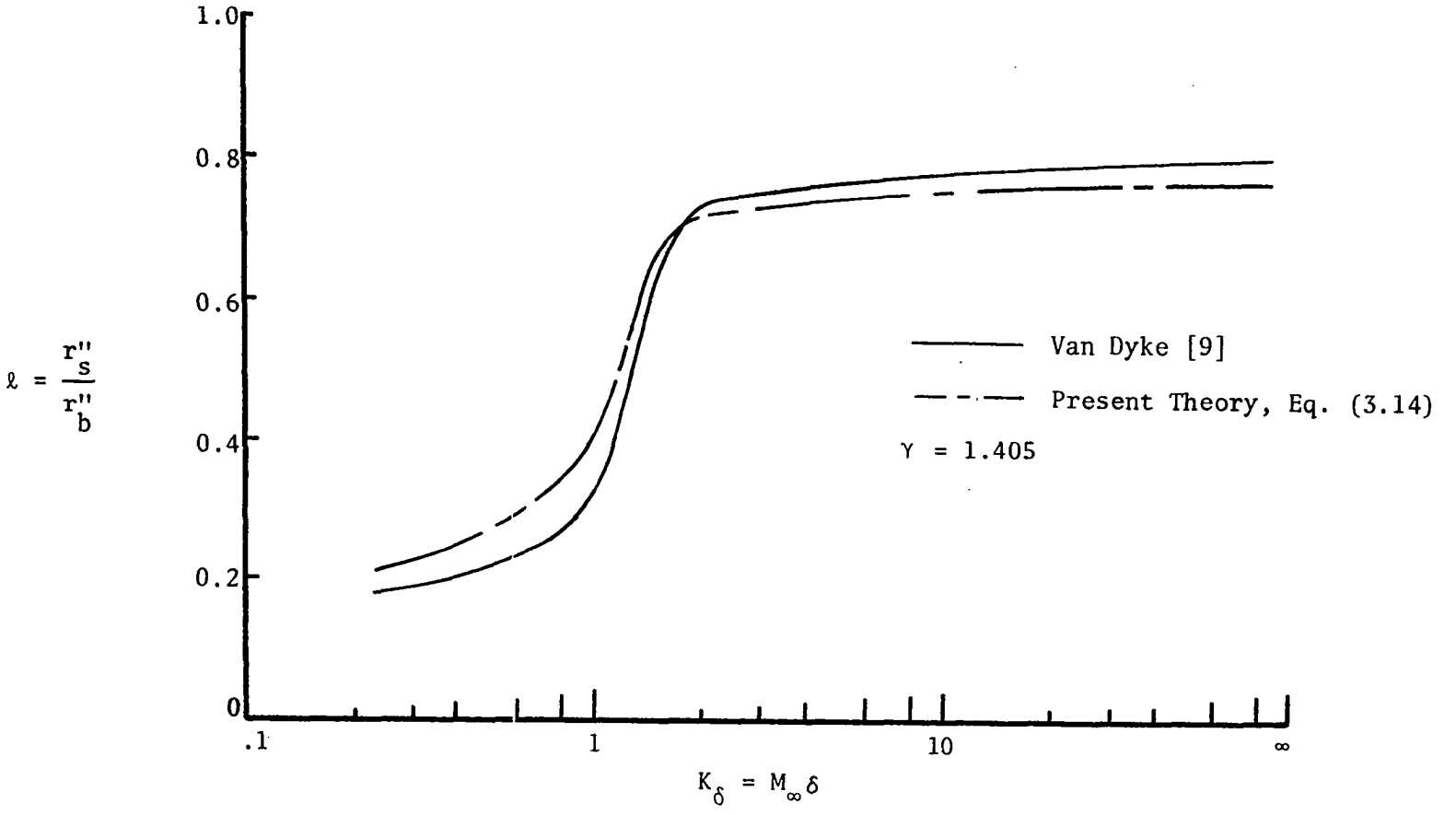


Figure 3.5. Curvature ratio for the plane ogive.

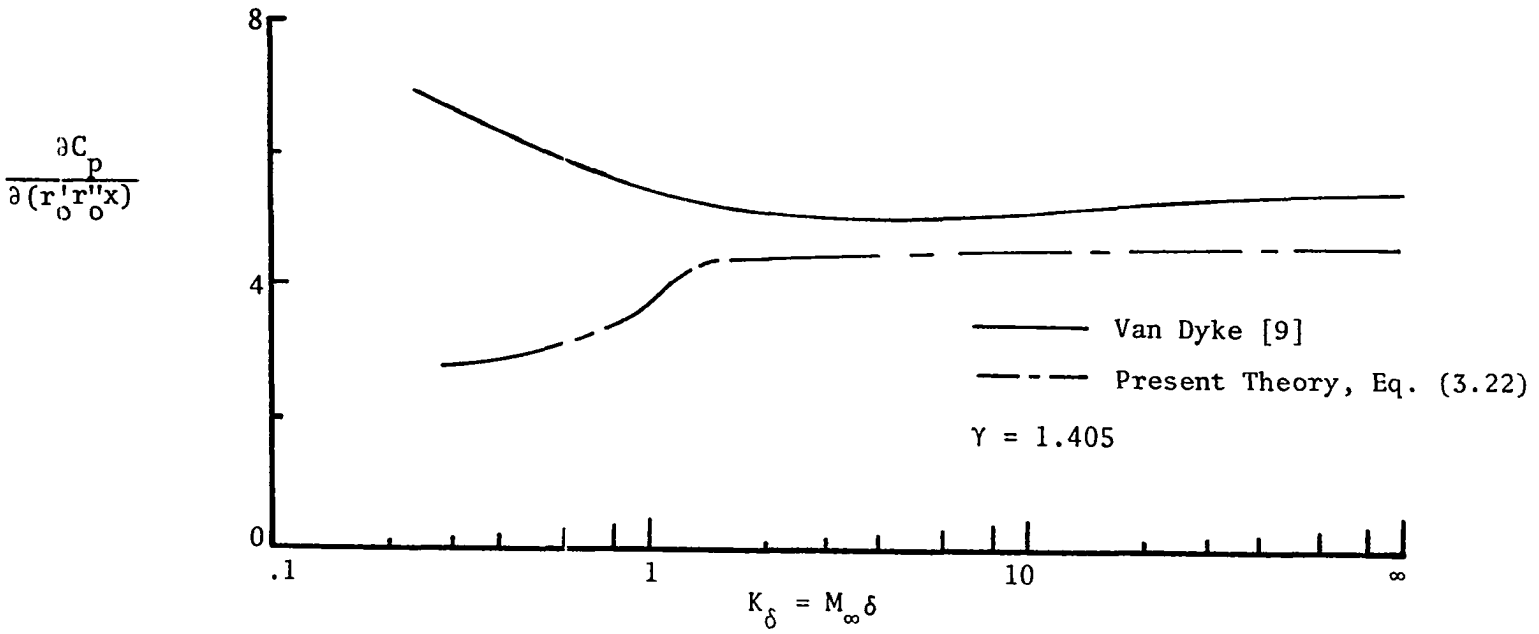


Figure 3.6. Initial pressure gradient on the plane ogive.

In this chapter we have found that conical and ogival shocks are supported by cones, wedges, and ogives. The bodies are given by algebraic expressions in terms of the shock parameters and ratio of specific heats. The body shapes agree well with those found by other methods and, in general, are obtained more easily. The surface pressures on a wedge agree exactly with those found by Linnell [39] and Van Dyke [9], whereas the cone surface pressures agree with the small disturbance values only in the Newtonian limit. The surface pressures and initial pressure gradients on ogives are in good agreement with the values computed by Van Dyke [9] for large K_δ.

CHAPTER IV

SLIGHTLY BLUNTED SHOCKS

General Considerations

In Chapter III we considered the flow past pointed bodies. The body shape was found to be given by the quadrature in Eq. (2.18) since the term $C/H^{1/\gamma}$ is equal to zero.

In this chapter we shall consider the flow past slender slightly blunted bodies. Two general types of shock shapes supported by these bodies will be considered - the power-law shock and the hyperbolic shock. Since the bodies are blunted, the term $C/H^{1/\gamma}$ in Eq. (2.18) is not zero. One of our tasks is to estimate and interpret the contribution of this term to the body shape.

The ensuing analysis is restricted to the limit M_∞ equal to infinity. In this limit the quadrature for the body shape supporting a power-law shock can be integrated exactly, and the quadrature for the body shape supporting a hyperbolic shock, although not integrable exactly, reduces to a rather simple form.

Power-Law Shock

Body Shape

A general form of the power-law shock shape to be used in the following analysis is

$$r_s = Ax^n \quad . \tag{4.1}$$

Throughout this chapter n is the shock power-law exponent only and, for convenience, will not be subscripted. With the use of Eq. (4.1) and the appropriate expressions for V_s, S, and v_2 the functions H and G for M_∞ equal to infinity are

$$H = v_\infty^2 \frac{\gamma A^2}{\gamma+1} n(3n-1)x^{2(n-1)} \quad ,$$

$$G = v_\infty^3 \frac{4\pi A^4 n}{\gamma+1} \left[\frac{\gamma-1}{\gamma+1} n + \tfrac{1}{2}(3n-1)\right] (2n-1)x^{4n-3}$$

for axisymmetric power-law shocks, and

$$H = v_\infty^2 \frac{2\gamma}{\gamma+1} A^2 n(2n-1)x^{2(n-1)}$$

$$G = v_\infty^3 \frac{4A^3 n}{\gamma+1} \left[\frac{\gamma-1}{\gamma+1} n + (2n-1)\right](3n-2)x^{3(n-1)}$$

for plane power-law shocks. The substitution of the above expressions into Eq. (2.18b) and subsequent integration yields

$$r_b^{j+1} = \frac{[(3-j)n-2+j]\{[(3+2j)\gamma+1]n-\gamma-1\}}{(\gamma+1)[(2+j)n-1][n(\gamma+2-j)-2+j]} r_s^{j+1} + r_o^{j+1}\left(\frac{x}{x_o}\right)^{2(1-n)/\gamma} \tag{4.2}$$

for the body shape. The first term on the right-hand side is contributed by evaluation of the quadrature. The second term accounts for the blunt nose, where r_o is some initial contribution to the body shape resulting from the bluntness effects and x_o is the axial coordinate at this point. Because of our original assumptions, the nose shape is not known (recall that we assumed all the energy added to the gas by the blunt nose was added instantaneously). Thus, it is necessary to develop some method which will enable us to estimate r_o and x_o within the provisions of hypersonic small disturbance theory.

A requirement of slender body theory is that the body slope δ satisfy the condition $\delta<<1$. If the Mach number is sufficiently large, the shock slope satisfies the same condition, that is, $\beta<<1$. In the following development β and δ are interpreted as the local shock and body slopes. Thus, if β is of order unity, the shock slope is sufficiently large to be considered in the nose region. Since the slender body approximations are not valid in the nose region, we shall use the condition $\beta = O(1)$ to evaluate r_o and x_o as follows.

Differentiation of the shock shape given by Eq. (4.1) yields

$$r_s' = Anx^{n-1} \quad ,$$

and thus

$$\beta \simeq Anx^{n-1} \quad .$$

We now assume that β is equal to unity when x is equal to x_o, that is,

$$Anx_o^{n-1} = 1 \quad .$$

It follows that

$$x_o = (An)^{1/(1-n)} \quad . \tag{4.3}$$

The above value for x_o insures that the point of evaluation of r_o is in the nose region of the shock and body. It follows from Eq. (4.1) that the shock radius at x_o is

$$r_{s_o} = A(An)^{n/(1-n)} \quad . \tag{4.4}$$

In addition it is known that in the region of the nose, the body is of the same order of magnitude as the shock. Furthermore, for small ε we assume

$$r_{b_o} \approx r_{s_o} \quad . \tag{4.5}$$

This assumption increases in accuracy as γ approaches unity. For values of γ larger than unity the body radius is overestimated initially. However, our objective is not to determine the nose shape, but to obtain a reasonable estimate of the influence of the entropy-displacement on the asymptotic body shape.

If we define the quantity ζ_{j+1} as

$$\zeta_{j+1} \equiv \frac{[(3-j)n-2+j]\{[(3+2j)\gamma+1]n-\gamma-1\}}{(\gamma+1)[(2+j)n-1][n(\gamma+2-j)-2+j]} \quad ,$$

Eq. (4.2) can be recast in the form

$$r_b^{j+1} = \zeta_{j+1} r_s^{j+1} + r_o^{j+1} \left(\frac{x}{x_o}\right)^{2(1-n)/\gamma} \quad . \tag{4.6}$$

At the initial condition x is equal to x_o and r_{b_o} is equal to r_{s_o}; therefore, solving (4.6) for r_o yields

$$r_o^{j+1} = (1- \zeta_{j+1}) r_{s_o}^{j+1} \quad . \tag{4.7}$$

Figure (4.1) illustrates the displacement effect of r_o. If Eqs. (4.4) and (4.7) are combined and substituted along with Eq. (4.3) into Eq. (4.6), the body shape is given by

$$r_b^{j+1} = \zeta_{j+1}(Ax^n)^{j+1} + (1-\zeta_{j+1}) \left[A^{\frac{(2-j)(n-1)+\gamma}{n}} \right]^{\frac{(\gamma+2-j)n-2+j}{(1-n)\gamma}} x^{\frac{j+1}{\gamma}} \cdot \frac{2(1-n)}{\gamma} \tag{4.8}$$

Equation (4.8) is the body shape for a power-law shock in the limit M_∞ equal to infinity. For a given shock shape and γ, the body is completely specified. However, there are certain restrictions on n which are enumerated in following sections.

Equation (4.8) has the same form as obtained by Guiraud *et al.* [24, pp. 174-177] for a solution of the inverse problem posed by Sychev [17]. They chose the shock shape as

$$r_s = KL\left(\frac{x}{L}\right)^n \quad ,$$

and continue the development with the pressure given by the self-similar or "homogeneous" solution. However, the other flow quantities are found from the Rankine-Hugoniot conditions across the detached shock, rather

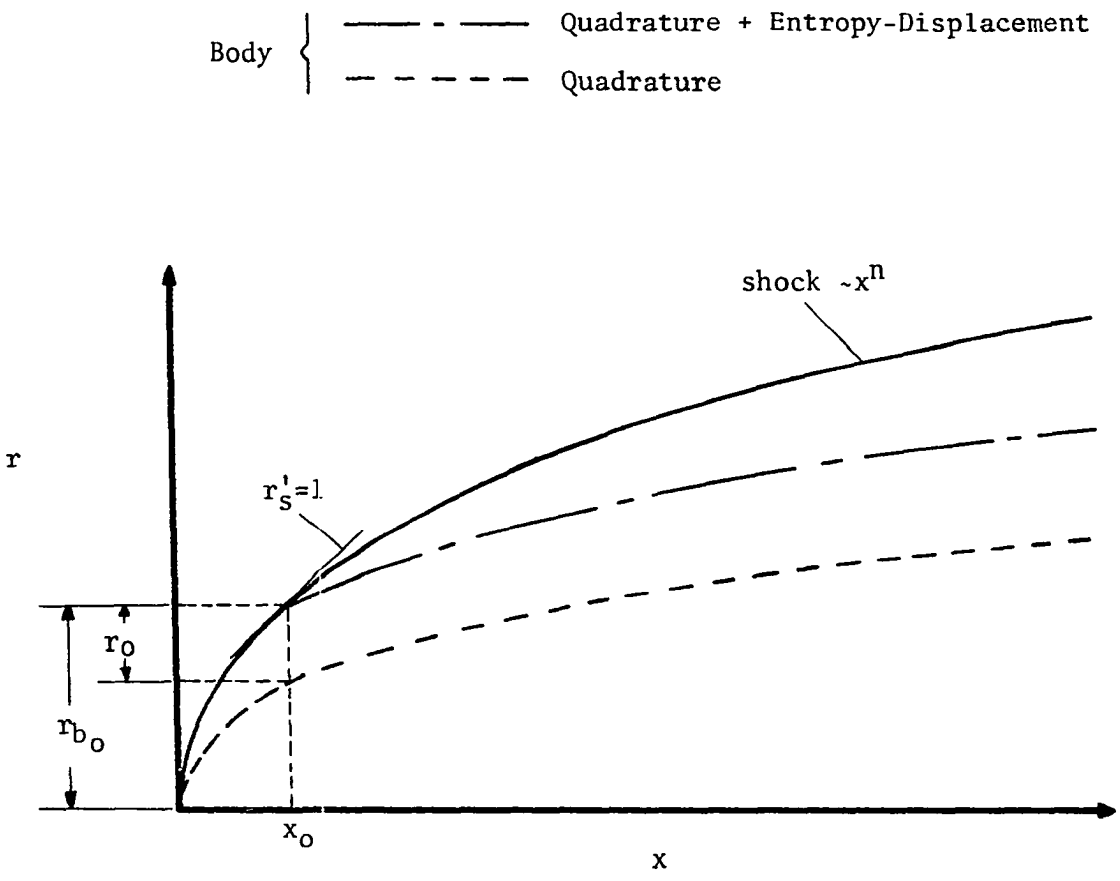


Figure 4.1. Illustration of the entropy-displacement effect.

than from the small-disturbance equations. A term is defined that represents the displacement effect of the entropy layer and enables the body shape to be described in the form

$$r_b^{j+1} \approx [\bar{\eta}_{b_H} KL(\frac{x}{L})^n]^{j+1} + \frac{\gamma-1}{\gamma+1}(\bar{p}_{b_H})^{-1/\gamma} I(j,\gamma,n) K^{-2/\gamma+(j+1)/(1-n)} L^{j+1} (\frac{x}{L})^{2(1-n)/\gamma} . \tag{4.9}$$

Here $\bar{\eta}_{b_H}$ is equal to r_b/r_s and $\bar{p}_{b_H}$ is equal to p_b/p_s as determined from the self-similar solution, while $I(j,\gamma,n)$ is computed from a quadrature. The first term on the right-hand side represents the self-similar body, whereas the second term is a result of the displacement effect of the entropy layer. This equation is written under the condition $2/(3+j) \leq n < 2(\gamma+1)/[(3+j)\gamma+2]$, since Sychev demonstrated that for $2(\gamma+1)/[(3+j)\gamma+2] < n \leq 1$ the displacement effect of the entropy layer is of smaller order than the error introduced by the small disturbance equations. When $n = 2/(3+j)$ the self-similar solution yields a vanishing body. Thus, η_{b_H} is equal to zero and Eq. (4.9) is written as

$$(\frac{r_b}{r_s})_{BW} = [\frac{\gamma}{\gamma+1}(\frac{2}{3+j})^{(\gamma-1)/\gamma}(\bar{p}_{b_{BW}})^{-1/\gamma}]^{1/(j+1)} K^{2(\gamma-1)/[(j+1)\gamma]} (\frac{x}{L})^{-[2/(3+j)](\gamma-1)/\gamma} , \tag{4.10}$$

where the subscript BW stands for "blast-wave". This result has also been obtained by Yakura [19, p. 450].

Before comparing Eqs. (4.8) and (4.9) further, we must establish the similarity of the second term on the right-hand side of Eq. (4.8) with the entropy-displacement term in Eq. (4.9).

Entropy-Displacement Effect

If the so-called entropy-displacement term in Eq. (4.8) is a reasonable approximation of the same term in Eq. (4.9) it must have a negligible displacement effect for the same values of n. To show that this is the case, we take the ratio $(r_b/r_s)^{j+1}$ in Eq. (4.8) and require that the second term on the right-hand side be of order β^2 or smaller. Thus, we set

$$(1-\zeta_{j+1})[A_n^{(2-j)(n-1)+\gamma}]^{\frac{j+1}{(1-n)\gamma}} \frac{x^{2(1-n)/\gamma}}{r_s^{j+1}} \simeq 0(\beta^2) \ . \tag{4.11}$$

A close examination reveals that the coefficient of x is approximately of order unity or smaller, that is,

$$(1-\zeta_{j+1})[A_n^{(2-j)(n-1)+\gamma}]^{(j+1)/[(1-n)\gamma]} \simeq 0(1) \ .$$

Furthermore, we know that

$$r_s^{j+1} \sim x^{(j+1)n}$$

and

$$\beta \sim x^{n-1} \ .$$

Hence, Eq. (4.11) can be recast in the form

$$x^{-(j+1)n}\, x^{2(1-n)/\gamma} \simeq x^{2(n-1)} \quad .$$

Consequently, the entropy-displacement term in Eq. (4.8) is negligible only if $n>n^*$ where n^* is given by

$$(j+1)n^* - \frac{2(1-n^*)}{\gamma} = 2(1-n^*)$$

or

$$n^* = \frac{2(\gamma+1)}{(3+j)\gamma+2} \quad .$$

This is recognized as the same result obtained by Sychev.

It appears that Eq. (4.8) is a good approximate form of Eq. (4.9). The proof of this is left to the following section. Although Eq. (4.9) is a rather straightforward expression itself, it should be noted that $\tilde{n}_{b_H}$ and $\tilde{p}_{b_H}$ must be obtained from a numerical solution of the small disturbance equations, and $I(j,\gamma,n)$ is determined from a quadrature that, in general, must be numerically evaluated. In contrast Eq. (4.8) is an algebraic expression in terms of the known parameters γ, n, and A, and the independent variable x.

Body Shape as a Function of n

Since we are dealing with power-law shocks over slender convex bodies, the range of n we shall consider in detail is $0<n<1$. However, it is of interest to consider briefly the special case n equal to unity.

If n is equal to unity the shock [given by Eq. (4.1)] is conical and A is equal to β. Consequently r_o is equal to zero, and the body

shape is given by the first term in Eq. (4.8) where

$$\zeta_{j+1} = \frac{2}{\gamma+1} \quad ,$$

from which it follows that

$$\frac{r_b}{r_s} = \left(\frac{2}{\gamma+1}\right)^{1/(j+1)} \quad . \tag{4.12}$$

This is precisely the result obtained from Eqs. (3.3) and (3.6) for the flow over cones and wedges with K_δ set equal to infinity.

For n in the range $2(\gamma+1)/[(3+j)\gamma+2] < n < 1$ we have determined that the entropy-displacement effect is negligible. Therefore, within the error of the small disturbance assumptions we have

$$\frac{r_b}{r_s} = (\zeta_{j+1})^{1/(j+1)} \tag{4.13}$$

from Eq. (4.8), and

$$\frac{r_b}{r_s} = (\bar{\eta}_{bH})^{1/(j+1)} \tag{4.14}$$

from Eq. (4.9). Kubota [40] and Mirels [41] numerically integrated the small disturbance equations to obtain values for $\bar{\eta}_{b_H}$. The basic equations used in this method are given by Mirels [42, p.9]. Another approach, an approximate analytical solution based on the work of Sakurai [10] and generalized by Mirels [41], is summarized in reference [42, pp. 21-22]. Using an integral approach, Chernyi [27] obtains an algebraic expression for the body shape similar to Eq. (4.13), but not valid for $n = 2/(3+j)$. Chernyi's technique is also summarized by Mirels [42, pp.

41-42]. Numerical data for the ratio of body shape to shock shape obtained from the methods just mentioned are tabulated in reference [42, p.11] and are listed in Table 4.1 along with data from Eq. (4.13). For axisymmetric bodies (j=1) numerical data from Eq. (4.13) agree rather well with the exact solution, especially for γ not too different from unity. The agreement is not as good for planar bodies (j=0), particularly for the larger values of γ; however, all of the approximate solutions deviate somewhat from the exact small disturbance solutions for large γ (e.g., $\gamma = 5/3$) and n approaching $2/(3+j)$.

If n lies in the range $2/(3+j) \leq n \leq 2(\gamma+1)/[(3+j)\gamma+2]$ the displacement effect of the entropy layer is important. Thus, the body shape is given by both terms in Eqs. (4.8) and (4.9). To illustrate the application of Eq. (4.8) we arbitrarily specify an axisymmetric shock with the shape

$$r_s = \sqrt{2}\, x^{.533} \quad . \tag{4.15}$$

The resulting body shape is

$$r_b = (1.11x^{1.067} + 1.086x^{.667})^{\frac{1}{2}} \quad , \tag{4.16}$$

for γ equal to 7/5.

For the planar case we choose the shock

$$r_s = x^{.70} \quad , \tag{4.17}$$

and the corresponding body is

$$r_b = .340x^{.70} + .478x^{.428} \quad , \tag{4.18}$$

for γ equal to 7/5.

Equations (4.15-16) and (4.17-18) are plotted in Figs. (4.2) and (4.3), respectively. In these figures the larger body represents

Table 4-1. Body Shape Associated with A Power-Law Shock (Zero Order Problem)

γ	β^a	NUMERICAL SOLUTION KUBOTA [40] r_b/r_s		APPROXIMATE SOLUTION SAKURAI[10] r_b/r_s		APPROXIMATE SOLUTION CHERNYI[27] r_b/r_s		APPROXIMATE SOLUTION Eq.(4.13) r_b/r_s	
		j=0	j=1	j=0	j=1	j=0	j=1	j=0	j=1
1.15	0	.930	.965	.930	.965	.930	.964	.930	.964
	1/3	.891	.945	.891	.945	.886	.941	.885	.940
	1/2	.852	.924	.852	.924	.843	.918	.841	.917
	5/8	.803	.898	.801	.897	.789	.888	.787	.887
	3/4	.716	.845	.710	.846	.698	.835	.695	.833
	7/8	.535	.735	.513	.724	.514	.717	.511	.715
	1	0	0	0	0	0	0	0	0
1.40	0	.833	.915	.833	.915	.833	.913	.833	.913
	1/3	.759	.875	.760	.875	.755	.869	.750	.867
	1/2	.695	.839	.695	.839	.688	.829	.679	.824
	5/8	.623	.796	.619	.795	.613	.783	.601	.775
	3/4	.513	.725	.499	.719	.501	.708	.490	.699
	7/8	.333	.589	.284	.561	.322	.567	.309	.555
	1	0	0	0	0	0	0	0	0
1.67	0	.749	.870	.749	.870	.749	.865	.749	.865
	1/3	.658	.819	.660	.819	.660	.812	.649	.810
	1/2	.585	.776	.586	.776	.588	.767	.570	.755
	5/8	.509	.727	.505	.726	.513	.717	.490	.700
	3/4	.404	.652	.385	.644	.408	.639	.381	.617
	7/8	.248	.518	.186	.480	.252	.502	.227	.477
	1	0	0	0	0	0	0	0	0

[a] $\beta = \frac{2}{j+1}\left(\frac{1}{n} - 1\right)$ in this table only.

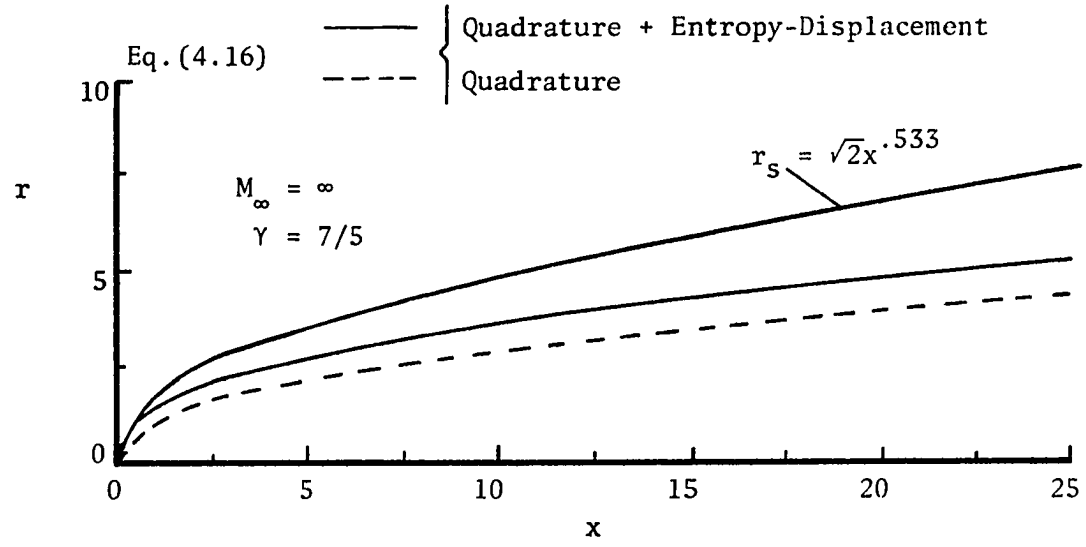


Figure 4.2. Body shape for an axisymmetric power-law shock.

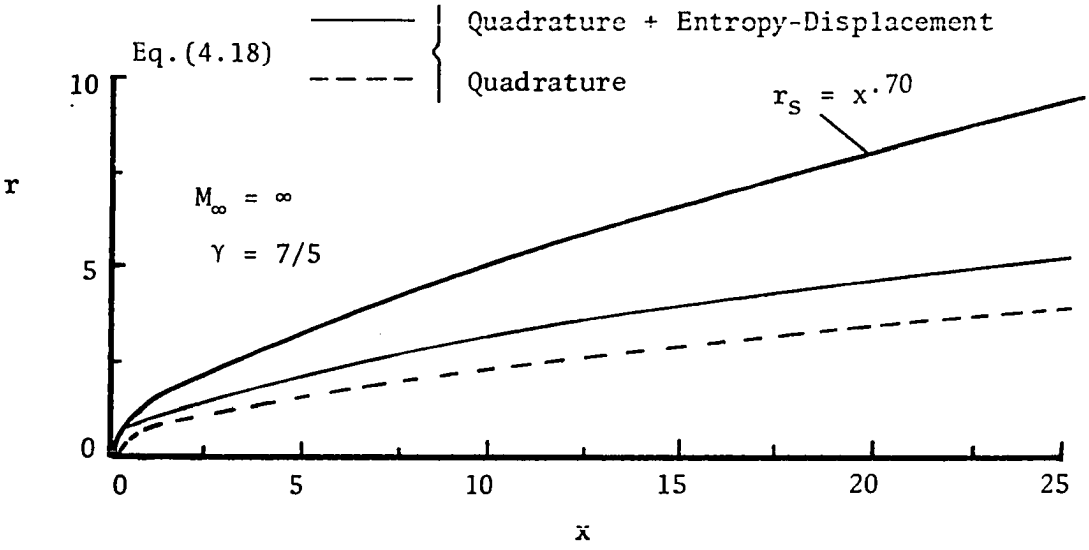


Figure 4.3. Body shape for a plane power-law shock.

the contributions from both the quadrature and entropy-displacement terms, whereas the smaller body is obtained from the quadrature term only. For the particular values of n chosen in the above examples it is apparent that the entropy-displacement effect contributes significantly to the body shape. As n increases toward $2(\gamma+1)/[(3+j)\gamma+2]$ the entropy-displacement effect becomes less important. This is also true as γ approaches unity. On the other hand when n decreases in value compared to the above example, the entropy-displacement term makes a greater contribution to the size of the body, and when $n = 2/(3+j)$ the entropy displacement effect is the body.

In the limit $n = 2/(3+j)$ the self-similar solutions of the small disturbance equations yield a vanishing body ($\bar{n}_{b_H}=0$). This particular solution is referred to as the constant-energy or blast-wave solution. Blast-wave solutions stem from the works of Sedov [3,5], Taylor [6], Sakurai [10,11], and Lees and Kubota [14]. From the blast-wave solutions we find that a power-law shock with $n = 2/(3+j)$ is supported by a body that does not grow with x. However, it was first shown by Sychev [17] numerically, and then by Yakura [19] analytically, that bodies for $n = 2/(3+j)$ vary asymptotically as $x^{2/[(3+j)\gamma]}$.

If we examine Eq. (4.8) we find that ζ_{j+1} is equal to zero for $n = 2/(3+j)$ and it follows that

$$r_b = \left[A^{\frac{-(2-j)(j+1)}{3+j}+\gamma}\left(\frac{2}{3+j}\right)^{\frac{2(\gamma+2-j)}{3+j}-2+j}\frac{j+3}{(j+1)\gamma}\right]x^{\frac{2}{(3+j)\gamma}}. \qquad (4.19)$$

Thus, we also find that the blast-wave shock produces a body which grows asymptotically with x.

A comparison between the numerical values computed from Eq. (4.19)

and those obtained by Yakura [19] and Guiraud [Eq. (4.10)] can be made by specifying the following shock shape

$$r_s = 2^{j/2} x^{2/(3+j)} \quad . \tag{4.20}$$

If the shock is axisymmetric the corresponding body obtained from Eq. (4.19) for γ equal to 7/5 is

$$r_b = 1.28 x^{5/14} \quad , \tag{4.21}$$

whereas Yakura and Guiraud found that

$$r_b = 1.39 x^{5/14} \tag{4.22}$$

In a similar manner we find that for the planar shock

$$r_b = 0.80 x^{10/21} \quad , \tag{4.23}$$

whereas Yakura and Guiraud obtained

$$r_b = 0.91 x^{10/21} \quad . \tag{4.24}$$

The agreement between Eqs. (4.21-22) and (4.23-24) is very good, especially when we consider the simplicity of our approximate analysis. For the axisymmetric shock further comparisons are made with the works of Sychev [17] and Schneider [26], with all of the results displayed in Fig. (4.4). In the case of the planar shock Eqs. (4.23-24) are compared in the plots in Fig. (4.5).

If n has a value $n<2/(3+j)$ there are no self-similar solutions to the small disturbance equations. Therefore, the solution given by

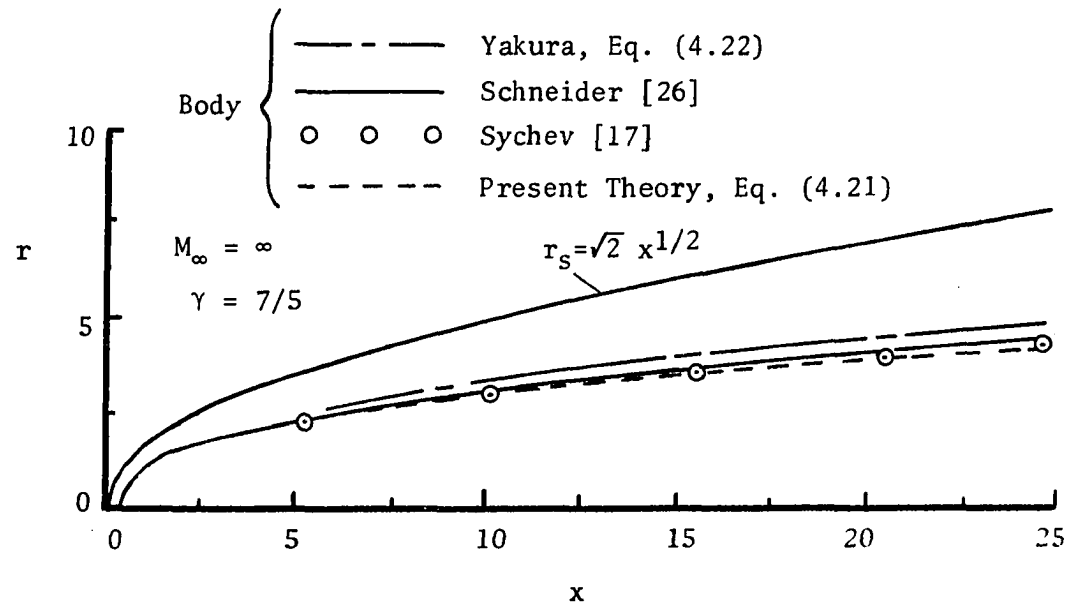


Figure 4.4. Body shapes for an axisymmetric parabolic shock.

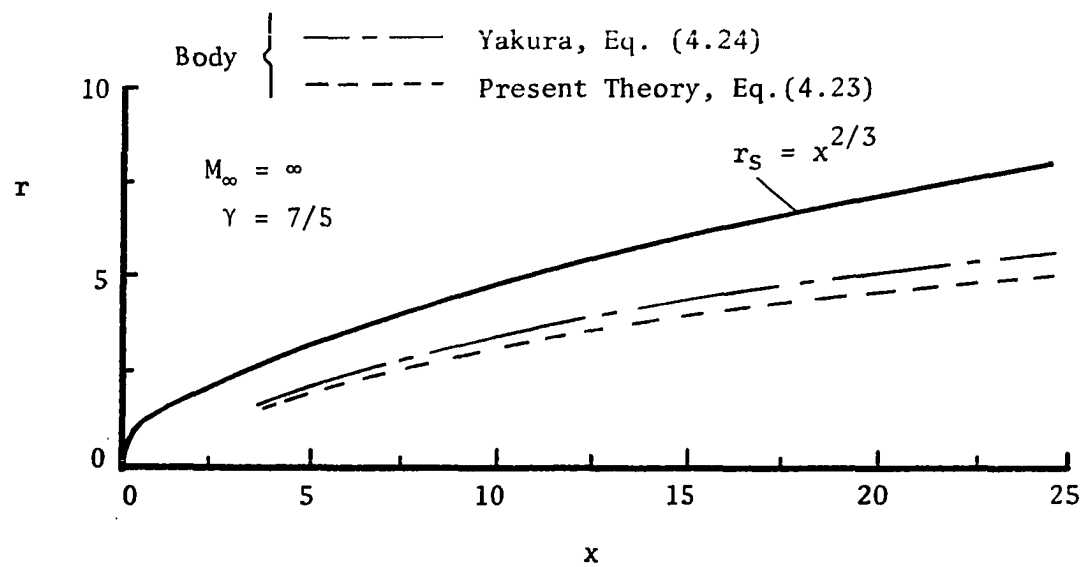


Figure 4.5. Body shapes for a plane parabolic shock.

Eq. (4.9) is not applicable for these values of n. Freeman [21] and Mirels [41,42] discuss solutions for this range of n.

Upon examination we find that the body given by the present theory, Eq. (4.8), is not realistic for $n<2/(3+j)$. The quadrature term contributes a negative quantity to the body shape, while the entropy-displacement contributes a term that grows faster than the shock for certain values of n. Hence, we shall consider the solution given by Eq. (4.8) to be valid only in the range $2/(3+j)\leq n\leq 1$.

Pressure Distribution

For a power-law shock, the pressure on the body surface can be found by substituting Eq. (4.1) into Eq. (2.28) with M_∞ equal to infinity. The resulting pressure distribution is

$$C_{p_b} = \frac{2(2-j)A^2 n}{\gamma+1}\,[n(2+j)-1]x^{-2(1-n)} \qquad (4.25)$$

In the limit n equal to unity, the shock is conical and A is equal to β. In this limit the pressure coefficient has the value

$$C_{p_b}/\delta^2 = 2^j(\gamma+1)^{1-j} \quad ,$$

which is recognized as that for the cone or wedge in the limit K_δ equal to infinity.

If the shock has a parabolic shape, that is, varies as $x^{2/(3+j)}$, then the pressure on the corresponding body is correctly given by the blast-wave solution. Thus, the blast-wave pressure is the correct pressure for a parabolic shock, but it corresponds to a body that grows

as $x^{2/[(3+j)\gamma]}$. If we specify an axisymmetric parabolic shock given by Eq. (4.20), the pressure obtained from Eq. (4.25) is

$$\frac{p_b}{\rho_\infty v_\infty^2} = \frac{0.5}{\gamma+1} x^{-1} \quad , \tag{4.26}$$

compared to Yakura's result

$$\frac{p_b}{\rho_\infty v_\infty^2} = \frac{0.373}{\gamma+1} x^{-1} \quad , \tag{4.27}$$

which is also the pressure found from the blast-wave solution. In a similar manner the surface pressure for a plane parabolic shock is

$$\frac{p_b}{\rho_\infty v_\infty^2} = \frac{8(0.50)}{9(\gamma+1)} x^{-2/3} \quad , \tag{4.28}$$

whereas Yakura obtained

$$\frac{p_b}{\rho_\infty v_\infty^2} = \frac{8(0.39)}{9(\gamma+1)} x^{-2/3} \quad . \tag{4.29}$$

Comparisons of the pressures from Eqs. (4.26-29) are made in Figs. (4.6) and (4.7). Also shown in Fig. (4.6) is the pressure obtained by Schneider [26]. Although the pressures given by the present theory are somewhat high the approximation is, in general, acceptable. For instance, as n approaches unity the pressures given by Eq. (4.25) become more accurate, and for n equal to unity (4.25) yields the exact value on the surface of a wedge.

Hyperbolic Shock

In the following sections expressions for the body shapes supporting axisymmetric and plane hyperbolic shocks are developed. The

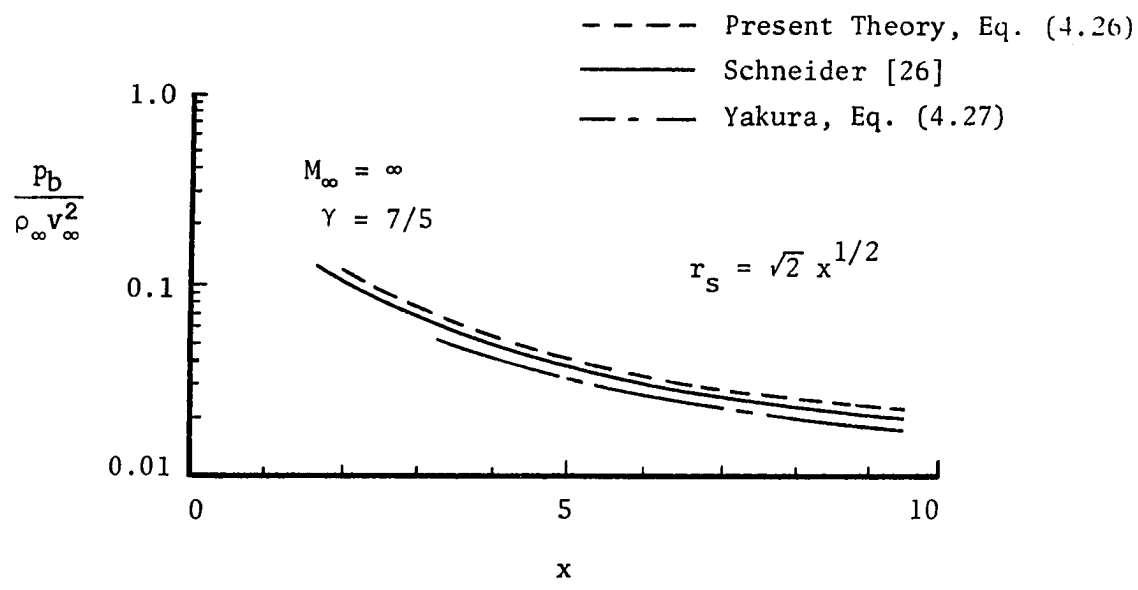


Figure 4.6. Body pressures for an axisymmetric parabolic shock.

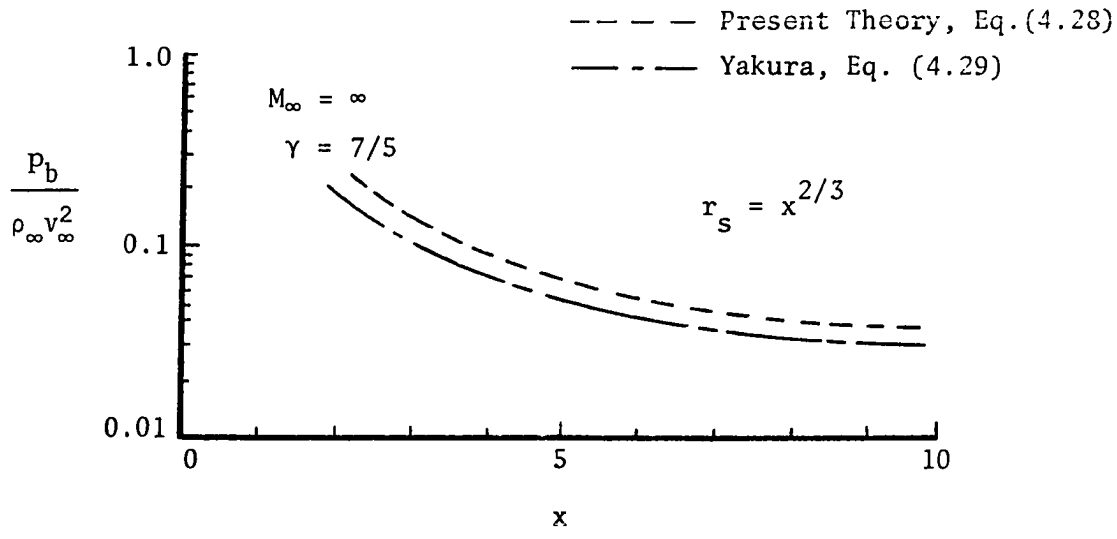


Figure 4.7. Body pressures for a plane parabolic shock.

analyses are carried out at M_∞ equal to infinity. Yakura [19] solved similar problems and found that the bodies were blunted cones and wedges.

Axisymmetric Case

We describe a hyperbolic shock by the formula

$$r_s = (A^2x + B^2x^2)^{\frac{1}{2}} \quad . \tag{4.30}$$

The functions H and G are obtained from (2.16) as

$$H = v_\infty^2 \frac{\gamma}{\gamma+1} \frac{A^4/4 + 2A^2B^2x + 2B^4x^2}{(A^2x + B^2x^2)} ,$$

and

$$G = v_\infty^3 \frac{4\pi\gamma}{(\gamma+1)^2}(A^2B^2 + 2B^4x) \quad .$$

If these expressions are substituted into Eq. (2.18b), the body shape can be written as

$$r_b^2 = \left(\frac{r_s^2}{\frac{A^4}{8B^2} + r_s^2}\right)^{1/\gamma} \cdot \left[\frac{4}{\gamma+1} \int_0^{r_s^2} \left(\frac{r_s^2}{\frac{A^4}{8B^2} + r_s^2}\right)^{1-\frac{1}{\gamma}} r_s dr_s + r_o^2 \left(\frac{\frac{A^4}{8B^2} + r_{s_o}^2}{r_{s_o}^2} \right)^{1/\gamma} \right] . \tag{4.31}$$

The second term on the right-hand side of (4.31) is a result of the entropy-displacement. We can evaluate r_o and r_{s_o}, in a manner similar to that for power-law shocks, by requiring that r_s' equal unity when x equals x_o. If this is accomplished and, in addition, we make the transformation of variable

$$W = \frac{8B^2}{A^4} r^2 \quad ,$$

Eq. (4.31) can be recast as

$$W_b = \left(\frac{W_s}{1+W_s}\right)^{1/\gamma} \cdot \left[\frac{2}{\gamma+1} \int_0^{W_s} \left(\frac{W}{1+W}\right)^{\frac{\gamma-1}{\gamma}} dW + W_o \left(\frac{1+W_{s_o}}{W_{s_o}}\right)^{1/\gamma}\right] \quad , \tag{4.32}$$

where

$$W_{s_o} = \frac{2B^2}{1-B^2}$$

$$W_o = (2B^2)^{\frac{\gamma-1}{\gamma}} \frac{(1+B^2)^{1/\gamma}}{1-B^2} - \frac{2}{\gamma+1} \int_o^{W_o} \left(\frac{W}{1+W}\right) dW \tag{4.33}$$

and

$0<B<1$.

The range of B does not severely restrict applications of the above theory since the asymptotic shock slope B should be less than unity to be consistent with the small disturbance approximations. Also, B must be greater than zero so that the variable W is non-zero. If Eqs. (4.32) and (4.33) are combined the body shape can be expressed as

$$W_b = \left(\frac{W_s}{1+W_s}\right)^{1/\gamma} \left[\frac{2}{\gamma+1} \int_{W_{s_o}}^{W_s} \left(\frac{W}{1+W}\right)^{\frac{\gamma-1}{\gamma}} dW + \frac{(2B^2)^{(\gamma-1)/\gamma} (1+B^2)^{1/\gamma}}{1-B^2}\right] \quad . \tag{4.34}$$

In general, the quadrature in Eq. (4.34) must be evaluated numerically. However, for W_s equal to infinity the body shape can be written in the form

$$r_b/r_s = \left(\frac{2}{\gamma+1}\right)^{\frac{1}{2}} , \qquad W_s = \infty . \tag{4.35}$$

Thus, the body shape is asymptotically conical. Yakura [19] found that an axisymmetric hyperbolic shock was supported by the flow over a blunted cone. He chose a shock with an asymptote of 22 degrees and found a body with an asymptote of 20.032 degrees for γ equal to 7/5. A plot of Eq. (4.34) for γ equal to 7/5 and B equal to 0.3839 radians (22 degrees) is displayed in Fig. (4.8). The body asymptote, computed from Eq. (4.35), is 0.3502 radians (20.06 degrees) which agrees very well with Yakura's result.

The pressure on the body surface is found by substituting Eq. (4.30) into Eq. (2.28) with M_∞ set equal to infinity. The pressure distribution can be expressed as

$$C_{p_b} = \frac{4B^2}{\gamma+1}\left[\frac{1+W_s}{W_s}\right] .$$

If B is defined in terms of the asymptotic cone angle θ_b as follows:

$$B^2 = \frac{\gamma+1}{2}\theta_b^2 \tag{4.36}$$

we can write

$$C_{p_b}/\theta_b^2 = 2\left[\frac{1+W_s}{W_s}\right] .$$

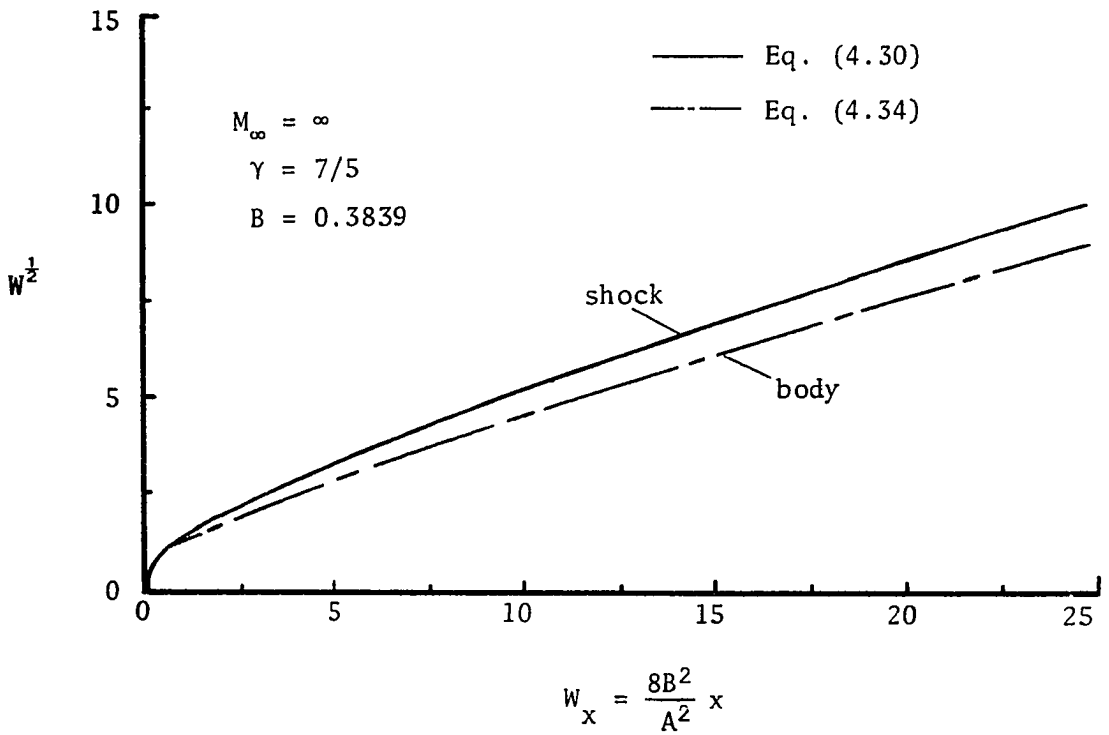


Figure 4.8. Body supporting an axisymmetric hyperbolic shock.

In the limit W_s equal to infinity the above expression reduces to

$$C_{p_b}/\theta_b^2 = 2 \quad , \qquad W_s = \infty \quad ,$$

which is the value we found for the pressure on the surface of a cone.

If we substitute the appropriate values for the hyperbolic shock into Eq. (2.32) with j equal to unity and M_∞ equal to infinity, and evaluate the resulting expression at x equal to zero, the nose drag coefficient is found to be

$$C_{D_N} = \frac{A^4}{r_N^2} \left[\frac{3\gamma-1}{2(\gamma^2-1)(\gamma+1)} \right] \quad , \tag{4.37}$$

where r_N is the radius of the nose. The variable W_s can, with the use of Eq. (4.30), be recast in the form

$$W_s = W_x + \frac{1}{8} W_x^2 \quad ,$$

where

$$W_x = (8B^2/A^2)x \quad .$$

We can remove the dependence of W_x on the shock parameters A and B with the application of Eqs. (4.36) and (4.37) and obtain

$$W_x = \left[\frac{32(3\gamma-1)}{\gamma-1} \right]^{\frac{1}{2}} \frac{\theta_b^2}{C_{D_N}^{\frac{1}{2}}} \frac{x}{d_N} \quad , \tag{4.38}$$

where $d_N = 2\, r_N$.

The total drag coefficient, obtained from Eq. (2.32) with M_∞ equal to infinity, can be written in terms of W_s and W_x as

$$C_D/\theta_b^2 = \frac{1}{\gamma-1}\left\{\left[\left(\frac{W_s}{W_b}\right)^2-1\right]\left[1+\frac{(4+W_x)^2}{W_x(8+W_x)}\right]+\right.$$

$$\left.\frac{1}{4}\frac{\gamma-1}{\gamma+1}\frac{(4+W_x)^2}{W_b^2}\right\}. \qquad (4.39)$$

Chernyi [28, pp. 226-231], with a solution of the direct problem, showed that the drag coefficient for a blunted cone has a minimum. This has also been experimentally verified e.g., Cleary [43]. Thus, slight blunting can decrease the drag of a cone. A plot of Eq. (4.39) is shown in Fig. (4.9) and it is apparent that the drag coefficient does not have a minimum. The difference between our solution and Chernyi's is that we have added a constraint to the problem by specifying the shock shape. The shock obtained by Chernyi has a slight inflection downstream whereas the shock given by Eq. (4.30) does not have an inflection. Basically, the two problems are not the same since Chernyi's body is conical except for the blunted nose, whereas the body given by (4.34) is conical only in the asymptotic sense.

Planar Case

For a plane hyperbolic shock we prescribe a shape given by

$$\bar{r}^{\,3/2} = \bar{x}^{\,3/2} - 1 , \qquad (4.40)$$

where $\bar{r}$ is equal to r/B, $\bar{x}$ is equal to x/A, and B/A is the slope of the

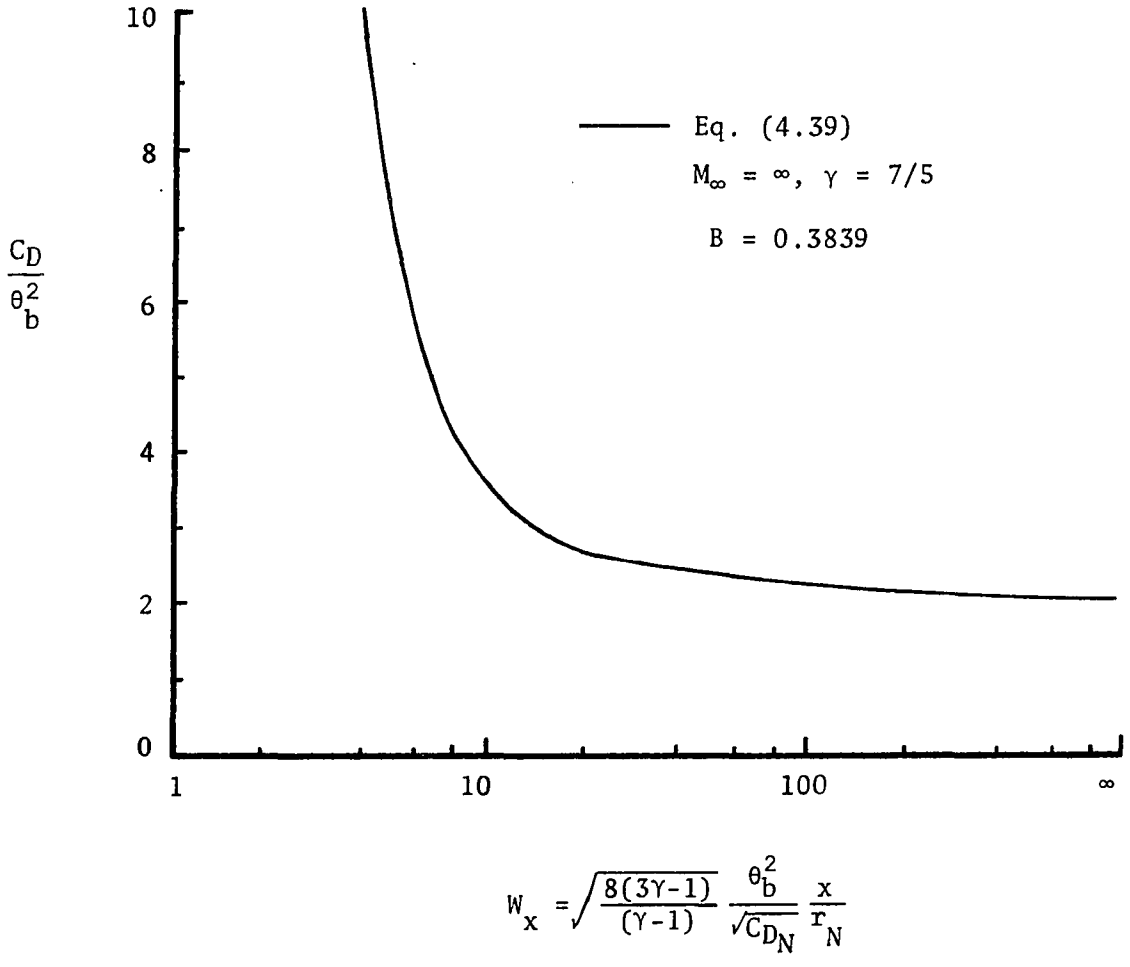


Figure 4.9. Drag coefficient for an axisymmetric hyperbolic shock.

shock asymptote. The shock shape for the planar hyperbolic shock must be given in a different form than the shock shape for the axisymmetric hyperbolic shock. The reason is that for small x, the shock radius given by Eq. (4.30) varies as $x^{\frac{1}{2}}$. However, the quadrature term in the general solution, Eq. (2.18), is not valid for power-law exponents less than 2/3 for planar shocks. This problem is eliminated with Eq. (4.40) since for values of $\bar{x}$ near unity the normalized shock thickness varies as $(\bar{x}^{3/2}-1)^{2/3}$.

For a shock given by Eq. (4.40) the functions H and G are:

$$H = v_\infty^2 \frac{2\gamma}{\gamma+1} \left(\frac{B}{A}\right)^2 \left[\frac{\bar{x}^{3/2-\frac{1}{2}}}{\bar{x}^{\frac{1}{2}}(\bar{x}^{3/2}-1)^{2/3}}\right] ,$$

$$G = v_\infty^3 \frac{4\gamma}{(\gamma+1)^2} \left(\frac{B}{A}\right)^3 \left[\frac{\bar{x}^{3/2+(\gamma+1)/(8\gamma)}}{\bar{x}^{3/2}}\right] .$$

Substitution of the above expressions into Eq. (2.18b) enables us to write the body shape in the form

$$\bar{r}_b = \frac{1}{H^{1/\gamma}} \left[\frac{2}{\gamma+1} \int_{\bar{x}_o}^{\bar{x}} \frac{G}{H^{\gamma-1/\gamma}} d\bar{x} + \bar{r}_{b_o} H_o^{1/\gamma}\right] , \qquad (4.41)$$

where

$$H = \frac{\bar{x}^{3/2} - \frac{1}{2}}{\bar{x}^{\frac{1}{2}}(\bar{x}^{3/2}-1)^{2/3}}$$

$$G = \frac{\bar{x}^{3/2} + (\gamma+1)/(8\gamma)}{\bar{x}^{3/2}}$$

$$\bar{x}_o = [1-(B/A)^3]^{-2/3}$$

$$H_o = \frac{1+(B/A)^3}{2(B/A)^2\bar{x}_o}$$

$$\bar{r}_{b_o} = \frac{(B/A)^2}{\bar{x}_o} \quad .$$

The second term on the right-hand side of Eq. (4.41) represents the displacement effect of the entropy layer. The procedure for obtaining the terms $\bar{x}_o$ and $\bar{r}_{b_o}$ is the same as that described previously for power-law and axisymmetric hyperbolic shocks.

A simple numerical integration will yield values for the body shape given by Eq. (4.41). For $\bar{x}$ equal to infinity, the quadrature in (4.41) can be evaluated exactly and the body shape can be written as

$$r_b/r_s = \frac{2}{\gamma+1} \quad , \qquad \bar{x} = \infty \quad , \tag{4.42}$$

which is the asymptotic shape for a blunted wedge. Yakura [19] found that the body supporting a plane hyperbolic shock is a blunted wedge. He specified a shock with a 24.30 degrees asymptote, and found that the body asymptote was 20 degrees for γ equal to 7/5. A plot of Eq. (4.41) for γ equal to 7/5 and B/A equal to 0.4241 radians (24.30 degrees) is shown in Fig. (4.10). The body asymptote, computed from Eq. (4.42), is 0.3532 radians (20.19 degrees) which is in good agreement with Yakura's result.

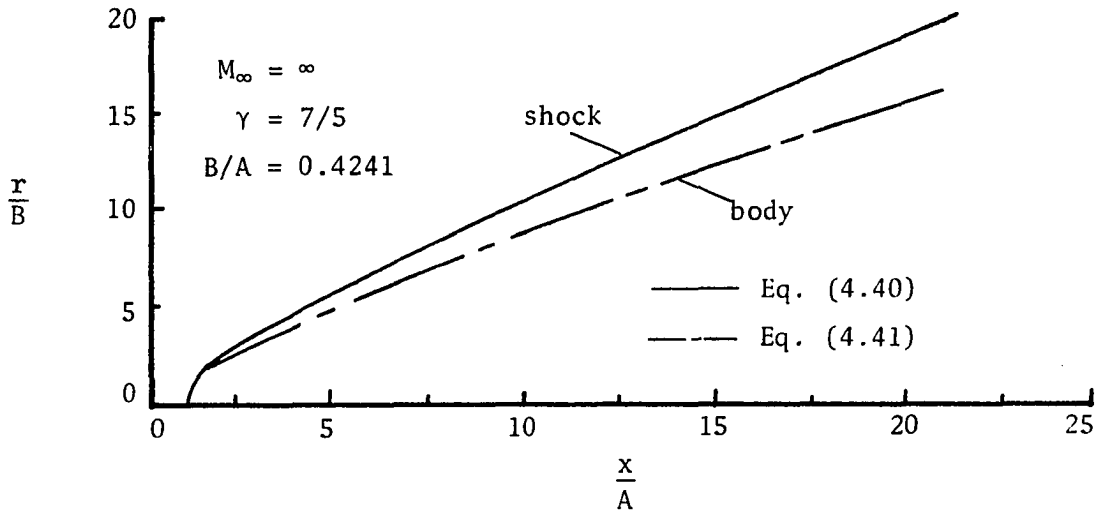


Figure 4.10. Body supporting a plane hyperbolic shock.

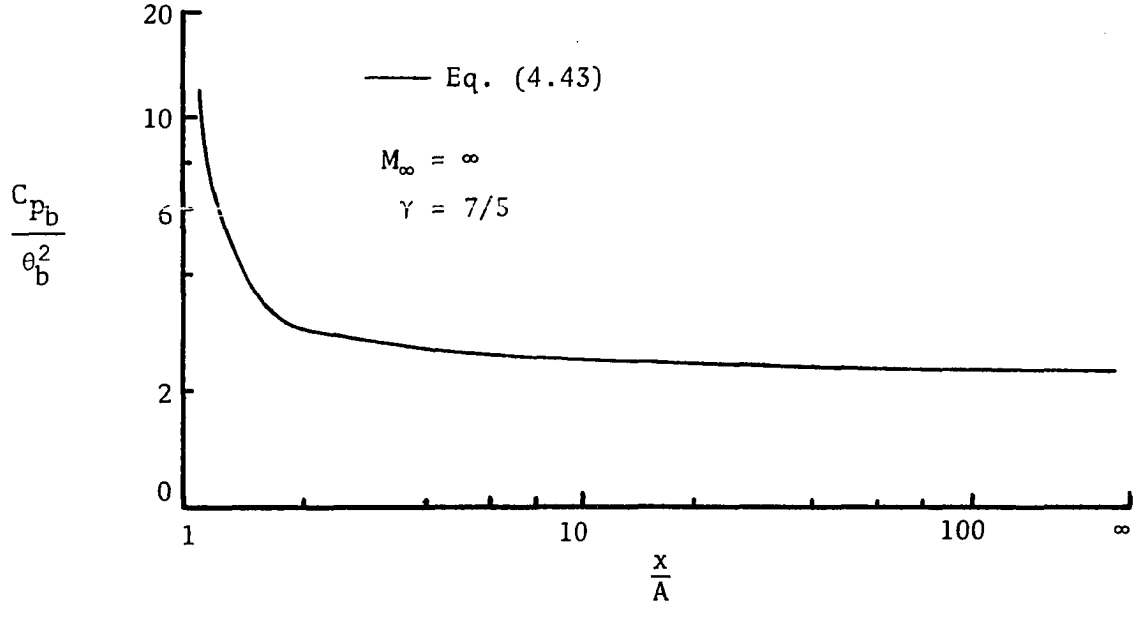


Figure 4.11. Body pressure for a plane hyperbolic shock.

The application of Eqs. (4.40) and (2.28) with M_∞ equal to infinity yield the following equation for the surface pressure:

$$C_{p_b} = \frac{2}{\gamma+1}\left(\frac{B}{A}\right)^2 \left[\frac{2\,\bar{x}^{3/2}-1}{\bar{x}^{1/2}(\bar{x}^{3/2}-1)^{2/3}}\right] .$$

However, since

$$\frac{B^2}{A^2} = \left(\frac{\gamma+1}{2}\right)^2 \theta_b^2$$

it follows that

$$C_{p_b}/\theta_b^2 = \frac{\gamma+1}{2}\left[\frac{2\bar{x}^{3/2}-1}{\bar{x}^{1/2}(\bar{x}^{3/2}-1)^{2/3}}\right] . \qquad (4.43)$$

A plot of Eq. (4.43) for γ equal to 7/5 is displayed in Fig. (4.11). For $\bar{x}$ equal to infinity (4.43) reduces to

$$C_{p_b}/\theta_b^2 = \gamma+1 , \qquad \bar{x} = \infty ,$$

which is recognized as the value of the surface pressure coefficient on a wedge for K_δ equal to infinity.

Our investigation of blunted shocks has been restricted to power-law and hyperbolic shapes in the limit M_∞ equal to infinity. For power-law shocks the body shape is expressed algebraically. We found that for certain values of the shock power-law exponent n_s the entropy-displacement thickness contributes significantly to the body shape. The body shape and surface pressures agree well with those found by Yakura [19], Guiraud *et al.* [24] and Schneider [26]. In the case of hyperbolic

shocks we found, as did Yakura [19], that the related bodies are blunted wedges and cones. The surface pressure far downstream for the blunted wedge agrees with the value given by Chernyi [28], but the surface pressure for the blunted cone is accurate only in the Newtonian Limit. Chernyi also found that a plot of the drag coefficient for a blunted cone exhibited a minimum. However, because of the restrictions we imposed on the flow by specifying the shock shape, the drag coefficient given by the present theory does not have a minimum.

CHAPTER V

CONSTANT RADIUS AND CONSTANT THICKNESS BODIES

Shock Shape and Pressure Distribution

In previous chapters we dealt with the inverse problem. In this chapter a special case of the direct problem is considered, that is, non-growing bodies. The shock shapes for these bodies were developed in Chapter II and are given by Eq. (2.26). If Eq. (2.26) is recast by a transformation into physical coordinates, the shock shape has the form

$$x = \frac{1}{K_j} \int_{r_{s1}}^{r_s} \frac{r^{j+1} dr}{[r^{j+1} + r_{b/2\varepsilon}^{j+1} + K_{j+2}(r^{j+1} - r_b^{j+1})^{-2\varepsilon}]^{\frac{1}{2}}}. \qquad (5.1)$$

Evaluation of the constants of integration requires a knowledge of the shock shape in the region of the nose. In general this information is not available from the present theory and must be obtained by some other means. If the nose shock shape is known, the downstream shock shape can be determined from Eq. (5.1). However, it is preferrable if the asymptotic shock shape is obtained without a knowledge of the nose shock shape. To accomplish this we shall assume that at the initial point of integration of Eq. (5.1), the shock is

attached to the body. For a flat-faced body we have the situation depicted in Fig. (5.1).

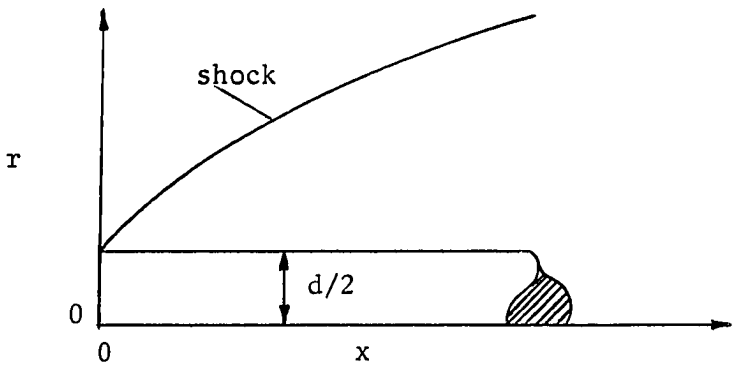


Figure 5.1. Illustration of the shock attachment.

Having made the assumption that the shock is attached to the leading-edge of the body, we require that the shock slope r_s' and the shock curvature r_s'' remain finite at the point of attachment. To satisfy these requirements we set the constants K_{j+2} equal to zero. Thus, differentiation of Eq. (5.1) yields

$$K_j = \frac{r_s' r_s^{j+1}}{(r_s^{j+1} + r_{b/2\varepsilon}^{j+1})^{\frac{1}{2}}} \quad . \tag{5.2}$$

The problem of determining the shock shape has been considerably simplified because K_j can now be evaluated in terms of the nose drag.

The drag on a slender body is given by Eq. (2.32). If Eq. (5.2) is substituted into (2.32) with M_∞ equal to infinity, the drag can be expressed as

$$D(x) = \frac{\rho_\infty v_\infty^2 2^{2-j}\pi^j}{\gamma+1}\left[\frac{1}{\gamma-1}\frac{r_s^{j+1}-r_b^{j+1}}{2r_s^{j+1}}K_j^2 + \frac{1}{\gamma+1}\frac{K_j^2}{r_s^{j+1}}(r_s^{j+1}+r_{b/2\varepsilon}^{j+1})\right]$$

which after further simplifications, reduces to

$$D(x) = D_N = \rho_\infty v_\infty^2 2^{2-j}\pi^j K_j^2\left[\frac{3\gamma-1}{2(\gamma^2-1)(\gamma+1)}\right] . \qquad (5.3)$$

As expected, the drag of a non-growing body is constant and is caused by the blunt nose. It follows that

$$K_j = \left[\frac{(\gamma^2-1)(\gamma+1)}{2(3\gamma-1)}\right]^{\frac{1}{2}} C_{D_N}^{\frac{1}{2}} r_N^{(j+1)/2} ,$$

where $r_N=r_b$ is the body radius or half the thickness. Furthermore, if we define the function $f_j'(\gamma)$ as

$$f_j'(\gamma) \equiv \left[\frac{(\gamma^2-1)(\gamma+1)}{2^{j+2}(3\gamma-1)}\right]^{\frac{1}{2}} ,$$

K_j can be recast in the form

$$K_j = f_j'(\gamma) C_{D_N}^{\frac{1}{2}} d^{(j+1)/2} , \qquad (5.4)$$

where d is the diameter or thickness of the body. Substitution of the non-dimensional variables $\bar{x} = x/d$, and $\bar{r} = r/d$ into Eq. (5.1) and subsequent integration yields

$$\bar{x} = \frac{C_{D_N}^{-\frac{1}{2}}}{4f_1'(\gamma)}\left\{\bar{r}_s(4\bar{r}_s^2 + \frac{1}{2\varepsilon})^{\frac{1}{2}} - \tfrac{1}{2}(1+\frac{1}{2\varepsilon})^{\frac{1}{2}} + \right.$$

$$\left.\frac{1}{4\varepsilon}\,\ell n\,\frac{\frac{1}{2}+[\frac{1}{4}+1/(8\varepsilon)]}{\bar{r}_s+[\bar{r}_s^2+1/(8\varepsilon)]}\right\} \qquad (5.5)$$

as the shock shape for a circular cylinder, and

$$\bar{x} = \frac{C_{D_N}^{-\frac{1}{2}}}{6\varepsilon^{3/2} f_o'(\gamma)} \left[(2\varepsilon\bar{r}_s - 1)(4\varepsilon\bar{r}_s + 1)^{\frac{1}{2}} - (\varepsilon - 1)(2\varepsilon + 1)^{\frac{1}{2}} \right] \tag{5.6}$$

as the shock shape for a flat-plate. As $\bar{r}$ tends to infinity the shock shape has the form

$$\bar{r} \sim f_1(\gamma) C_{D_N}^{\frac{1}{4}} \bar{x}^{\frac{1}{2}} , \qquad \bar{r} \to \infty , \tag{5.7}$$

for the circular cylinder, and

$$\bar{r} \sim f_o(\gamma) C_{D_N}^{1/3} \bar{x}^{2/3} , \qquad \bar{r} \to \infty , \tag{5.8}$$

for the flat-plate, where

$$f_j(\gamma) = \left[\frac{3-j}{2-j} f_j'(\gamma) \right]^{(2-j)/(3-j)} . \tag{5.9}$$

The pressure on the body surface is given in general form by Eq. (2.28). The term r_s'' can be expressed in terms of known quantities by differentiating Eq. (5.2). The result is

$$r_s'' = (j+1) K_j^2 r_s^{-(2+j)} \left[-r_s^{-(j+1)} \left(r_s^{j+1} + r_{b/2\varepsilon}^{j+1} \right) + \tfrac{1}{2} \right] ,$$

which upon substitution into Eq. (2.28) yields

$$\frac{p_b}{p_\infty} = \frac{2}{\gamma+1} f_j'^2 \frac{C_{D_N}}{\bar{r}^{j+1}} + 1 . \tag{5.10}$$

As $\bar{r}$ tends to infinity the surface pressure can be written in the form

$$\frac{\Delta p}{\frac{1}{2}\rho_\infty V_\infty^2} \sim \left[\frac{\gamma-1}{8(3\gamma-1)} \right]^{\frac{1}{2}} C_{D_N}{}^{\frac{1}{2}} \bar{x}^{-1}$$

$$\sim f_1^*(\gamma) C_{D_N}{}^{\frac{1}{2}} \bar{x}^{-1} , \qquad \bar{r} \to \infty, \tag{5.11}$$

for the circular cylinder, and

$$\frac{\Delta P}{\frac{1}{2}\rho_\infty V_\infty^2} \sim \left[\frac{\sqrt{2}(\gamma+1)^{\frac{1}{2}}(\gamma-1)}{3(3\gamma-1)} \right]^{2/3} C_{D_N}{}^{2/3} \bar{x}^{-2/3}$$

$$\sim f_o^*(\gamma) C_{D_N}{}^{2/3} \bar{x}^{-2/3} , \qquad \bar{r} \to \infty , \tag{5.12}$$

for the flat-plate.

Comparisons with other Theories and Experiments

In the development of Eqs. (5.5) and (5.6) we assumed that the shock is attached to the body as depicted in Fig. (5.1). The nose shape is unknown and is imagined as being flat. Thus, there is a certain amount of arbitrariness involved concerning the location of the flat nose of the theoretical body when we compare our data with the data from other theories and experiments. As an example, consider the hemisphere cylinder sketched in Fig. (5.2)



(a)



(b)

Figure 5.2. Location of the nose for the theoretical body.

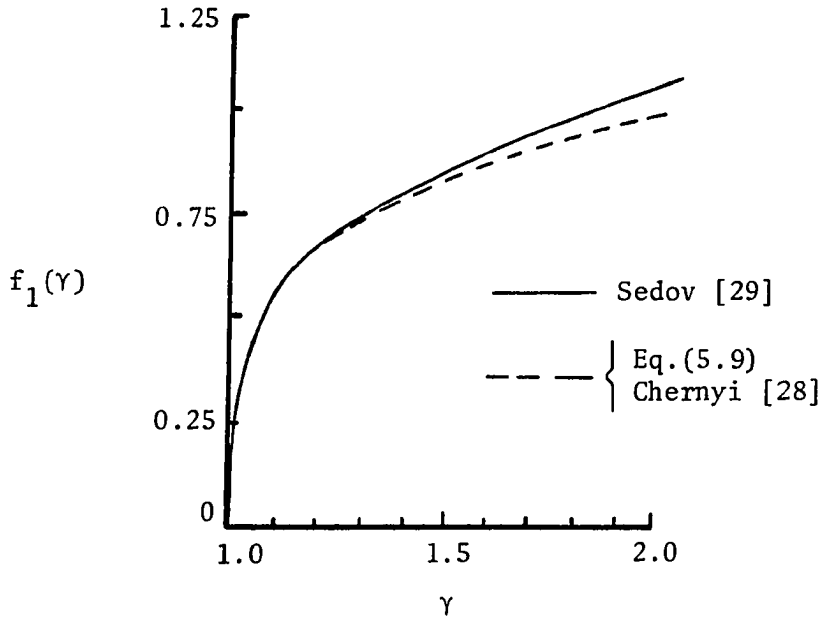
The nose of the body used in the present theory, shown by the dotted lines, could be placed at the shoulder of the hemisphere cylinder as in Fig. (5.2a). Another possibility is that both bodies could be matched at the nose as in Fig. (5.2b). The method we shall use is that depicted in Fig. (5.2b).

In the figures to follow the abcissas for all of the shock shapes are given in terms of x/d, and are measured relative to the nose of both bodies as shown in Fig. (5.2b). This is also true for the pressures when compared with the theoretical data of Van Hise, for example, Figs. (5.8) and (5.9). However, the experimental pressures given by Mueller [see Figs.(5.14-17)] are measured relative to the

shoulder of the particular nose cylinder combination. Thus, the pressures obtained from Eq. (5.10) and displayed in these figures are suitably adjusted. For instance, if the shoulder for the experimental model occurs at x/d equal to $\frac{1}{2}$, then this location is x_s/d equal to zero. The pressure at this location from the present theory is that obtained for x/d equal to $\frac{1}{2}$ in Eq. (5.10).

Equations (5.7-8) and (5.11-12) are asymptotic forms of the solutions for the shock shape and pressure distribution. In a functional form, they correspond to the exact solutions for a violent explosion of a line and plane charge (blast-wave solutions) as presented by Sedov [29]. Chernyi [28, pp. 209,215] obtains the same functional forms for the flow past a circular cylinder and flat-plate. He also considered the flow past blunted cones and wedges and obtained analytic expressions for the shock shape and pressure distribution in the limit δ (body half angle) equal to zero. In this limit the functions $f_j(\gamma)$ and $f_j^*(\gamma)$ obtained by Chernyi are algebraically identical to those given by the present solutions. The variations of f_j and f_j^* with γ are shown in Figs. (5.3) and (5.4), and are compared with the numerical values found by Sedov.

Van Hise [44] studied the induced pressures and shock shapes on long bodies of revolution with varying nose bluntness. He used the method of characteristics and assumed a perfect gas. The fluid mediums investigated were air and helium, and the Mach number range was 5 to 40. He also found that the shock shapes and pressures computed by the theory of characteristics could be approximated by semi-empirical equations



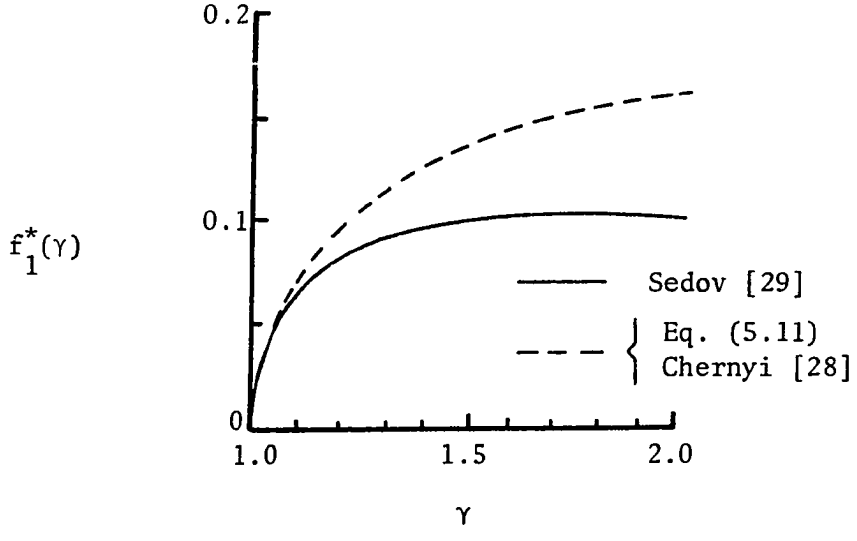
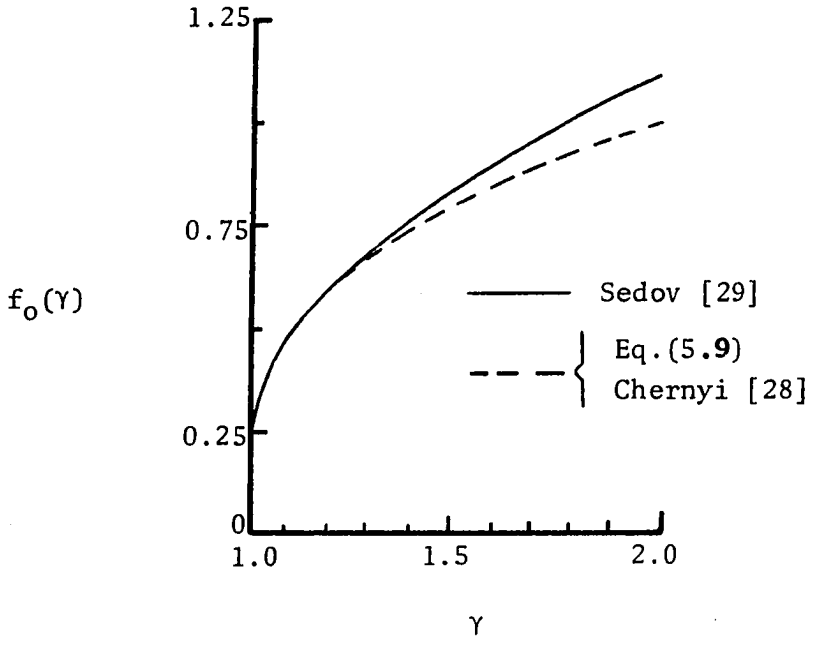


Figure 5.3. Variation of f_1 and f_1^* with γ.



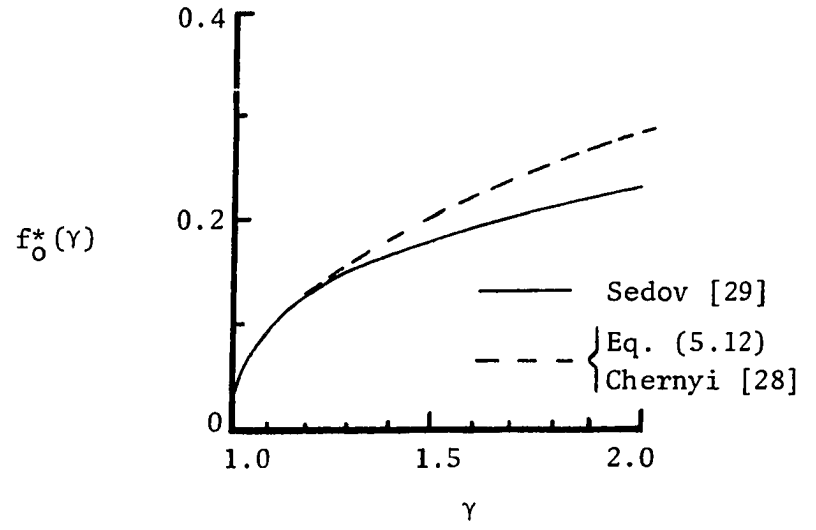


Figure 5.4. Variation of f_o and f_o^* with γ.

from second-order blast-wave theory. These equations for air and helium, respectively, are:

$$\bar{r} = 0.98(\bar{x}\, C_{D_N}{}^{\frac{1}{2}})^{0.46} \quad , \tag{5.13a}$$

$$\frac{p}{p_\infty} = 0.06\, \frac{M_\infty^2 C_{D_N}{}^{\frac{1}{2}}}{\bar{x}} + 0.55 \quad , \tag{5.13b}$$

and

$$\bar{r} = 1.07(\bar{x}\, C_{D_N}{}^{\frac{1}{2}})^{0.46} \quad , \tag{5.14a}$$

$$\frac{p}{p_\infty} = 0.075\, \frac{M_\infty^2 C_{D_N}{}^{\frac{1}{2}}}{\bar{x}} + 0.55 \quad . \tag{5.14b}$$

Lukasiewicz [45] presents blast-analogy solutions derived from the first and second-order blast-wave approximations developed by Sakurai [10,11]. The second-order approximations given by Lukasiewicz for γ equal to 7/5 are

$$\bar{r} = \frac{M_\infty^2 C_{D_N}(0.774)}{M_\infty^2 (C_{D_N}/\bar{x})^{2/3} - 1.09} \quad , \tag{5.15a}$$

$$\frac{p}{p_\infty} = 0.121\, M_\infty^2 (C_{D_N}/\bar{x})^{2/3} + 0.56 \tag{5.15b}$$

for plane flow, and

$$\bar{r} = M_\infty C_{D_N}{}^{\frac{1}{2}} (0.834) \left(\frac{\bar{x}}{M_\infty^2 C_{D_N}{}^{\frac{1}{2}}}\right)^{\frac{1}{2}} \left(1 + \frac{2.86\, \bar{x}}{M_\infty^2 C_{D_N}{}^{\frac{1}{2}}}\right)^{\frac{1}{2}} \quad , \tag{5.16a}$$

$$\frac{p}{p_\infty} = 0.074\, \frac{M_\infty^2 C_{D_N}{}^{\frac{1}{2}}}{\bar{x}} + 0.44 \tag{5.16b}$$

for axisymmetric flow.

Figures (5.5-9) display shock shapes and pressure distributions which are typical of the results obtained by Van Hise. Equations (5.5) and (5.10) representing the shock shapes and surface pressures from the present theory are also shown. In addition, in Figs. (5.5), (5.7), and (5.9) these results are compared with Eqs. (5.16) given by Lukasiewicz.

Generally, the agreement among the theories presented is good. For the shock shapes the agreement of the data is quite good for x/d not too near the nose. The surface pressures agree rather well for x/d not too near the shoulder. In Figs. (5.8) and (5.9) the pressures from Eq. (5.10) are computed with the counterpressure term ($p_\infty = 1.0$) neglected.

Mueller *et al.* [46] experimentally investigated the induced pressures and shock shapes on axisymmetric cylindrical models with various nose shapes. The tests were accomplished in the Langley Research Center 2-inch helium tunnel at free-stream Mach numbers from 15.6 to 21. The models were 0.090-inch-diameter circular cylinders with a length of 5 inches.

Figures (5.10-13) display the shock coordinates obtained by Mueller for circular cylinders with a modified hemispherical nose, hemispherical nose, 90° conical nose, and a flat-nose, respectively. Figures (5.14-17) show the variation in surface pressure for the same nose-cylinder combinations. Also shown in all figures are the smooth curves computed from Eqs. (5.5) and (5.10). The shock shapes are seen to agree very well for x/d not too near the nose. In Figs. (5.11) and (5.13) the data obtained by Vas (discussed below) are displayed, and yield shapes

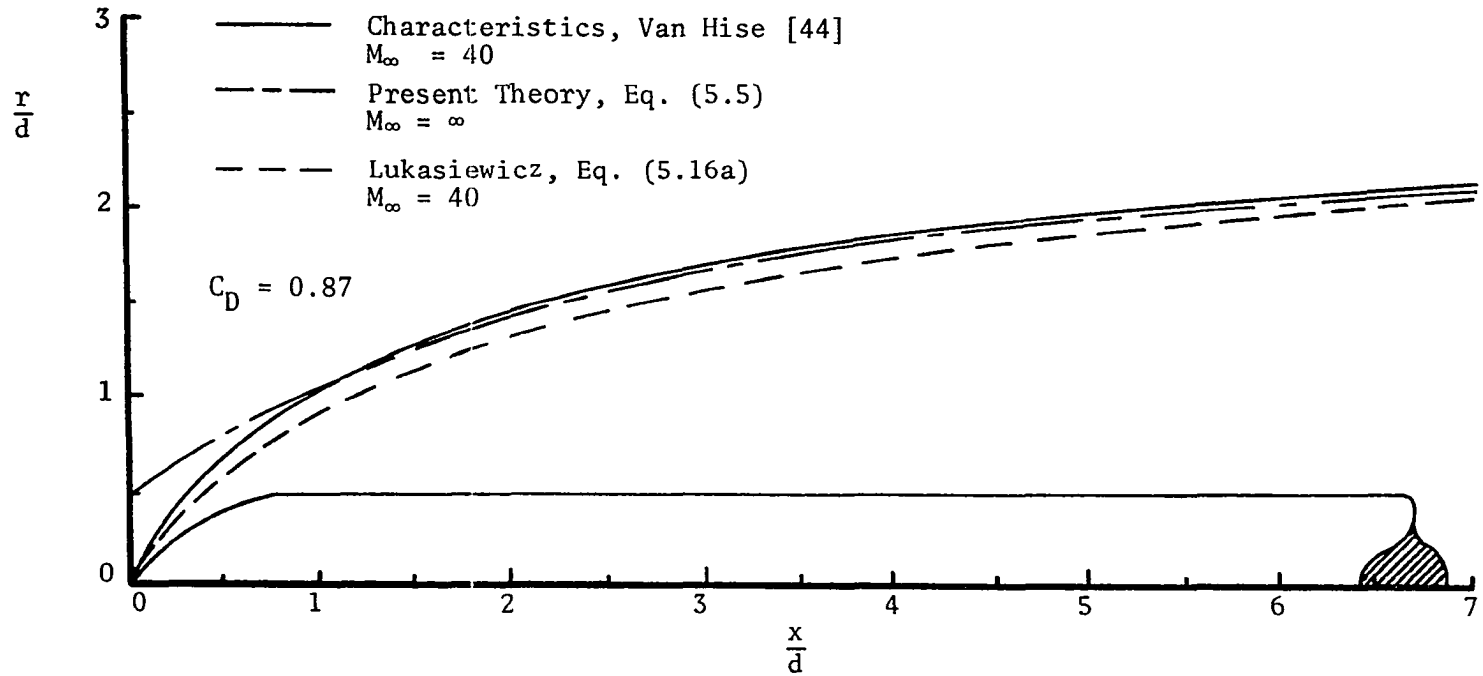


Figure 5.5. Shock shape for a circular cylinder with a pointed hemispherical nose (γ = 7/5).

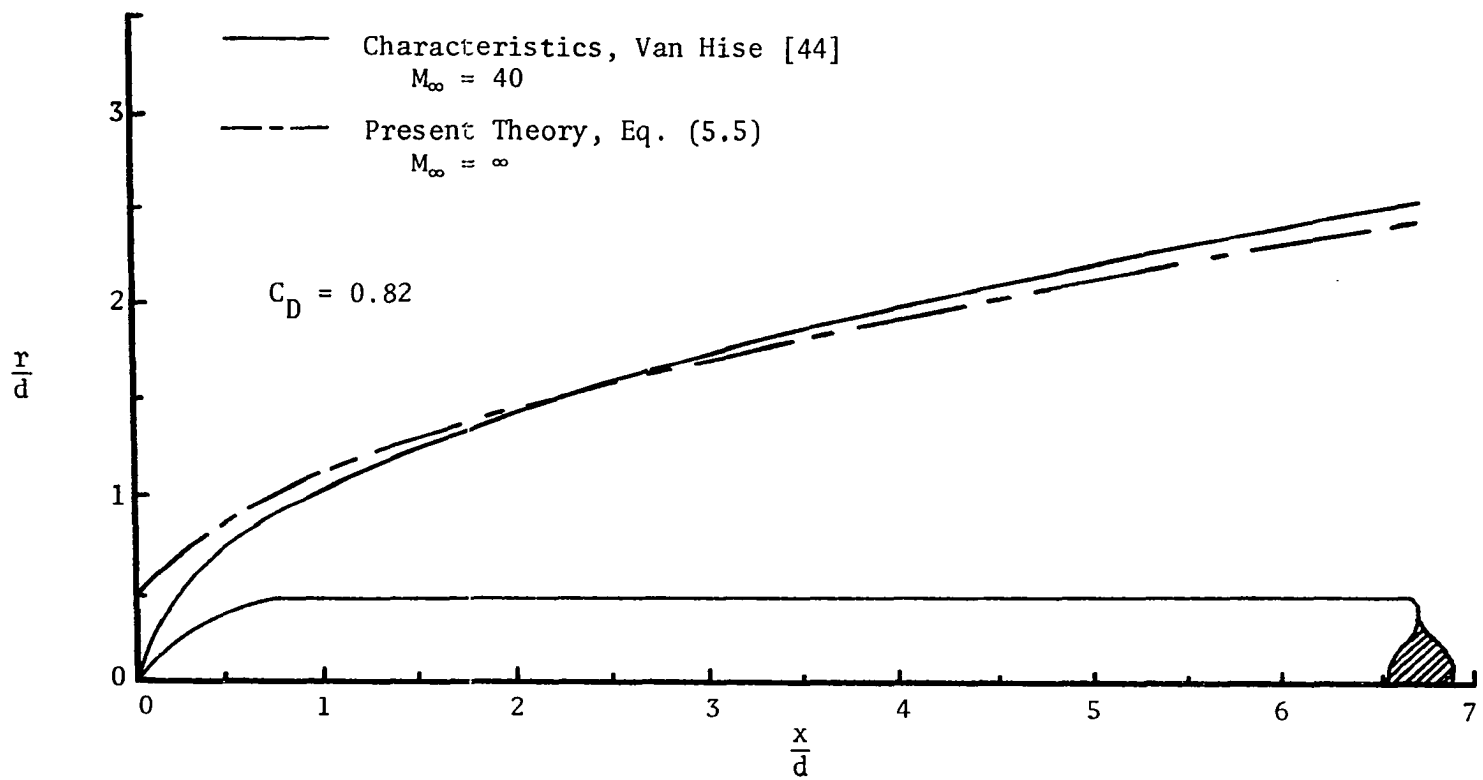


Figure 5.6. Shock shape for a circular cylinder with a pointed hemispherical nose (γ=5/3).

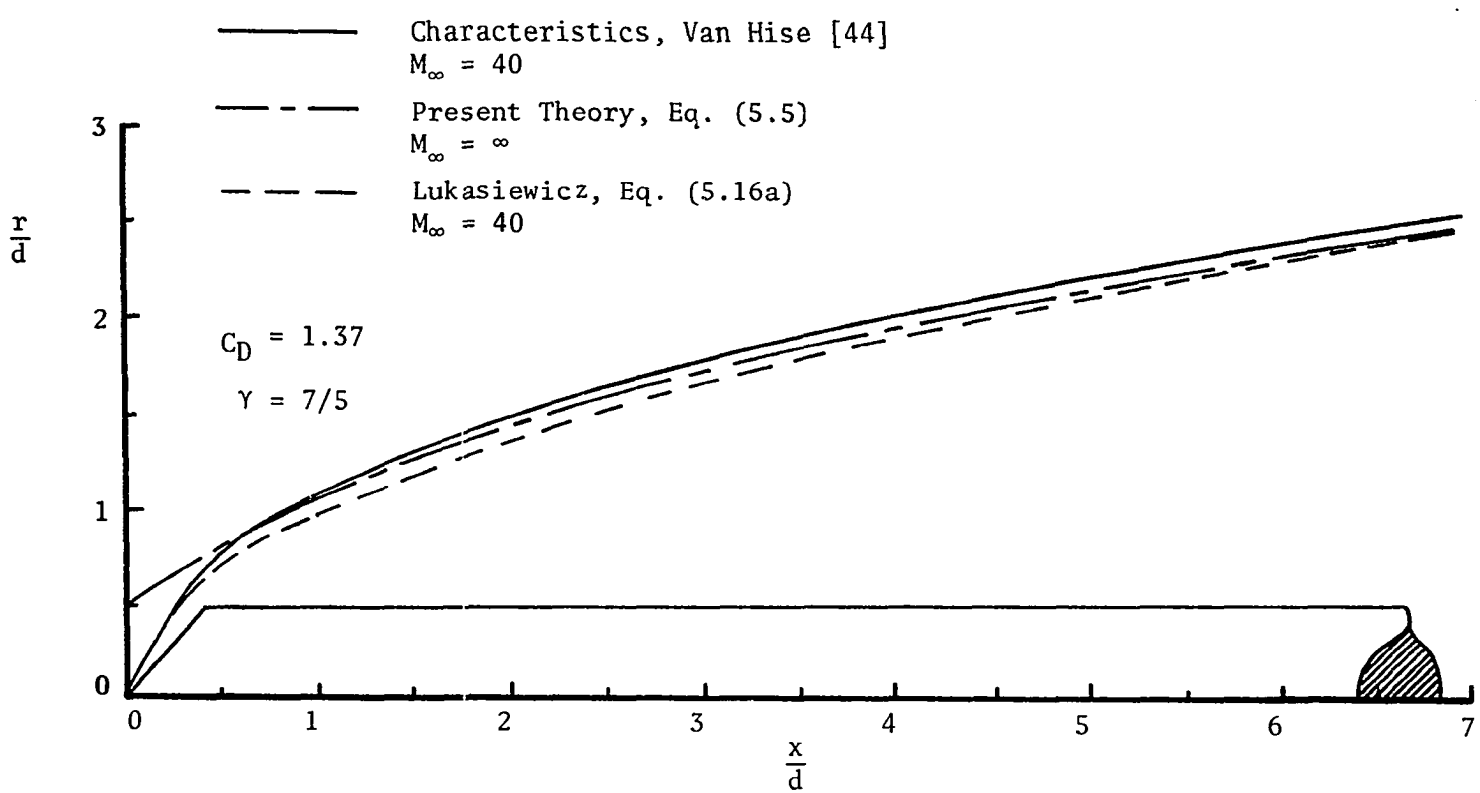


Figure 5.7. Shock shape for a circular cylinder with a conical nose.

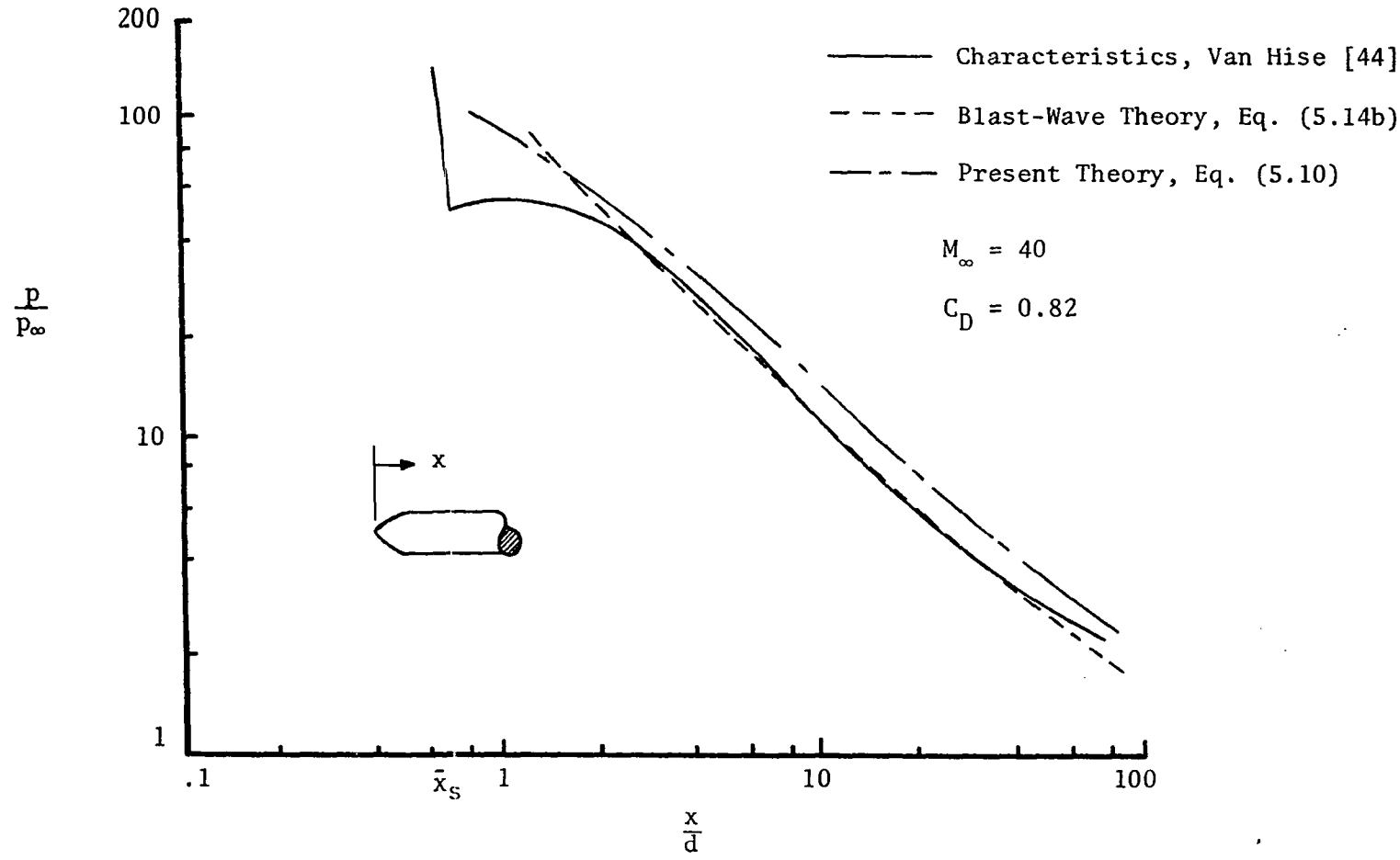


Figure 5.8. Surface pressure on a circular cylinder with a pointed hemispherical nose (γ=5/3).

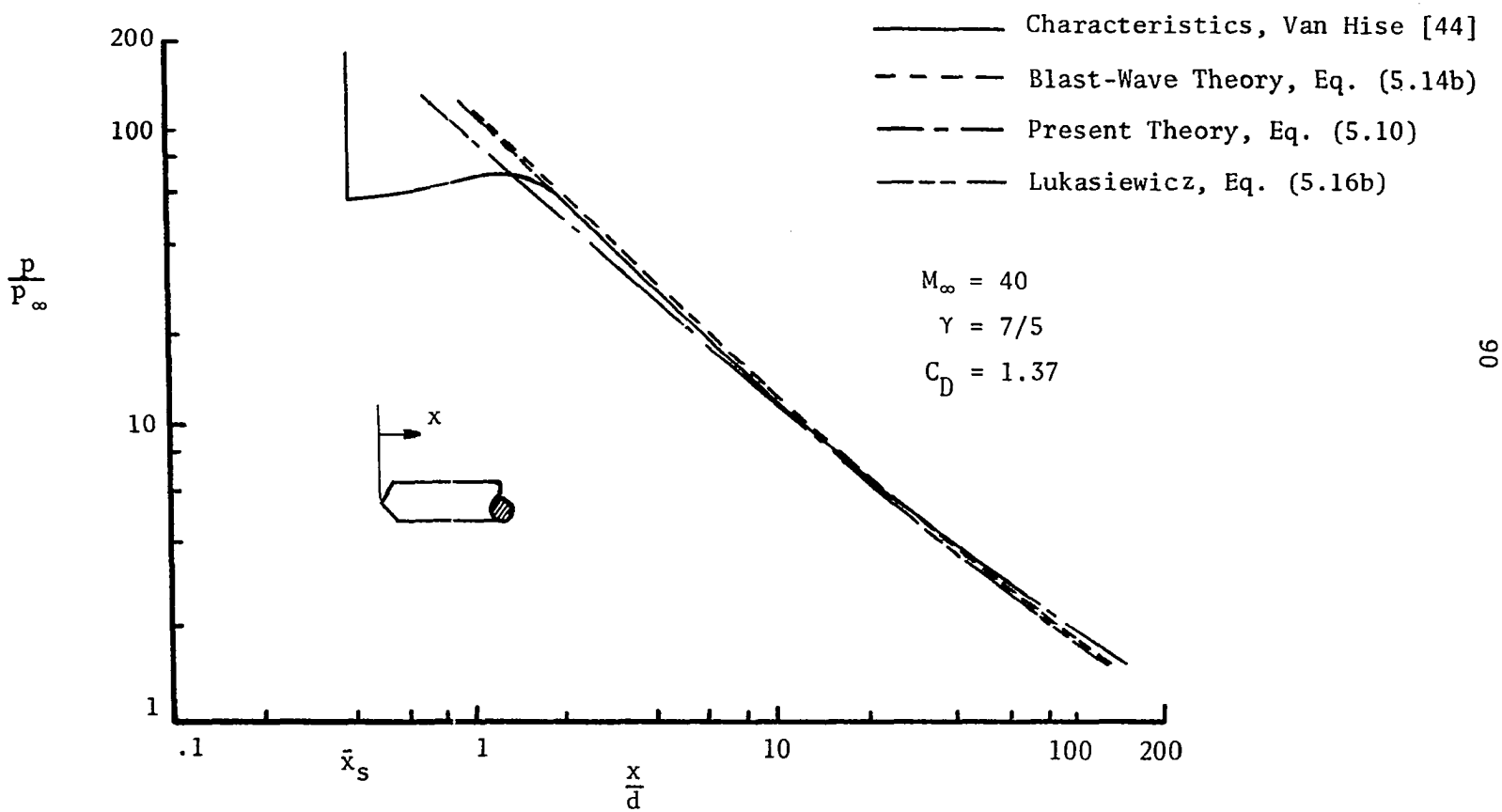


Figure 5.9. Surface pressure on a circular cylinder with a conical nose.

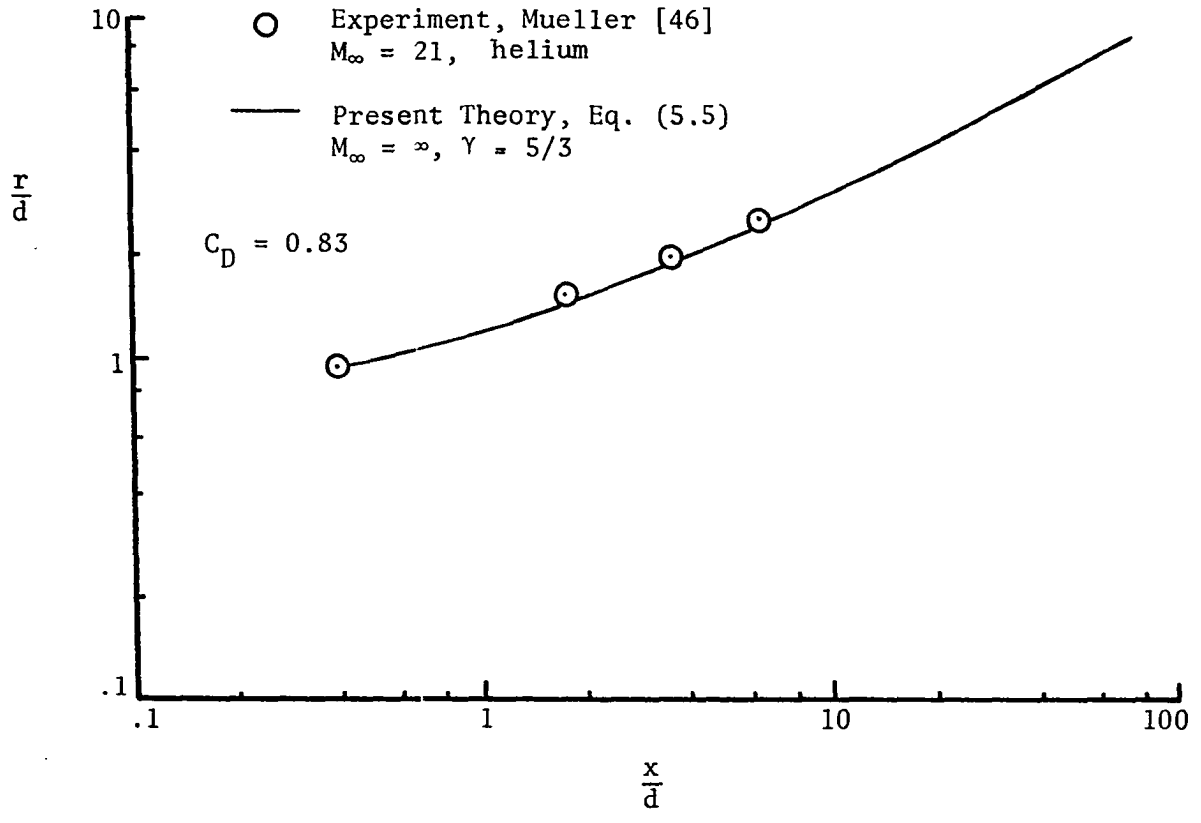


Figure 5.10. Shock coordinates for a circular cylinder with a modified hemispherical nose.

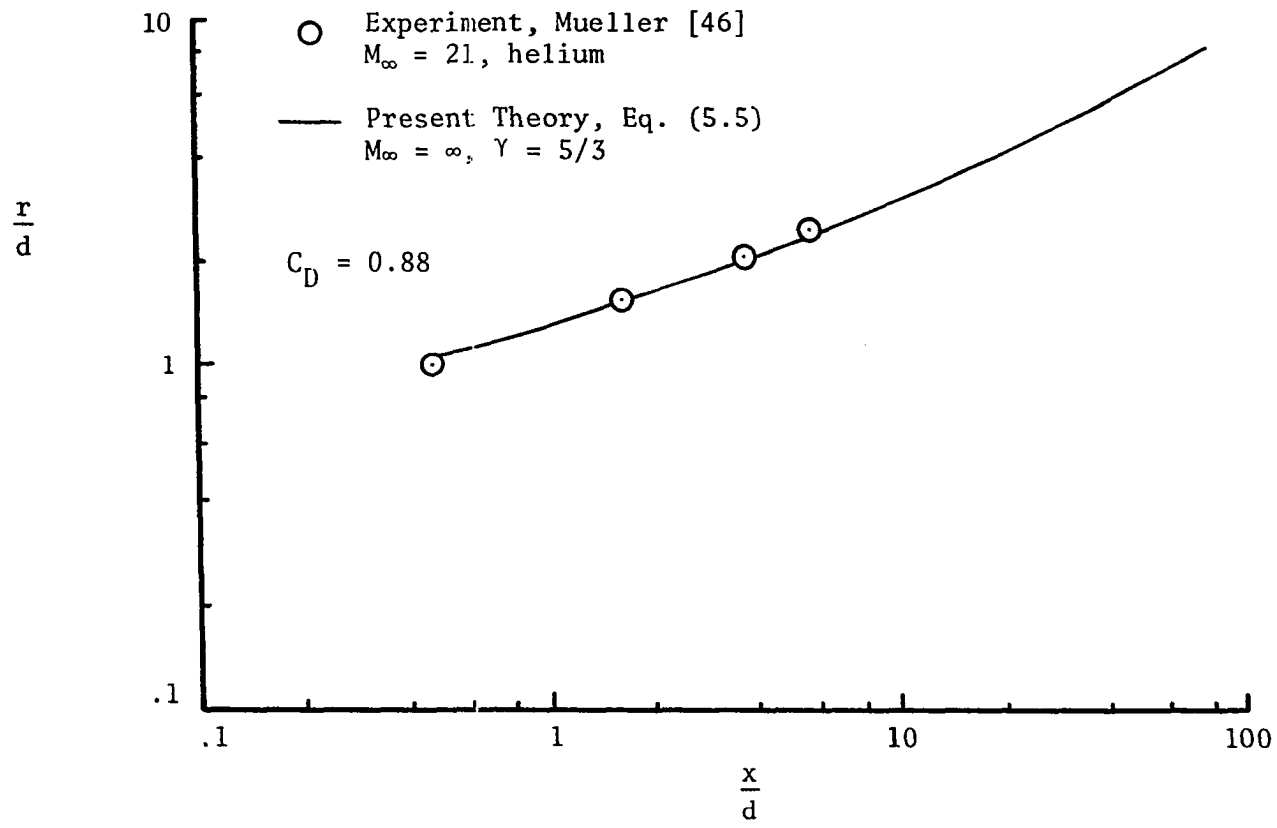


Figure 5.11. Shock coordinates for a circular cylinder with a hemispherical nose.

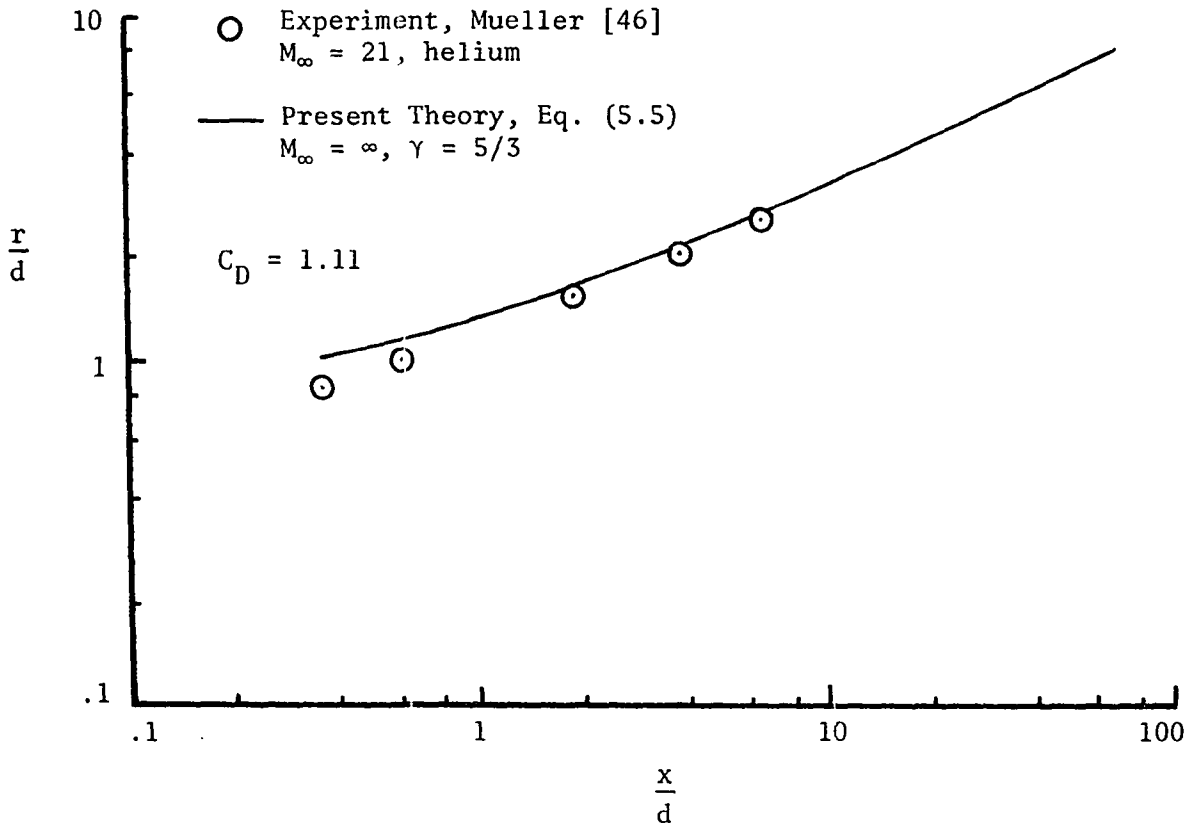


Figure 5.12. Shock coordinates for a circular cylinder with a 90° conical nose.

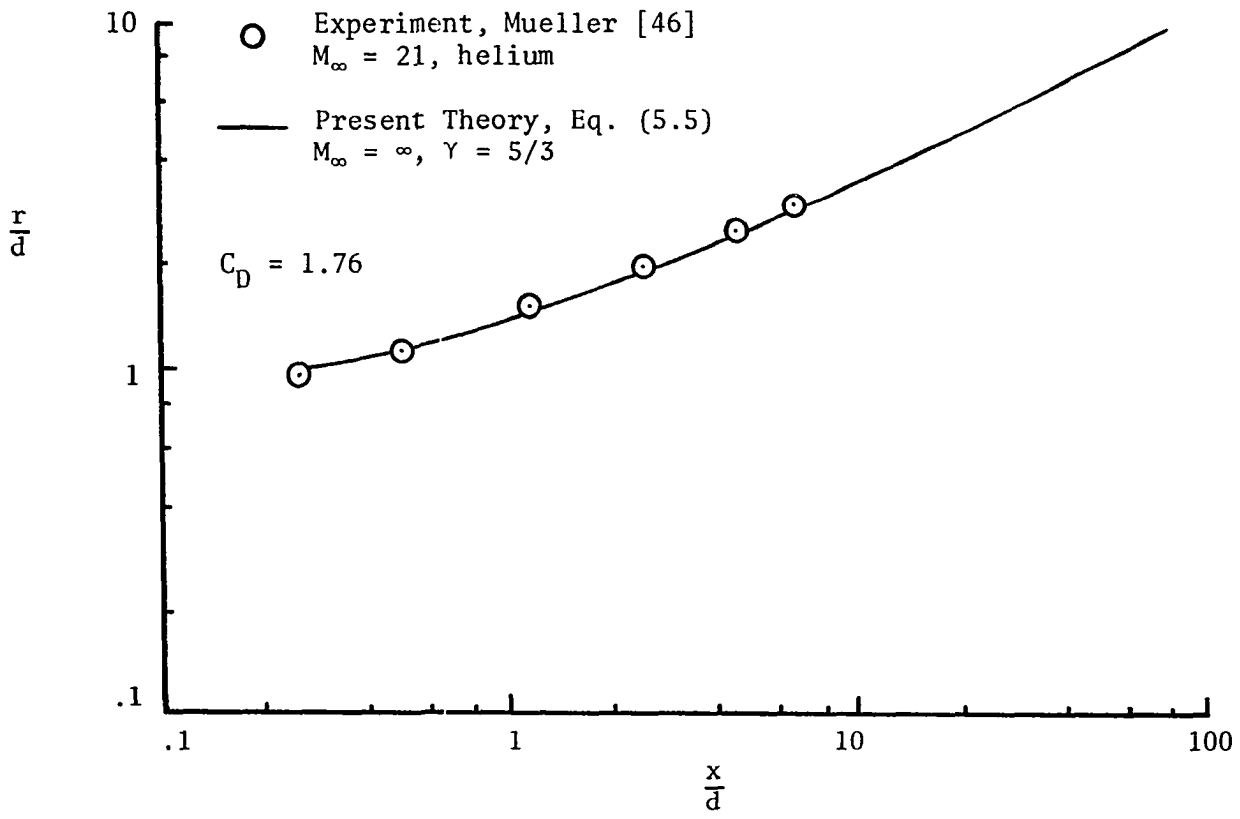


Figure 5.13. Shock coordinates for a circular cylinder with a flat nose.

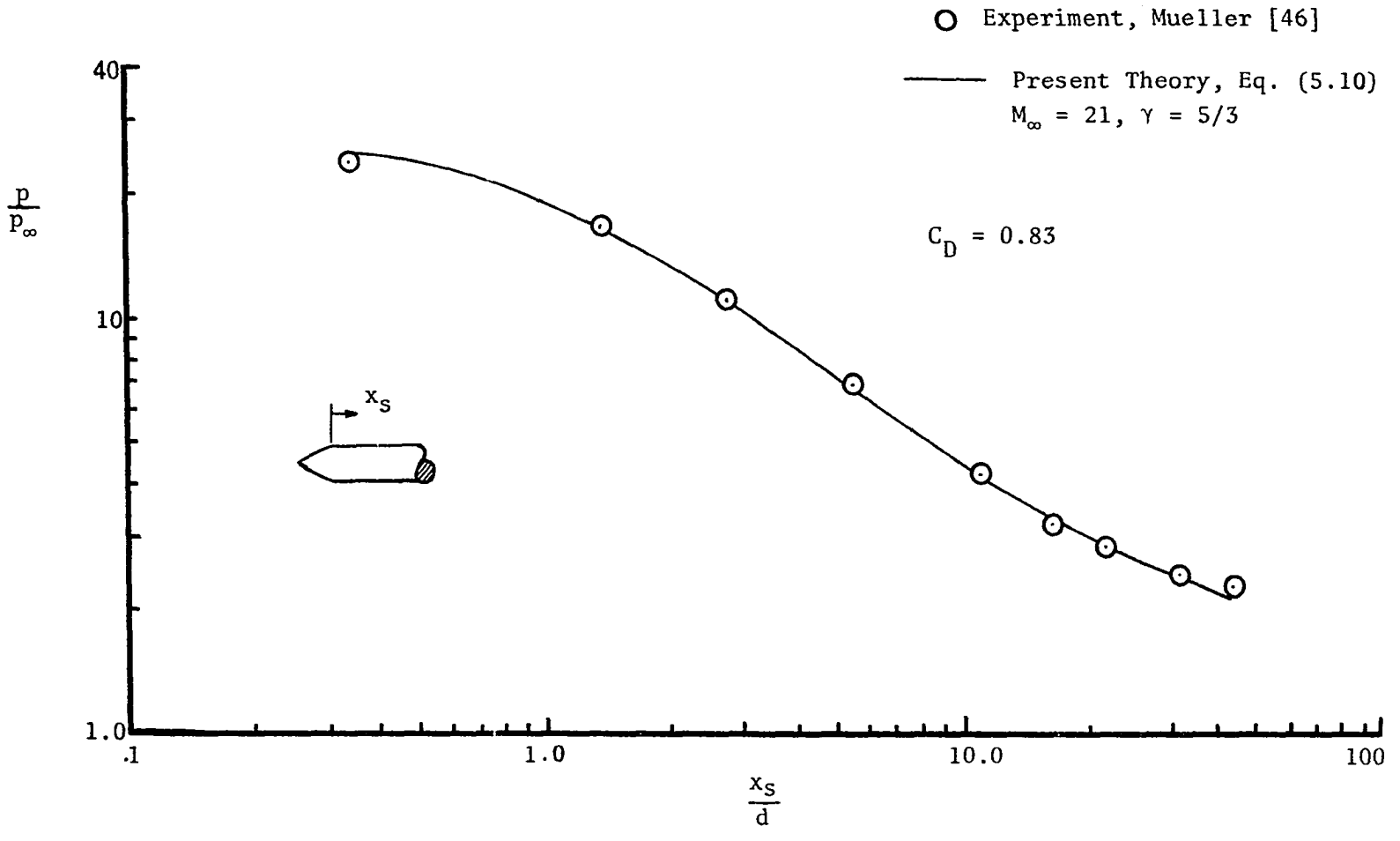


Figure 5.14. Surface pressure on a circular cylinder with a modified hemispherical nose.

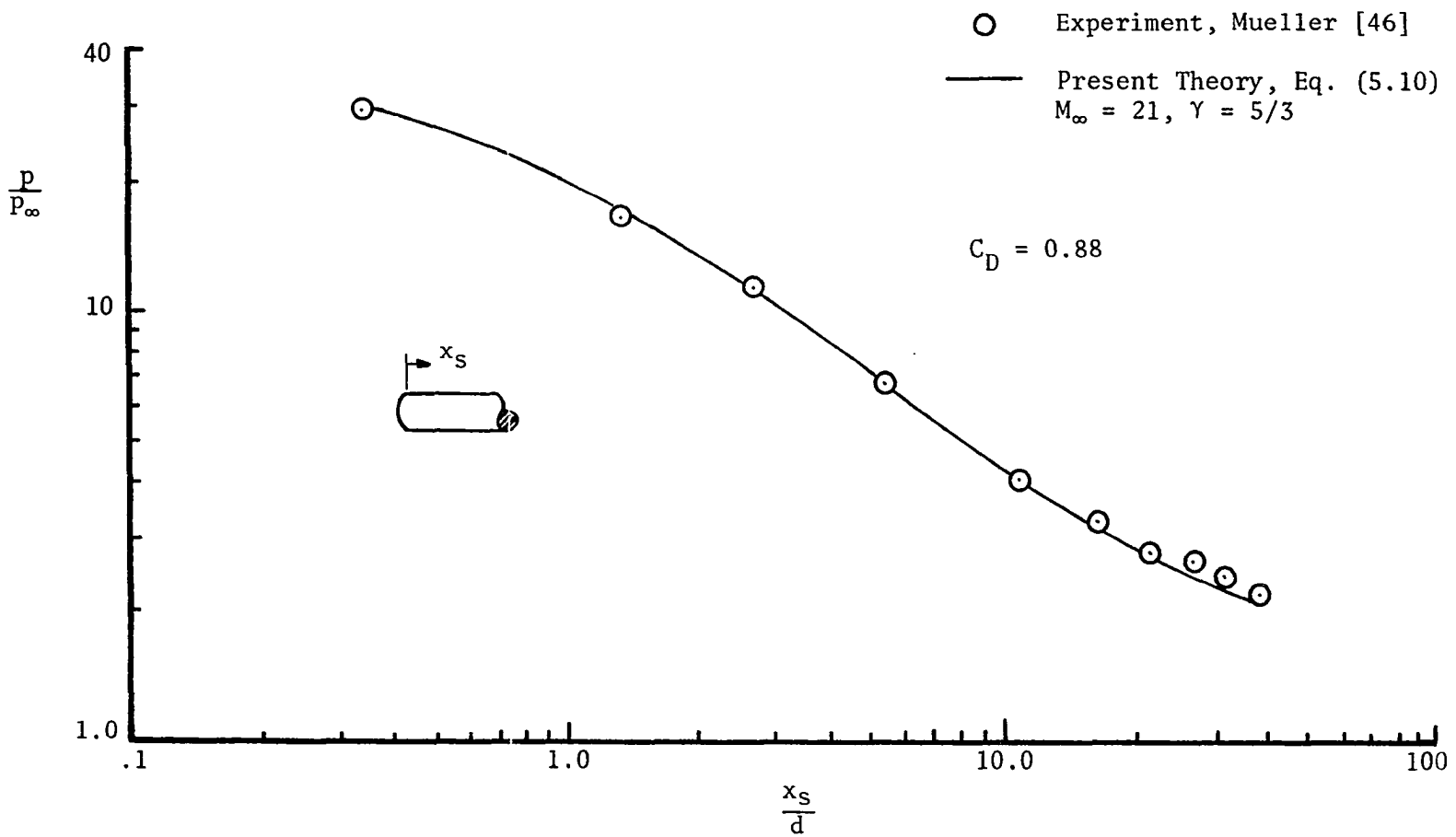


Figure 5.15. Surface pressure on a circular cylinder with a hemispherical nose.

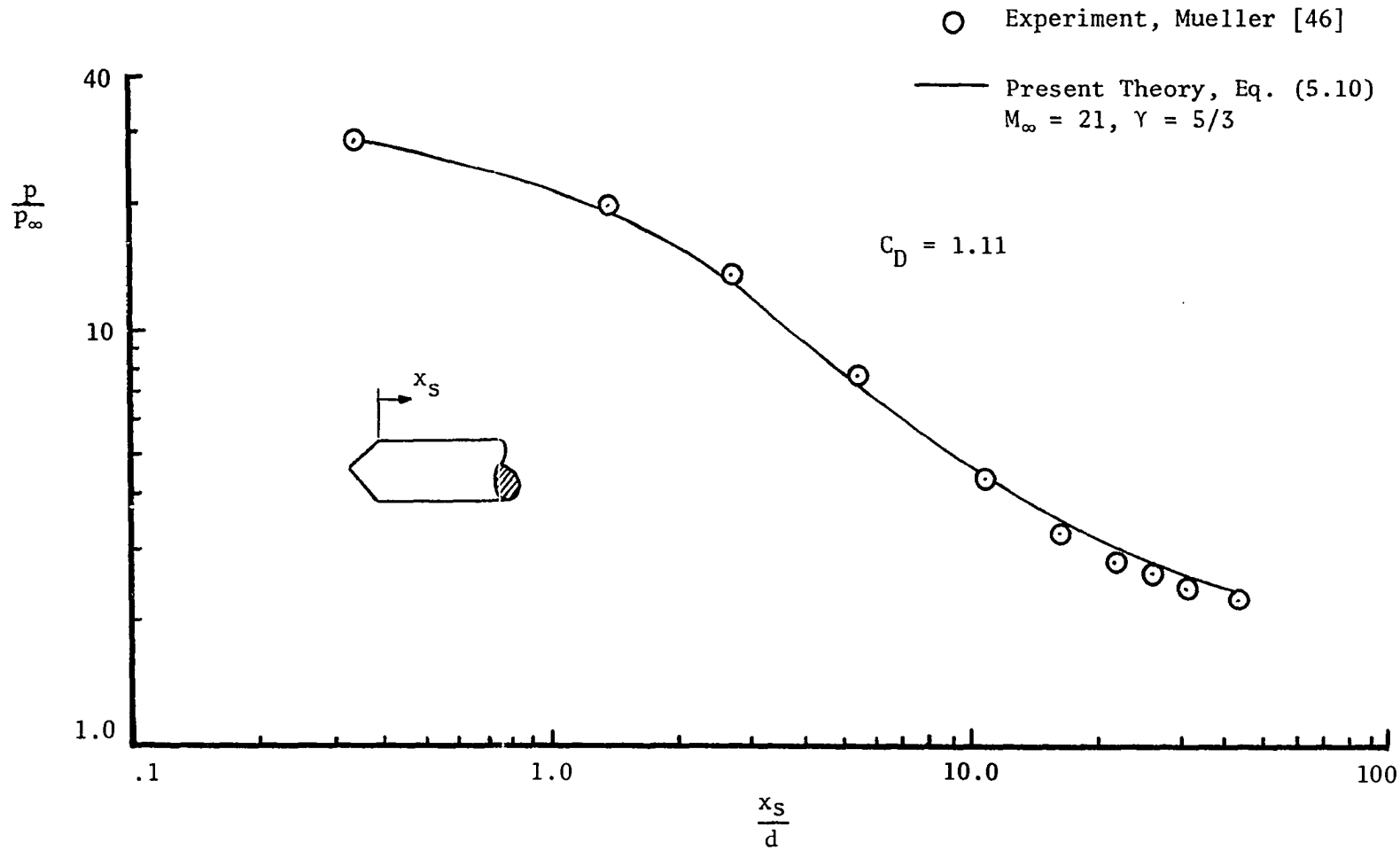


Figure 5.16. Surface pressure on a circular cylinder with a 90° conical nose.

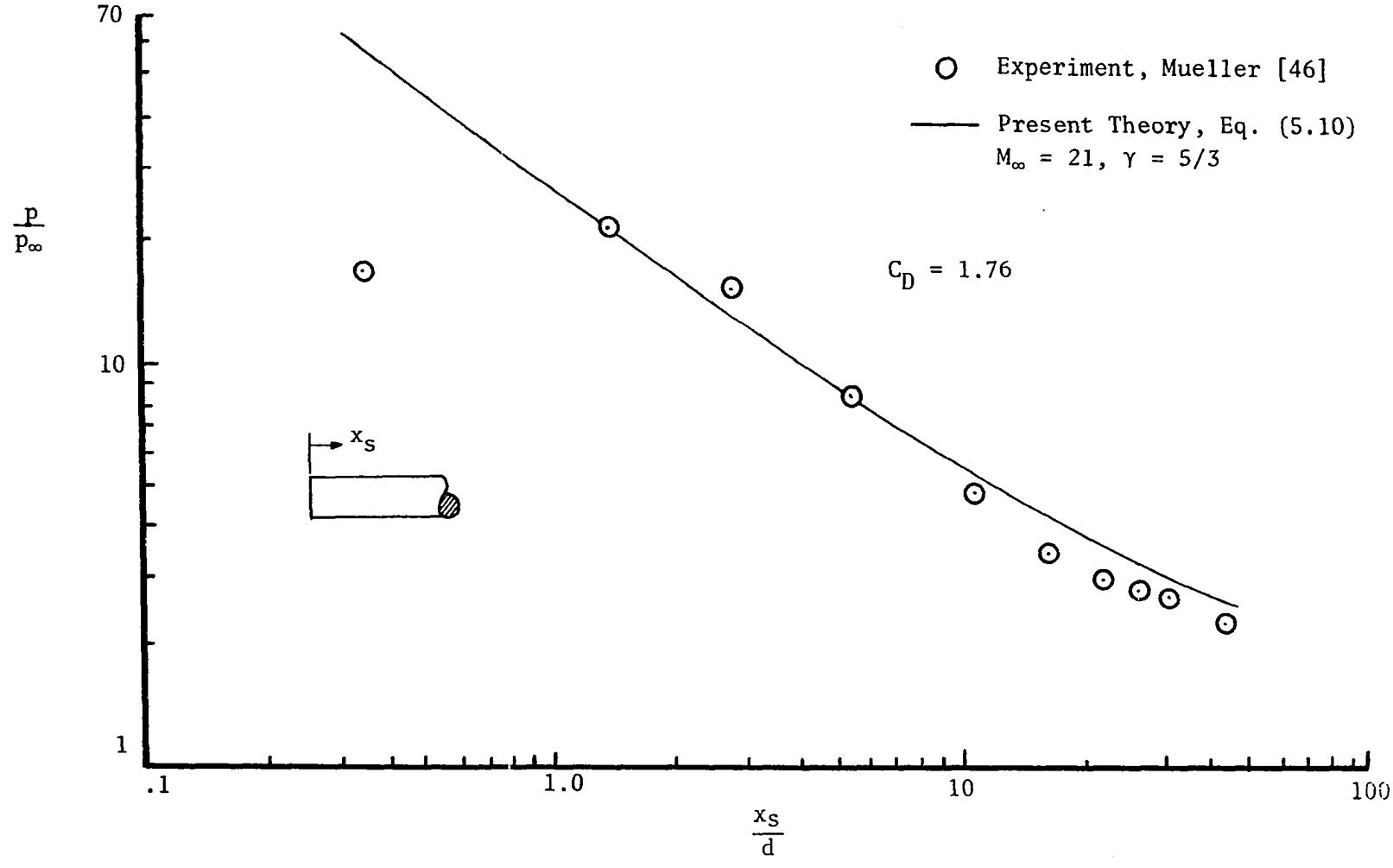


Figure 5.17. Surface pressure on a circular cylinder with a flat nose.

which are somewhat larger than those found by Mueller and the present theory. This is probably due in part to the relatively low Mach number ($M_\infty \simeq 13$) of the tests conducted by Vas.

Vas *et al.* [47] experimentally investigated the shock shapes about cylinders and flat-plates with hemispherical, hemicylindrical and flat leading edges. Tests were conducted in the Princeton University helium hypersonic tunnel at a Mach number of approximately 13. They found that the shock shapes could be approximated quite well by

$$\bar{r} = 2.0\ \bar{x}^{0.49} \tag{5.17a}$$

and

$$\bar{r} = 1.75\ \bar{x}^{0.50} \tag{5.17b}$$

for flat plates with square and round leading edges, respectively, and

$$\bar{r} = 1.4\ \bar{x}^{0.42} \tag{5.18a}$$

and

$$\bar{r} = 1.1\ \bar{x}^{0.45} \tag{5.18b}$$

for circular cylinders with flat and hemispherical noses, respectively. The shock shapes observed for the flow around the cylinders are displayed in Figs. (5.11) and (5.13). Shock shapes from the tests conducted for flat-plates are shown in Figs. (5.18) and (5.19), and are compared with the shapes computed from Eq. (5.6).

Cheng *et al.* [16] obtained the shock shapes for the flow over flat-nosed flat plates, in the Cornell Aeronautical Laboratory hypersonic shock tunnel, for a Mach number of about 12. Data points for the

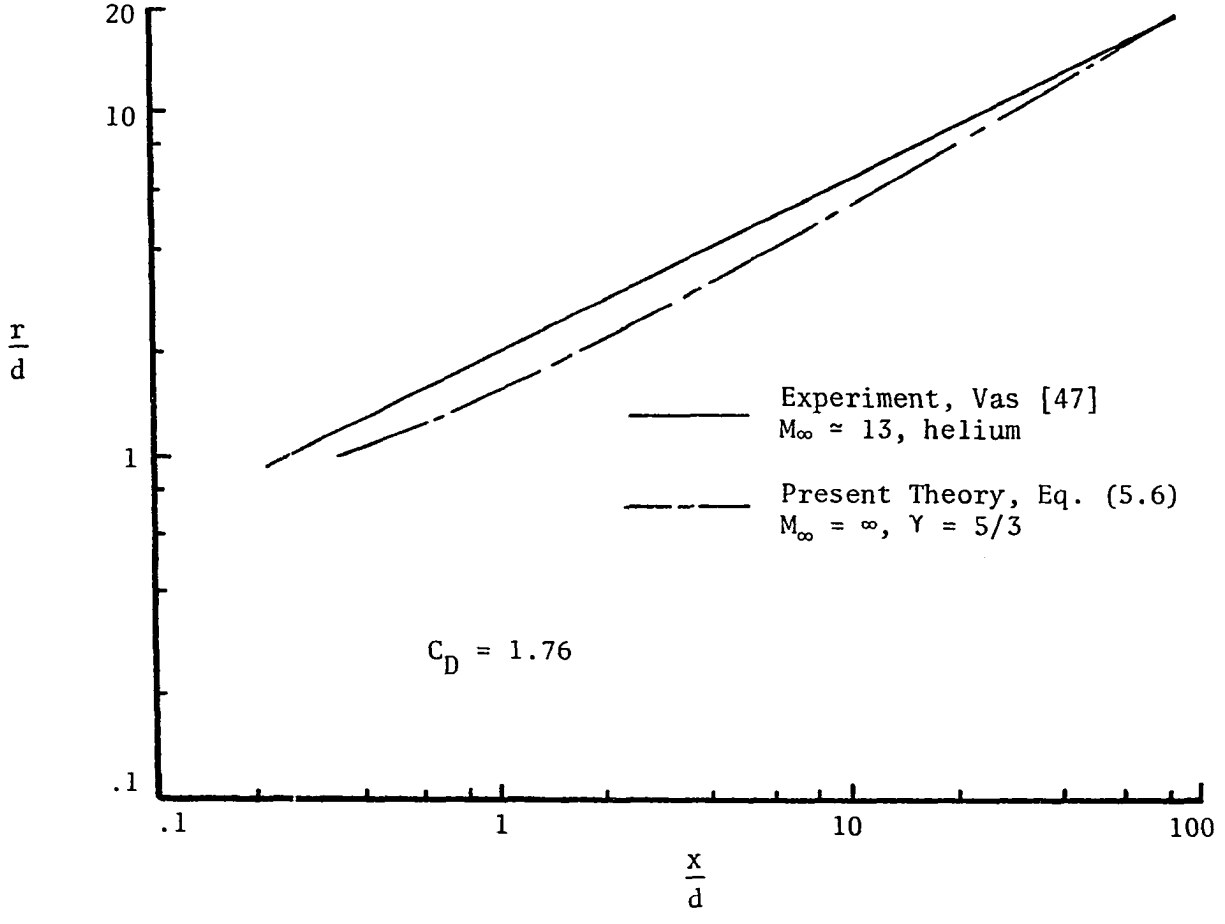


Figure 5.18. Shock coordinates for a flat leading-edge plate in helium.

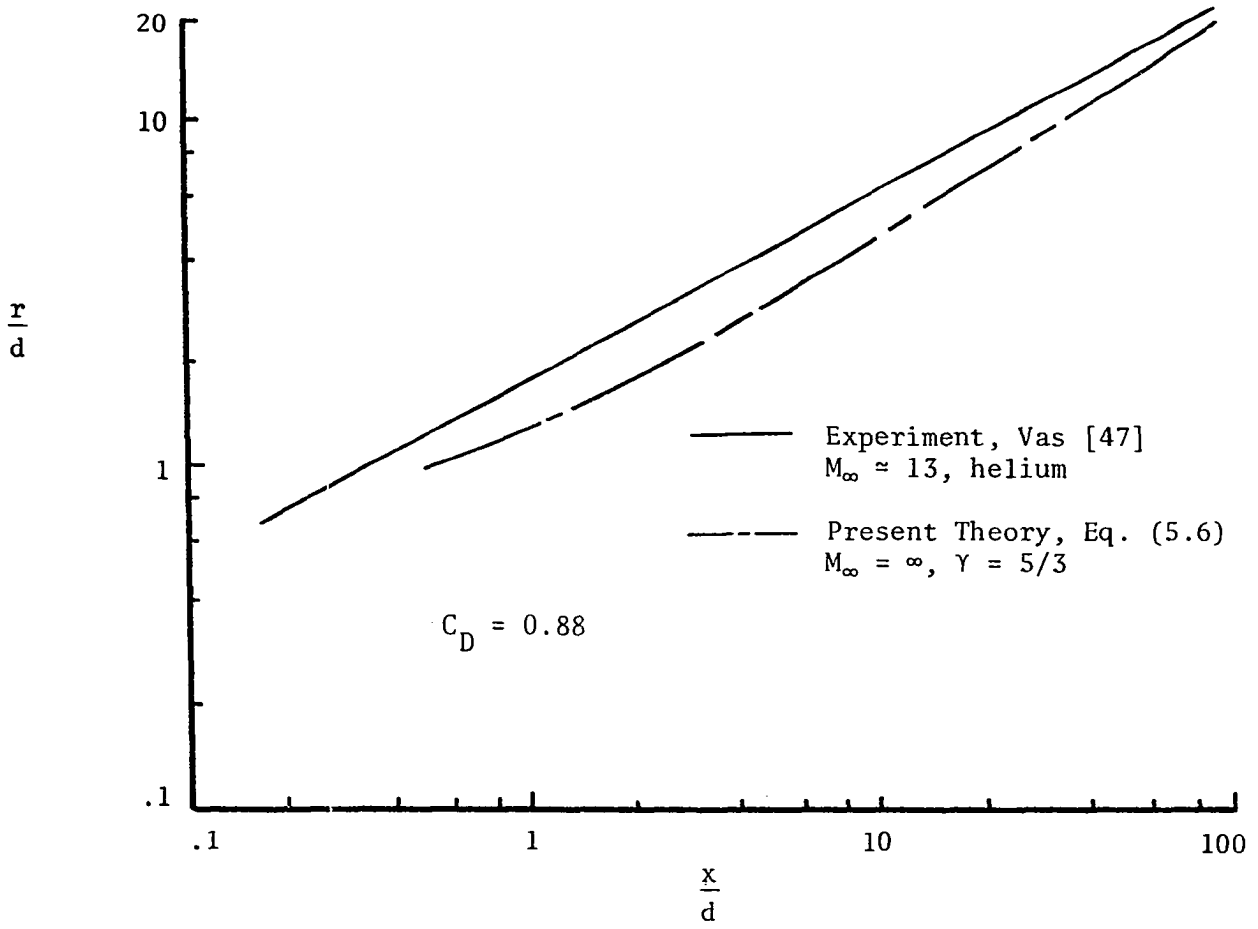


Figure 5.19. Shock coordinates for a flat-plate with a hemicylindrical leading-edge.

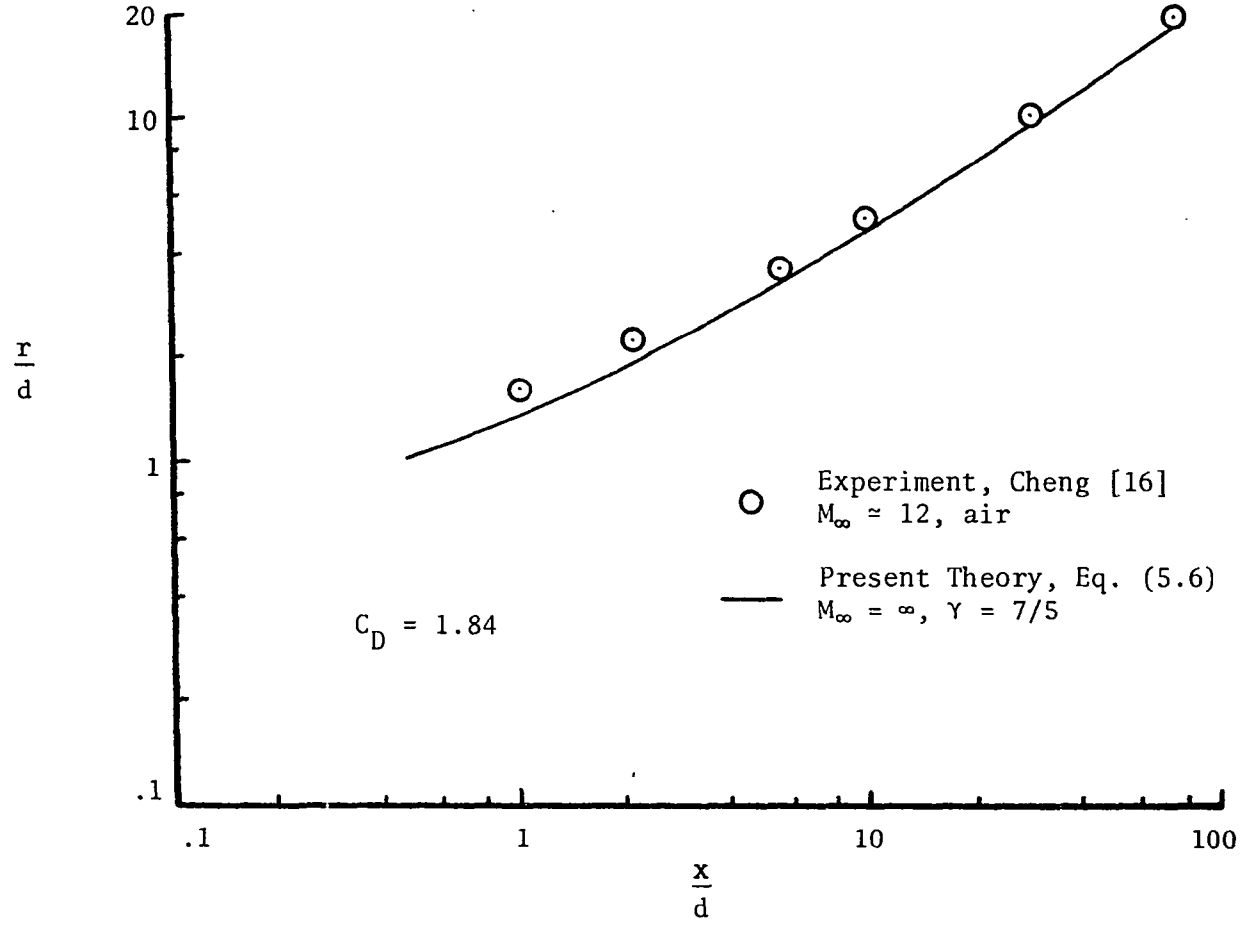


Figure 5.20. Shock coordinates for a flat leading-edge plate in air.

correlated shock shapes from several models are plotted in Fig. (5.20). Also shown are curves given by Eq. (5.6) of the present theory, and Eq. (5.15a) from Lukasiewicz's development.

The agreement among the various data is, in general, considered good especially for larger values of x/d. Again, Vas's data yield shock coordinates somewhat larger than the present theory for values of x/d not too large. However, the power-law exponent predicted by Vas [see Eqs. (5.17)] is considerably lower than the present theory which yields a value of about 0.61 for x/d≈25. This accounts for the improved agreement between the shock coordinates for large x/d.

Additional Considerations

From the preceeding analysis it is evident that for aerodynamically blunt non-growing bodies, the present theory yields acceptable approximate analytical solutions. However, if the nose of a non-growing body is very slender, such as the cone-cylinder depicted in Fig. (5.21), some additional considerations are necessary.



Figure 5.21. The slender cone-cylinder.

For slender conical and ogival forebodies the nose shock shapes can be found from the analyses presented in Chapter III. It follows that by properly joining the nose shock with the afterbody shock given by Eq. (5.1), a shock which seems to be valid downstream of the nose is determined. As an example, we consider three alternative methods for determining the shock shape about a cone-cylinder.

With the first method the shock shape over the conical portion of the body is known from Eq. (3.3). If the shock slope r_s' is to be continuous at the shoulder, then the shock slope found from Eq. (5.1) must have the same value as that given by the conical solution. At the shoulder we assume r_s'' is equal to zero. With r_s' and r_s'' specified the constants of integration K_j and K_{j+2} are evaluated; subsequently, the afterbody shock shape is found by integrating Eq. (5.1). In the second method we again begin with a known conical shock. However, we assume the surface pressure at the shoulder is known. This enables us, with the use of Eq. (2.28), to determine r_s''. The analysis then proceeds as described in the first method. The third approach requires the application of Eq. (5.5). In this case the conical nose is replaced by a specified drag coefficient. The afterbody shock, given by Eq. (5.5), is considered as being attached at the shoulder of the cone-cylinder shown in Fig. (5.21). This approach is similar to that used for the blunt-nosed cylinders discussed previously.

Of these three methods, the first is in best agreement with experiment near the nose, but all three methods yield essentially the same shock far downstream. In Fig. (5.22) the shock shape for a 45° pointed

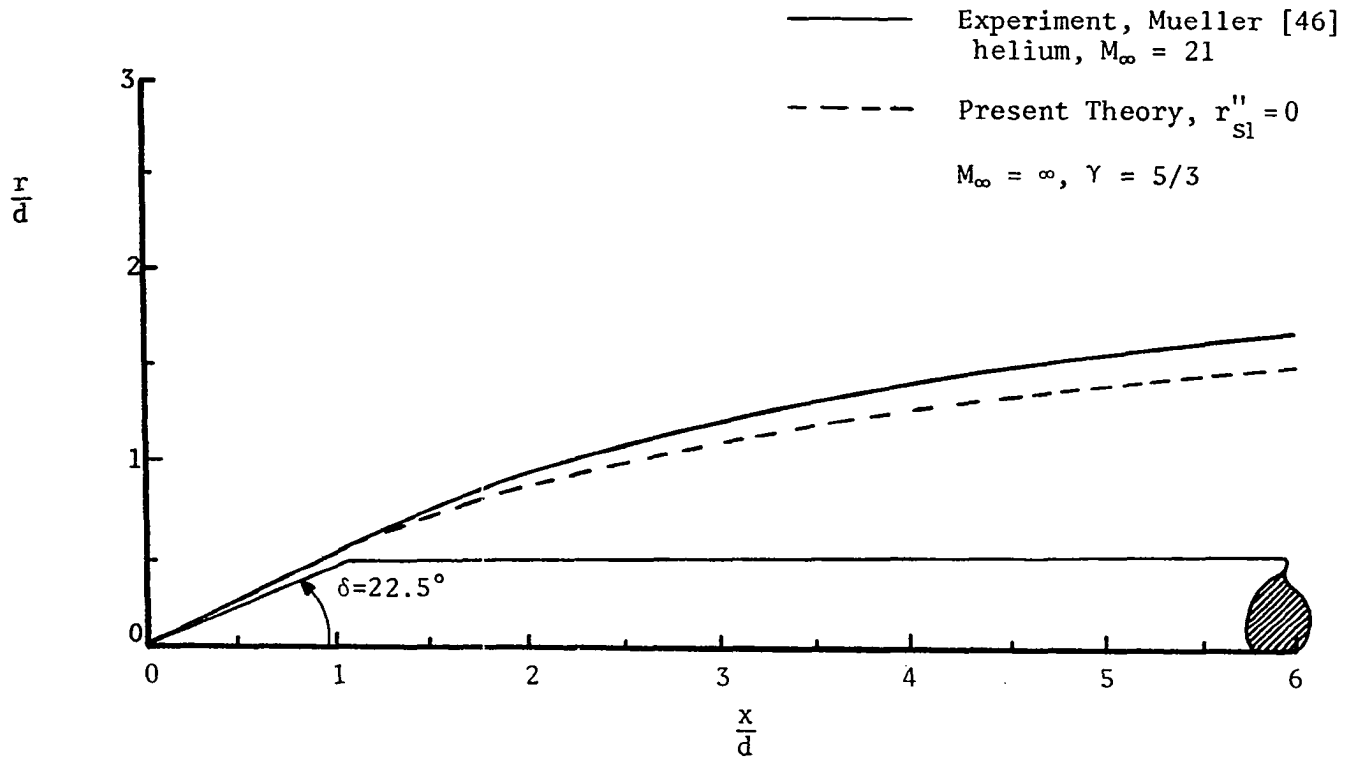


Figure 5.22. Comparison of shock shapes for a slender cone-cylinder.

cone-cylinder, obtained from experiment by Mueller, is displayed along with a plot from the first method described above. Although the comparison is not bad near the nose, the growth of the two shocks is fundamentally different downstream. The experimental shock grows as $\bar{x}^{.55}$, whereas the present theory predicts a shock that grows approximately as $\bar{x}^{.48}$ for points not too near the nose. It appears that the slender nose significantly influences the downstream shock growth, such that the shock does not behave in the same manner as the shock for a blunt-nosed cylinder. Thus, application of the theory to non-growing bodies should be restricted to those bodies that are aerodynamically blunt.

In this chapter we studied the direct problem applied to circular cylinders and flat-plates for M_∞ equal to infinity. We found that the shock shapes do not grow as a simple power-law, but only approach this type of behavior as x approaches infinity. For x equal to infinity our development yields a shock that grows as a blast-wave, that is, $x^{2/(3+j)}$. For real flows the shock weakens downstream from the nose and eventually degenerates into a Mach wave. It follows that for real flows (finite Mach number) the shock tends to vary as x far downstream rather than $x^{2/(3+j)}$ as predicted by theory for M_∞ equal to infinity. Thus, the shock shapes developed with the present theory agree reasonably well with those found from experiments for locations not too near the nose, yet not so far downstream that the real shock has weakened significantly.

CHAPTER VI

INTERPRETATION OF BODY SHAPES

In Chapter IV we discussed power-law shocks where $r_s \sim x^{n_s}$. We found that for n_s equal to unity, the bodies are cones and wedges with n_b^* equal to n_s. In the range $2(\gamma+1)/[(3+j)\gamma+2] < n_s < 1$ the body can be approximated to order β^2 with a simple power-law shape given by Eq. (4.13), and n_b is equal to n_s. For $2/(3+j) < n_s < 2(\gamma+1)/[(3+j)\gamma+2]$ the displacement effects of the entropy layer are greater than order β^2. In this range the body is given by Eq. (4.8) with $n_b < n_s$. When $n_s = 2/(3+j)$ we found that the body shape is given by Eq. (4.19) with $n_b = 2/[(3+j)\gamma]$. Our solutions for the inverse problem are not valid for $0 < n_s < 2/(3+j)$ because the bodies generated in this range are not realistic. This limitation is not unique to the present theory. For instance, it is not obvious why there are no self-similar solutions in this range. Despite a number of attempts there does not appear to be a satisfactory asymptotic theory for hypersonic flow over the full range of slender blunt-nosed bodies. For further discussions of this problem the reader is referred to Mirels [41,42], Freeman [21], and Guiraud *et al.* [24].

---

*The body power-law exponent.

The similarity solutions of the small disturbance equations yield shock shapes for power-law bodies of the form $r_s \sim x^{n_s}$. In the range $2/(3+j) < n_s < 1$ the self-similar solutions yield n_s equal to n_b. For the values $0 < n_b < 2/(3+j)$ the shock power-law exponent is $n_s = 2/(3+j)$. This behavior is displayed in Figs. (6.1) and (6.2) for axisymmetric and planar bodies, respectively. Also shown by the smooth dashed curves are the variations in the shock and body power-law exponent, from the present theory, as described in the previous paragraph.

In Chapter V shock shapes for n_b equal to zero were obtained from a solution of the direct problem for non-growing bodies. The shock coordinates for these bodies are displayed in Figs. (5.10-13) and (5.18-20) and are compared with experimental values. Since these plots are logarithmic the slope at any point is the local value of n_s. It is apparent that the shock shapes are not simple power-law types since the slopes vary with $\bar{x}$. The change in slope is less evident for $\bar{x}$ greater than about 1 for circular cylinders and $\bar{x}$ greater than about 2 for flat-plates. However, the slopes are continually increasing and approach the limiting or "blast-wave" slopes ($\frac{1}{2}$ for circular cylinders and 2/3 for flat-plates) only as $\bar{x}$ approaches infinity. It is evident from the equations for the shock shapes, Eqs. (5.5) and (5.6), that the slopes do not depend on the nose shape, but are dependent on γ. For purposes of comparison with experiment values of n_s for n_b equal to zero are chosen from Figs. (5.10-13) and (5.18-20) at $\bar{x}$ equal to

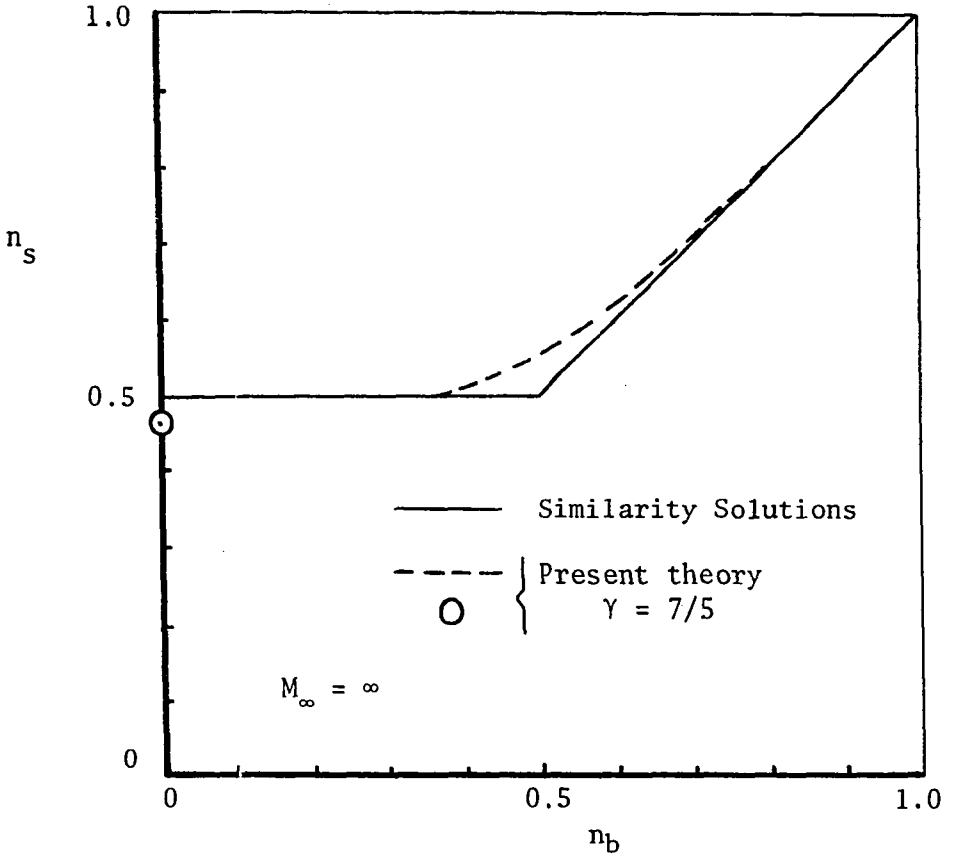


Figure 6.1. Variation of the shock power-law exponent for axisymmetric bodies.

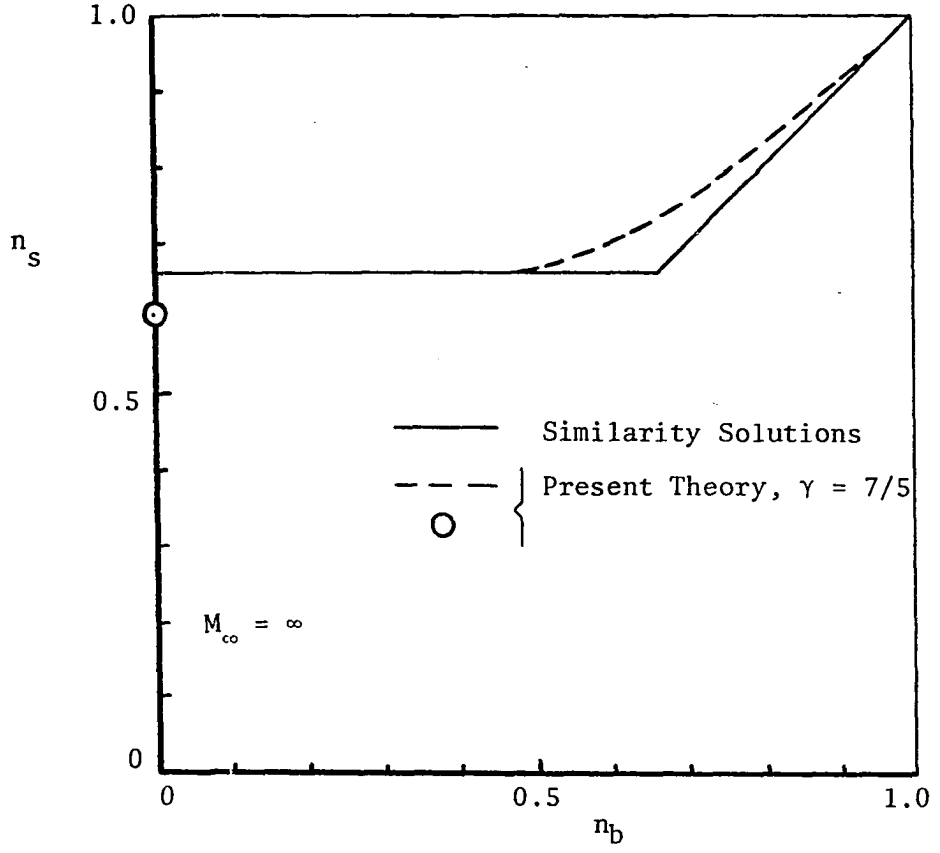


Figure 6.2. Variation of the shock power-law exponent for planar bodies.

25. This particular value is arbitrary, but is chosen well downstream of the nose region where the slope changes most rapidly, and yet within the physical limitations of most practical bodies. For γ equal to 7/5 we find that n_s is equal to approximately 0.465 for circular cylinders and approximately 0.61 for flat-plates.

In Figs. (6.3) and (6.4) the solid segment of the smooth curve is the variation in the power-law exponent from the present theory as plotted previously in Figs. (6.1) and (6.2). The value of n_s for n_b equal to zero determines the n_s axis intercept. These values are given above for γ equal to 7/5. The dashed segment of the smooth curve is drawn in to demonstrate the most likely behavior of n_s with n_b in the range where our solutions are not available. In Fig. (6.3) our data are compared with the experimental data of Freeman *et al.* [48] and Beavers [49] for axisymmetric blunted bodies. In Fig. (6.4) data points from the experiments of Hornung [50] are compared with the present theory for plane blunted bodies.

The tests conducted by Freeman were accomplished at M_∞ equal to 8.8, in nitrogen, in the N.P.L. 6 inch shock tunnel. The models were complete power-law shapes with n_b equal to 0, 1/10, 1/3, 1/2, 3/4 and 1. Model lengths were 6 inches and base diameters 2 inches. Freeman noted that n_s varied considerably with the position of measurement. Data were taken in a range $0.2<x/\ell<1.0$ with the magnitude of variation shown in Fig. (6.3). The actual data points displayed are for the x/ℓ equal to 0.5 position measurement. The experiments conducted by Beavers were made in the Rosemont Aeronautical Laboratory hypersonic wind tunnel at

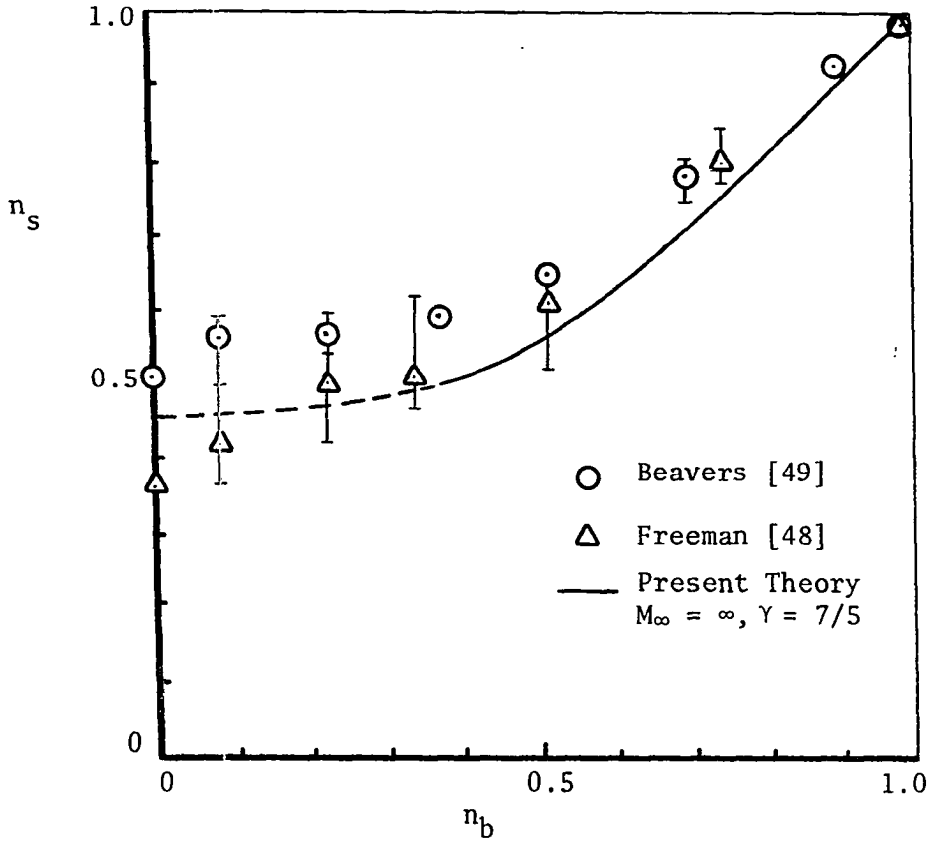


Figure 6.3. Comparison of the variation of n_s with n_b between the present theory and experiments (j = 1).

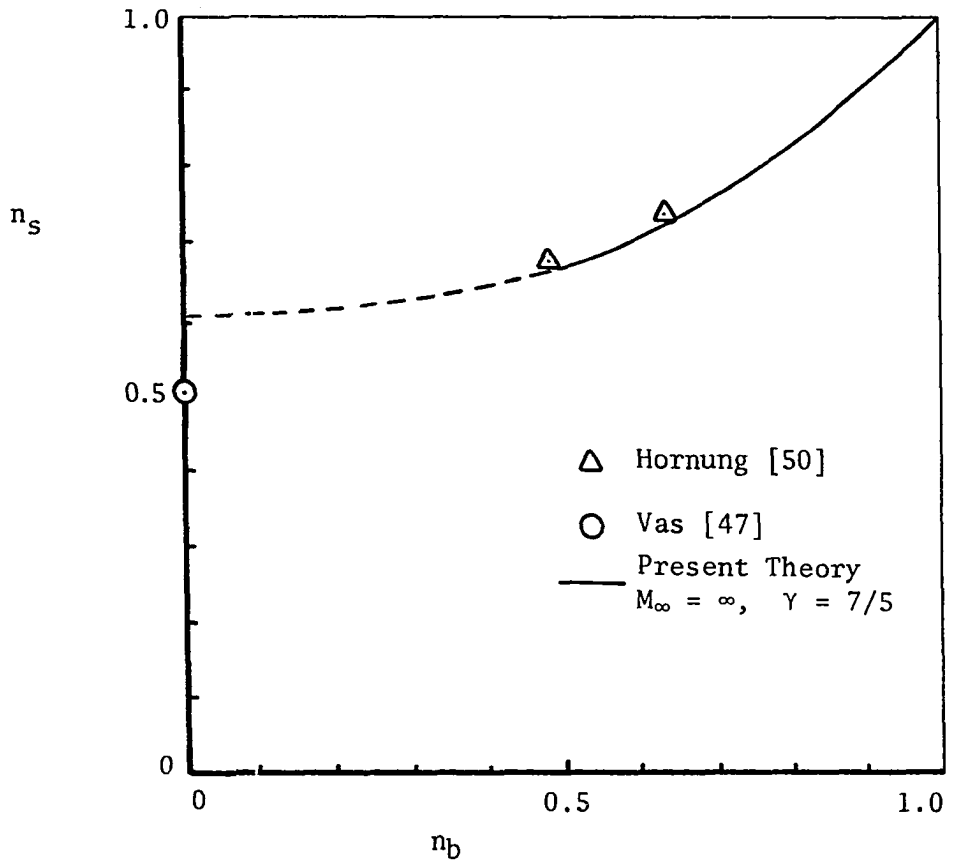


Figure 6.4. Comparison of the variation of n_s with n_b between the present theory and experiments (j = 0).

M_∞ equal to 7.7. Beavers found that the variation of n_s was not noticeable for values of x/ℓ greater than about 0.2 for n_b equal to 0.85, and x/ℓ greater than about 0.6 for n_b equal to zero. Values of n_b tested were 0, 0.1, 0.25, 0.4, 0.5, 0.7, 0.85 and 1.0. The lengths of the test models for which data is shown in Fig. (6.3) are 7 inches. All bodies had a maximum diameter of 2 inches.

Although there is a noticeable spread in the experimental data presented by Freeman and Beavers, both groups of data plot as a smoothed version of the similarity solution shown in Fig. (6.1). The present theory plots as a smooth curve also, but as previously mentioned part of the curve is drawn arbitrarily. Except for n_b equal to zero we seem to agree more closely with Freeman's results.

Some of the differences between the experimental data of Freeman and Beavers, and between the experiments and the present theory can be explained as follows. First, experimental evidence was gathered at relatively low Mach numbers which differed from about Mach 7 to Mach 13, whereas the theory is developed for M_∞ equal to infinity. Second, the fineness ratios (ℓ/d) of the experimental bodies were small, varying from 2 to 3.5, but the theory is developed independently of finite lengths. Freeman [48] notes that both the Mach number and fineness ratio influence the experimental measurement of the variation in n_s with n_b.

The experimental data presented in Fig. (6.4) by Hornung were obtained in air with a free-stream Mach number of about 8. The models

were plane power-law bodies with n_b equal to 1/2 and 5/8. The models were 10 inches long and 5 inches wide with d equal to 0.01 inch for n_b equal to 5/8, and d equal to 0.225 inch for n_b equal to 1/2. The data points from these tests fall very nearly on the smooth curve drawn from our analysis. Also shown for n_b equal to zero is the experimental data point from Vas's work.

CHAPTER VII

CONCLUSIONS

The following conclusions and recommendations are made as a result of the development and application of an integral approximation for the shock shapes over slender bodies in inviscid hypersonic flow.

Concluding Remarks

Applications of the solution for the inverse problem to pointed shocks, that is, cones, wedges and ogives yield bodies that can be expressed algebraically in terms of the shock parameters and the ratio of specific heats. The computed shapes agree well with other methods for K_δ greater than unity, and generally are obtained much more easily. The surface pressures on a wedge agree exactly with those found by Linnell [39] and subsequently by Van Dyke [9], whereas surface pressures for cones are found to agree with small disturbance values only in the Newtonian limit. The surface pressures and initial pressure gradients for ogives agree well with the small disturbance values given by Van Dyke [9] for $K_\delta >> 1$.

The inverse problem applied to blunted shocks was restricted to M_∞ equal to infinity. For power-law shocks the body shape was expressed algebraically. It was also shown that for certain values of the shock power-law exponent n_s the entropy-displacement thickness plays an important role in the determination of the body shape. Agreement of the power-law shock shapes, body shapes, and surface pressures with other theories is, in general, quite good. However, there appears to be some discrepancy between the theories and experiments. In the case of hyperbolic shocks the body shape is expressed in terms of a simple quadrature. We found, as did Yakura [19], that these bodies are blunted wedges and cones. However, because of the restrictions we imposed on the flow by specifying the shock shape, the drag coefficient on a blunted cone given by the present theory does not exhibit a minimum as found by Chernyi [28].

The direct problem applied to circular cylinders and flat-plates for M_∞ equal to infinity yields shock shapes that do not grow as a simple power-law. We found that these shocks grow more slowly than the blast-wave, and approach the blast-wave behavior only as x approaches infinity. These results are in good agreement with other theories e.g., Van Hise [44] and experiments, although there is some spread among the experimental data.

The simplicity gained by the present integral method, which accounts for only the gross flow properties, is necessarily accompanied by a loss of information concerning the behavior of the flow quantities in the shock layer. Also, the small disturbance requirements are violated

in the nose region (as well as in the entropy layer) and as a result the body nose shapes are unknown. In addition, far downstream the present solutions are not valid because the strong shock requirements are violated. This accounts, in part, for the differences in the shock shapes given by the present theory for M_∞ equal to infinity and the experimental data recorded for finite Mach number.

Recommendations for Future Research

The work presented here dealing with slender blunted shocks was accomplished for M_∞ equal to infinity. This, of course, enabled the simplest solutions to be obtained. Future work should include attempts to simplify the solutions for finite Mach numbers.

The general quadrature solution is readily applicable to other simple body shapes. For instance solutions could be obtained for the exponential shock similar to that investigated by Chernyi [28]. Also, solutions for $n_s > 1$ could be found from the quadrature solution for the inverse problem.

A more rigorous development of the entropy-displacement effects should be made. One approach could be an expansion procedure with the inner region taken near the nose, and the outer region taken far from the nose.

Future experimental efforts should be made at very high Mach numbers ($M_\infty \simeq 20$ and greater) and bodies with relatively large fineness ratios ($\ell/d \simeq 10$ and greater). In this way more realistic comparisons between theory and experiment can be made, e.g., the shock power-law exponent behavior with respect to the body power-law exponent.

LIST OF REFERENCES

1. Guderly, J. P., "Starke kugelige und zylindrishe Verdichtungstösse in der Nähe des Kugelmittelpunkts bzw. der Zylinderachse," Luftfahrtforchung, Vol. 19 (1942), pp. 302-312.
2. Hayes, W. D., "On Hypersonic Similitude," Quarterly of Applied Mathematics, Vol. 5 (1947), pp. 105-106.
3. Sedov, L. I., "On Certain Unsteady Motions of a Compressible Fluid," Prikladnaya matematika i mechanika, Vol. 9 (1945), pp. 293-311.
4. Tsien, H.S., "Similarity Laws of Hypersonic Flows," Journal of Mathematical Physics, Vol. 25 (1946), pp. 247-251.
5. Sedov, L. I., "Propagation of Strong Blast Waves," Prikladnaya matematika i mechanika, Vol. 10 (1946), pp. 241-250.
6. Taylor, G. I., "The Formation of a Blast Wave by a Very Intense Explosion," Proceedings of the Royal Society of London, Ser. A 201, (1950), pp. 159-186.
7. Bam-Zelikovich, G. M., Bunimovich, A. I., and Mikhailova, M. P., "The Motion of Slender Bodies at Hypersonic Speeds," Collection of Papers, No. 4, Teoretich. Gidromekhanika. Oborongiz, Moscow, 1949.
8. Goldsworthy, F. A., "Two-Dimensional Rotational Flow at High Mach Number Past Thin Airfoils," Quart. J. Mech. Appl. Math., Vol. 5 (1952), pp. 54-63.

9. Van Dyke, M. D., "A Study of Hypersonic Small Disturbance Theory," Rept. 1194 (1954), NACA.

10. Sakurai, A., "On the Propagation and Structure of the Blast Wave, I," J. Phys. Soc. Japan, Vol. 8 (1953), pp. 662-669.

11. Sakurai, A., "On the Propagation and Structure of the Blast Wave, II," J. Phys. Soc. Japan, Vol. 9 (1954), pp. 256-266.

12. Lin, S. C., "Cylindrical Shock Waves Produced by Instantaneous Energy Release," J. Appl. Phys., Vol. 25 (1954), pp. 54-57.

13. Cheng, H. K., and Pallone, A. J., "Inviscid Leading-Edge Effect in Hypersonic Flow," J. Aero. Sci., Vol. 23 (1956), pp. 700-702.

14. Lees, L., and Kubota, T., "Inviscid Hypersonic Flow over Blunt-Nosed Slender Bodies," J. Aero. Sci., Vol. 24 (1957), pp. 195-202.

15. Chernyi, G. G., "Hypersonic Flow around a Body by An Ideal Gas," Izv. Akad. Nauk SSSR, Otd. Tekhn. Nauk., No. 6 (1957), pp. 77-85.

16. Cheng, H. K., Hall, J. G., Golian, T. C., and Hertzberg, A., "Boundary-Layer Displacement and Leading-Edge Bluntness Effects in High Temperature Hypersonic Flow," J. Aero. Sci., Vol. 28, No. 5 (1961), pp. 353-381, 410.

17. Sychev, V. V., "On the Theory of Hypersonic Gas Flow with a Power-Law Shock Wave," J. Appl. Math. Mech., Vol. 24 (1960), pp. 756-764.

18. Guiraud, J. P., "Ecoulement Hypersonique d'un Fluide Parfait sur une Plague Plane Comportant un Bord d'Attague d'Epaisseur Finie," Comptes Rendus, Acad. Sci., Paris, Vol. 246 (1958), pp. 2842-2845.

19. Yakura, J. K., "Theory of Entropy Layers and Nose Bluntness in Hypersonic Flow," Hypersonic Flow Research, Vol. 7 (F.R. Riddell, ed.), Academic Press, New York, 1962, pp. 421-470.

20. Freeman, N. C., "Newtonian Theory of Hypersonic Flow at Large Distances From Bluff Axially Symmetric Bodies," Hypersonic Flow Research, Vol. 7 (F.R. Riddell, ed.), Academic Press, New York, 1962, pp. 345-377.

21. Freeman, N. C., "Asymptotic Solutions in Hypersonic Flows: An Approach to Second-Order Solutions of Hypersonic Small-Disturbance Theory," Research Frontiers in Fluid Dynamics, Vol. XV (R.J. Seegar and G. Temple, eds.), Interscience, New York, 1965, pp. 284-307.

22. Vaglio-Laurin, R., "Asymptotic Flow Pattern of a Hypersonic Body," PIBAL Rept. No. 805, 1964, Dept. of Aerospace Engr. and Appl. Mech., Polytechnic Inst. of Brooklyn, Brooklyn, N.Y..

23. Guiraud, J. P., "Asymptotic Theory in Hypersonic Flow," ONERA T.P., No. 132 (1964). Also in "Proc. Internatl. Symp. on Fundamental Phenomena in Hypersonic Flow," (J.G. Hall, ed.), Cornell Univ. Press, Ithaca, N. Y., 1966, pp. 70-84.

24. Guiraud, J. P., Vallee, D., and Zolver, R., "Bluntness Effects in Hypersonic Small Disturbance Theory," Basic Developments in Fluid Dynamics, Vol. 1 (M. Holt, ed.), Academic Press, New York, 1965, pp. 127-247.

25. Stewartson, K., and Thompson, B. W., "On One-Dimensional Unsteady Flow at Infinite Mach Number," Proc. Roy. Soc. (London), Ser. A 304 (1968). pp. 255-273.

26. Schneider, W., "A Uniformly Valid Solution for the Hypersonic Flow Past Blunted Bodies," J. Fluid Mech., Vol. 31, part 2, 1968, pp. 397-415.

27. Chernyi, G. G., "Application of Integral Relationships in Problems of Propagation of Strong Shock Waves," J. Appl. Math. Mech., Vol. 24 (1960), pp. 159-165.

28. Chernyi, G. G., Introduction to Hypersonic Flow, 1st ed., Academic Press, New York, 1961.

29. Sedov, L. I., Similarity and Dimensional Methods in Mechanics, Academic Press, New York, 1959.

30. Hayes, W. D., and Probstein, R. F., Hypersonic Flow Theory, 2nd ed., Vol. I, Inviscid Flows, Academic Press, New York, 1966.

31. Seeger, R. J., and Temple, G., eds., Research Frontiers in Fluid Dynamics, Vol. XV, Interscience, New York, 1965, pp. 284-307. See ref. [21].

32. Riddell, F. R., ed., Hypersonic Flow Research, Vol. 7, Academic Press, New York, 1962, pp. 345-377, 421-470. See refs [19,20].

33. Cox, R. N., and Crabtree, L. F., Elements of Hypersonic Aerodynamics, Academic Press, New York, 1965.

34. von Kármán, Th., and Dryden, H. L., Advances in Applied Mechanics, Vol. VII, Academic Press, New York, 1962, pp. 1-54, 317-319. See ref. [42].

35. Chernyi, G. G., "Integral Methods for the Calculation of Gas Flows with strong Shock Waves," J. Appl. Math. Mech., Vol 25 (1961), pp. 138-147.

36. Cole, J. D., "Newtonian Flow Theory for Slender Bodies," J. Aero. Sci., Vol. 24 (1957), pp. 448-455.

37. Rasmussen, M. L., "On Hypersonic Flow Past an Unyawed Cone," AIAA J., Vol. 5 (1967), pp. 1495-1497.

38. Sims, J. L., "Tables for Supersonic Flow Around Right Circular Cones at Zero Angle of Attack," SP-3004 (1964), NASA.

39. Linnell, R. D., "Two-Dimensional Airfoils in Hypersonic Flows," J. Aero. Sci., Vol. 16 (1949), pp. 22-30.

40. Kubota, T., "Investigation of Flow around Simple Bodies in Hypersonic Flow," Mem. 40, Guggenheim Aero. Lab., 1957, Calif. Inst. of Tech..

41. Mirels, H., "Approximate Analytical Solutions for Hypersonic Flow over Slender Power-Law Bodies," TR R-15 (1959), NASA.

42. Mirels, H., "Hypersonic Flow over Slender Bodies Associated with Power-Law Shocks," Advances in Applied Mechanics, Vol. VII (Th. von Kármán and H. L. Dryden, eds.), Academic Press, New York, 1962, pp. 1-54, 317-319.

43. Cleary, J. W., "An Experimental and Theoretical Investigation of the Pressure Distribution and Flow Fields of Blunted Cones at Hypersonic Mach Numbers," TN D-2969 (1965), NASA.

44. Van Hise, V., "Analytic Study of Induced Pressure on Long Bodies of Revolution with Varying Nose Bluntness at Hypersonic Speeds," TR R-78 (1961), NASA.

45. Lukasiewicz, J., "Blast-Hypersonic Flow Analogy-Theory and Application," ARS J., Vol. 32 (1962), pp. 1341-1346.

46. Mueller, J. N., Close, W. H., and Henderson, A., Jr., "An Investigation of Induced-Pressure Phenomena on Axially Symmetric, Flow-Aligned, Cylindrical Models Equipped with Different Nose Shapes at Free-Stream Mach Numbers From 15.6 to 21 in Helium," TN D-373 (1960), NASA.

47. Vas, I.E., Bogdonoff, S. M., Hammitt, A. G., "An Experimental Investigation of the Flow Over Simple Two-Dimensional and Axial Symmetric Bodies," Jet Propulsion, Vol. 28 (1958), pp. 97-104.

48. Freeman, N. C., Cash, R. F., and Bedder, D., "An Experimental Investigation of Asymptotic Hypersonic Flows," J. Fluid Mech., Vol. 18 (1964), pp. 379-384.

49. Beavers, G. S., "Shock-Wave Shapes on Hypersonic Axisymmetric Power-Law Bodies," AIAA J., Vol. 7 (1969), pp. 2038-2040.

50. Hornung, H. G., "Inviscid Hypersonic Flow Over Plane Power-Law Bodies," J. Fluid Mech., Vol. 27 (1967), pp. 315-336.

APPENDIX A

H_0, H_1, H_2, G_1, AND G_2 FOR THE OGIVE OF REVOLUTION

H_0, H_1, H_2, G_1 AND G_2 FOR THE OGIVE OF REVOLUTION

The shock shape for the ogive of revolution given by Eq. (3.8) is

$$r_s = \beta x(1+\lambda x+\omega x^2+\ldots) \quad .$$

The substitution of this shock shape into Eq. (2.16) and expansion for small x yields the following expressions for H and G:

$$H = H_0(1+H_1x+H_2x^2+\ldots)$$

$$G = \frac{1}{v_\infty} \frac{4\pi}{\gamma+1} (\beta^2v_\infty^2-a_\infty^2)H_0x(1+G_1x+G_2x^2+\ldots) \quad ,$$

where

$$H_0 = a_\infty^2 + \frac{2\gamma}{\gamma+1} (\beta^2v_\infty^2-a_\infty^2)$$

$$H_1 = \frac{2\gamma}{\gamma+1} \frac{\lambda}{H_0} (5\beta^2v_\infty^2+a_\infty^2)$$

$$H_2 = \frac{2\gamma}{\gamma+1} \frac{1}{H_0} [(5\beta^2v_\infty^2-3a_\infty^2)\lambda^2+(9\beta^2v_\infty^2+3a_\infty^2)\omega]$$

$$G_1 = \frac{\lambda}{H_0} [3 \frac{\gamma-1}{\gamma+1} (3\beta^2v_\infty^2+a_\infty^2)+ \frac{3}{2} \beta^2v_\infty^2(\frac{7\beta^2v_\infty^2-a_\infty^2}{\beta^2v_\infty^2-a_\infty^2})]$$

$$G_2 = \frac{2\lambda^2}{H_0} \{\frac{\gamma-1}{\gamma+1} [9\beta^2v_\infty^2-a_\infty^2 + \frac{4(\beta^2v_\infty^2+a_\infty^2)^2}{\beta^2v_\infty^2-a_\infty^2}] + \beta^2v_\infty^2(\frac{16\beta^2v_\infty^2-2a_\infty^2}{\beta^2v_\infty^2-a_\infty^2})\}$$

$$+ \frac{2\omega}{H_0} [4 \frac{\gamma-1}{\gamma+1} (2\beta^2v_\infty^2+a_\infty^2)+\beta^2v_\infty^2(\frac{11\beta^2v_\infty^2+a_\infty^2}{\beta^2v_\infty^2-a_\infty^2})] \quad .$$

APPENDIX B

A_1, B_1, AND C_1 FOR THE OGIVE OF REVOLUTION

A_1, B_1, AND C_1 FOR THE OGIVE OF REVOLUTION

The body shape for the ogive of revolution is obtained if we substitute the complete expressions for H and G given in Appendix A into Eq. (2.18b). The resulting expression is expanded for small x, integrated, and manipulated to obtain

$$r_b = \delta x[1+A_1\lambda x+(B_1\omega+C_1\lambda^2)x^2+\ldots] \quad ,$$

where δ is the initial body slope and A_1, B_1, and C_1 are:

$$A_1 = \frac{(19\gamma-7)(\gamma+1)K_\delta^4+6(13\gamma+1)K_\delta^2+72}{12(\gamma+1)(1+\gamma K_\delta^2)K_\delta^2}$$

$$B_1 = \frac{(5\gamma-3)(\gamma+1)K_\delta^4+(23\gamma-1)K_\delta^2+24}{2(\gamma+1)(1+\gamma K_\delta^2)K_\delta^2}$$

$$C_1 = \frac{k_1K_\delta^8+k_2K_\delta^6+k_3K_\delta^4+k_4K_\delta^2-2880(3\gamma+1)}{288(\gamma+1)^2(1+\gamma K_\delta^2)K_\delta^4}$$

where

$$k_1 = 7(-49\gamma^2+26\gamma+23)(\gamma+1)^2$$

$$k_2 = 24(\gamma+1)(-203\gamma^2+12\gamma+11)$$

$$k_3 = 36(-445\gamma^2-298\gamma-29)$$

$$k_4 = 288(-63\gamma-23) \quad .$$